

Report

R-20-13

December 2022



Methodology for rock mechanics modelling of the Forsmark site

Eva Hakami

Diego Mas Ivars

Caroline Darcel

SVENSK KÄRNBRÄNSLEHANTERING AB

SWEDISH NUCLEAR FUEL
AND WASTE MANAGEMENT CO

Box 3091, SE-169 03 Solna
Phone +46 8 459 84 00
skb.se

SVENSK KÄRNBRÄNSLEHANTERING

ISSN 1402-3091

SKB R-20-13

ID 1945707

December 2022

Methodology for rock mechanics modelling of the Forsmark site

Eva Hakami, Rejlers AB

Diego Mas Ivars, Svensk Kärnbränslehantering AB

Caroline Darcel, Itasca Consultants SAS

Keywords: Data collection, Intact rock strength, In situ stress, Fracture properties, Stiffness, Sealed fractures, Stress modelling, H-M modelling, Safety assessment.

This report is published on www.skb.se

© 2022 Svensk Kärnbränslehantering AB

Preface

A series of methodology reports support the programmes for investigation and modelling during the execution of planned underground constructions at Forsmark. The series includes the following disciplines: geometric modelling of ground elevation and regolith, deterministically modelled geological structures, discrete fracture network (DFN) modelling (stochastic, semi-stochastic and deterministic modelling of structural-hydraulic fracture data), rock mechanics modelling, thermal properties modelling, integrated hydrological and hydrogeological modelling, hydrogeochemical modelling, and transport modelling. Report numbers (ID), acronyms, and titles are shown below.

ID	Acronym	Title
R-20-10	DGMM	Methodology for deterministic geologic modelling of the Forsmark site.
R-20-11	DFNMM1	Methodology for discrete fracture network modelling of the Forsmark site. Part 1 – Concepts, Data and Interpretation Methods.
R-20-12	DFNMM2	Methodology for discrete fracture network modelling of the Forsmark site. Part 2 – Application examples.
R-20-13	RMMM	Methodology for rock mechanics modelling of the Forsmark site.
R-20-14	HGMM	Methodology for hydrological and hydrogeological modelling of the Forsmark site.
R-20-15	HCMM	Methodology for hydrochemical modelling of the Forsmark site.
R-20-16	ERMM	Methodology for elevation and regolith modelling of the Forsmark site.
R-20-17	TRPMM	Methodology for site descriptive and safety assessment transport modelling of the Forsmark site.
R-20-18	THPMM1	Methodology for modelling of thermal properties of the Forsmark site. Part 1 – Recommended data and interpretation methods.
R-20-19	THPMM2	Methodology for modelling of thermal properties of the Forsmark site. Part 2 – Background and methodology development.

This methodology report, RMMM, describes how to acquire data concerning in situ stress field, rock mechanics properties for the intact rock, for fractures and the rock mass. It further explains how the rock mechanics parameters will be coupled to hydro-mechanical fracture parameters and be integrated in discrete network modelling. Besides supporting the programmes for investigation and modelling during constructions, other end users of this methodology are safety assessment and repository design.

Abstract

The objective of this report is to give an account of all methods planned to be used in constructing a descriptive model for rock mechanics properties at the Forsmark site, designated to serve as a final repository of radioactive waste. Many of the methods and parameters previously used for site-descriptive modelling in the surface-based site investigation phase will be retained, and this report focuses on motivating and describing parts that have been added or modified in the strategy.

The report starts with a chapter presenting the role of rock mechanics and principal rock mechanics concerns in the safety assessment, also including a description of some central concepts and nomenclature for rock mechanics. This is followed by a review of all rock mechanics areas that are covered by the detailed site investigations and associated site description: in situ rock stress field, intact rock properties, fracture properties and rock mass properties.

The main changes of the strategy, compared with the one used in the previous site description, are the following:

The stress model will incorporate additional supporting measurement data, using a new method (LVDT-cell method), which can be applied when the rock excavation has begun. Measurement data will be analysed and presented handling the stress as a tensor entity. Additional support for the stress model will be established through evaluation of so-called core and ring diskings of drill cores and the borehole wall stability. The variation in in situ rock stress that is expected due to deformation zones in the region will be simulated with improved numerical methods.

For the intact rock a description of scale effects will be added based on complementary laboratory testing using different sample sizes. An extended database from laboratory testing will also improve the basis for the description of the different rock types occurring in the area. New parameters in the description are fracture toughness and CAI (Cerchar abrasive index). Point load test is a strength measurement method that will be evaluated for possible use as a complementary method in the excavation phase.

For the description of single open fractures, they will be subdivided into two categories depending on if they have been observed as water-conductive in the borehole, or not. This is done to enable an improved description covering different types of fractures, which is of importance for the safety assessment. The strategy for fractures also includes additional laboratory tests performed at different boundary conditions, a study of scale dependence and an improved description of the fracture surface roughness. For the water-bearing fractures (established by flow logging) the estimated mechanical property parameters will be associated with larger uncertainty and cannot, to the same extent, be based directly on laboratory testing. However, a separate handling of water-bearing fractures will enable an improved description and it will include estimates of larger scale undulation, and its influence on fracture shear resistance, and also a suggestion for handling of the hydro-mechanical coupling between mechanical deformation and hydraulic aperture change.

The sealed fractures will be described separately with strength and stiffness properties, as for the open fractures. This is motivated by the fact that sealed fractures are expected to occur relatively frequently in the deposition area. The estimation of strength and stiffness parameters for sealed fractures will be based on testing.

Concerning the naturally fractured rock mass properties, the strategy is to primarily use the DFN-based approach (Discrete Fracture Network) in the modelling, which means that the parameters are calculated with theoretical models for how deformation and strength depend on the properties of the fracture network and the rock stresses in the area. New models for both the fracture network (DFN) and its application within rock mechanics will be used in future site descriptions.

Sammanfattning

Syftet med denna rapport är att redovisa samtliga metoder som planeras för att upprätta en beskrivning av de bergmekaniska egenskaperna på den utsedda platsen för slutförvar i Forsmark. Många av metoderna och parametrarna som använts till platsbeskrivningen i det markbaserade platsundersökningsskedet kommer att bibehållas, och denna rapport fokuserar på motivering och beskrivning av de delar som har tillkommit eller förändrats i strategin.

Rapporten inleds med ett kapitel som presenterar bergmekanikens roll och huvudsakliga frågeställningar inom säkerhetsanalysen för slutförvar, och även beskriver några centrala begrepp och nomenklatur inom bergmekanik. Sedan följer en genomgång av samtliga områden inom bergmekanik som ingår i de detaljerade platsundersökningarna och motsvarande platsbeskrivning: bergspänningsfältet in situ, intakta bergets egenskaper, sprickors egenskaper och bergmassans egenskaper.

De väsentligaste förändringarna i strategin, i förhållande till den som tillämpades i tidigare platsbeskrivning, är följande:

Spänningsmodellen kommer att innehålla ytterligare stödande mätdata från en ny bergspänningsmätmetod (LVDT-cellen) som kan användas när utbrytningen har påbörjats. Mätdata kommer att analyseras och presenteras med hänsyn till spänningen som en tensor. Ytterligare stöd för spänningsprediktionen kommer att sökas genom utvärdering av så kallad "core diskning" och "ring diskning" och även från stabiliteten i borrhållsväggarna. Variationen av in situ bergspänningar som kan förväntas på grund av deformationszoner i regionen kommer att modelleras med förbättrade numeriska metoder.

För det intakta berget tillkommer beskrivning av skaleffekter baserat på kompletterade laboratorieprovning med olika provstorlek. En utökad databas från laboratorieprovning kommer även att förbättra underlaget för beskrivningen av de olika förekommande bergarterna i området. Tillkommande parametrar är brottseghet och nötningsindex CAI (Cerchar abrasivity index). Punktlasttester är en mätmetod för hållfasthet som kommer att utvärderas för att eventuellt användas som komplement i byggskedet.

För beskrivning av öppna sprickor kommer dessa att indelas i två kategorier beroende på om de har observerats som vattenförande i borrhålen eller inte. Det görs för att kunna förbättra beskrivning avseende alla olika typer av sprickor, vilket är väsentligt i säkerhetsanalyser. Strategin innehåller för sprickor även ytterligare laboratorieprovning med olika randvillkor, en studie av skalberoende samt förbättrad beskrivning av sprickyrtornas råhet. För de vattenförande sprickorna (identifierade med flödesloggning) är uppskattningen av egenskapsparametrar förknippad med större osäkerheter, och kan inte, i samma utsträckning, direkt baseras på laboratorieprovning. Men en separat hantering av vattenförande sprickor kommer att förbättra beskrivningen. Den kommer att inkludera en bedömning av sprickors storskaliga undulering och dess inverkan på skjuvhållfasthet samt förslag till hantering av den hydro-mekaniska kopplingen mellan sprickors rörelser och motsvarande förändringar i hydraulisk apertur.

De läkta sprickorna kommer att beskrivas separat med hållfasthetsparametrar som för de öppna. Det motiveras av att läkta sprickor förväntas att uppträda i relativt stor omfattning i depositionsområdet. Uppskattningen av läkta sprickors hållfasthet kommer att baseras på provning.

För den naturlig uppspruckna bergmassans egenskaper är strategin att huvudsakligen använda en så kallad teoretisk approach, vilket innebär att parametrarna beräknas med teoretiska modeller för hur deformationen och hållfastheten beror av spricknätverkets egenskaper och spänningar som finns i området. Nya modeller för såväl spricknätverket i sig (DFN) och dess applikation inom bergmekanik kommer att användas i kommande platsbeskrivningar.

Contents

1	Introduction	9
1.1	Background	9
1.2	Purpose of the rock mechanics methodology report	12
2	Rock mechanics concepts and nomenclature	13
2.1	Rock mechanics engineering and failure modes	14
2.2	Scale aspects in rock mechanics	16
2.3	Definition of excavation damage zone concepts	18
2.3.1	EDZ – Excavation Damage Zone	19
2.3.2	EIZ – Excavation Influence Zone	20
2.4	Spalling	22
2.4.1	Observations of spalling	22
2.4.2	Theoretical models for spalling	28
2.4.3	Strategies for improved spalling prediction	30
2.5	Rock mechanics concerns in the safety assessment	32
2.6	Rock mass properties descriptors	35
2.6.1	Fracture systems as Discrete Fracture Network models	36
2.6.2	Fracture size range selection for modelling applications	37
3	In situ stress	39
3.1	Modelling approach	39
3.2	Measurement methods	41
3.2.1	Overcoring methods	41
3.2.2	Hydraulic test methods	44
3.2.3	Breakout observations	44
3.2.4	Core dinking and ring dinking	46
3.2.5	Co-visualisation of borehole stress measurement results	50
3.3	Stress modelling – large scale	52
3.4	Description of spatial variability in stress field	57
3.5	Description of uncertainty in stress field	57
3.6	Stress models for hydro-mechanical analyses	58
4	Intact rock properties	59
4.1	Strength properties of intact rock	59
4.1.1	Compressive strength	59
4.1.2	Crack initiation stress	60
4.1.3	Tensile strength	61
4.1.4	Fracture toughness	63
4.1.5	Cerchar Abrasivity Index – CAI	64
4.2	Deformation properties of intact rock	65
4.3	Intact rock property parameter – Summary table	66
4.4	Scale effect in properties of intact rock	67
4.5	Creep – Time dependent behaviour of intact rock	69
5	Single open fracture properties	71
5.1	Fracture normal and shear stiffness	71
5.2	Fracture shear strength and dilation	73
5.3	Fracture aperture	75
5.4	Fracture surface geometry properties	76
5.4.1	Small scale surface geometry – Roughness	76
5.4.2	Large scale surface geometry – Undulation	76
5.5	Influence of sample scale on fracture parameters	77
5.5.1	Fracture scale issue	77
5.5.2	Upscaling for smaller fractures	80
5.5.3	Strategy for mechanical property estimations for larger fractures	82

5.6	Coupled H-M properties of single fractures	82
5.6.1	The need for coupled models for fractures	82
5.6.2	Coupling fracture stress and transmissivity	83
5.6.3	Water-bearing fractures – PFL fractures	88
5.7	Additional influencing factors on laboratory fracture test results and property models	89
5.7.1	Boundary conditions during laboratory testing	89
5.7.2	Variation in fracture infilling materials and side wall alteration	90
5.7.3	Coupling between temperature and fracture properties	90
5.7.4	Creep – Time dependent behaviour for single fractures	91
6	Sealed fracture properties	93
6.1	Frequency of sealed fractures	93
6.2	Potential influence on safety assessment from sealed fractures	95
6.3	Selection of parameters for sealed fracture description	96
7	Rock mass properties of fracture domains and deformation zones	97
7.1	DFN-based analytical approach	97
7.1.1	Rock mass effective elastic and strength properties	97
7.1.2	Stress dependent rock mass equivalent permeability	100
7.2	DFN-based numerical approach	100
7.3	Empirical approach	101
8	Rock mechanics modelling improvement strategy	103
	References	105

1 Introduction

1.1 Background

The Swedish Nuclear Fuel and Waste Management Company's (SKB) task is to take care of all the radioactive waste in Sweden, from nuclear power plants and industries, in a safe way. The system for managing Swedish radioactive waste comprises several facilities that together provide a safe chain of operation, Figure 1-1. The radioactivity level of the waste determines how it is managed.

Operational waste from nuclear power plants, which includes used protective clothing, replaced components and filter materials that have been used to decontaminate reactor water, as well as radioactive waste from hospitals, industry and research are deposited at the Final Repository for Short-lived Radioactive Waste (SFR). This repository is located at Forsmark in bedrock about 50 metres below sea level and will be expanded with an additional repository area at 150 m depth (SFR-PSU).

Spent nuclear fuel from nuclear power stations is transported by SKB's specially built vessel M/S Sigrid to the Central Interim Storage Facility for Spent Nuclear Fuel (CLAB), outside Oskarshamn, and will eventually be moved to the Spent Nuclear Fuel Repository that SKB plans to construct at Forsmark.

SKB is also planning a final repository for long-lived radioactive waste, SFL. This project has not, however, progressed as far as the others.

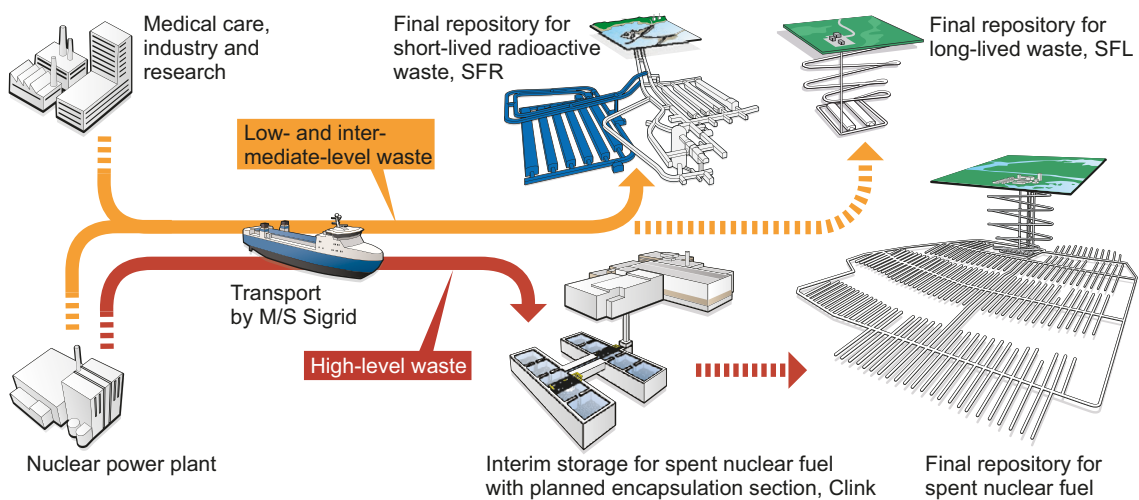


Figure 1-1. The Swedish system for dealing with radioactive waste. The facilities that still have to be constructed are indicated by dotted arrows.

The planned Final Repository for Spent Nuclear Fuel (SFK) forms the last link in the chain for managing the spent nuclear fuel, and it is planned to be built at Forsmark in south-east of Sweden (Figure 1-2). The spent fuel will be deposited in the repository in sealed canisters placed in vertical deposition holes distributed in horizontal rock vaults and surrounded by bentonite clay at a depth of about 500 metres in the rock. These canisters will be made of copper with inserts of nodular cast iron, and will each contain about 2 tonnes of spent nuclear fuel, and the encapsulation plant is planned to be constructed at Oskarshamn.

The general layout and the multibarrier concept for the Spent Nuclear Fuel Repository is illustrated in Figure 1-3. The repository will be composed of facilities above ground as well as access ramp and shafts to the underground repository area (Figure 1-4).



Figure 1-2. The location of the Forsmark site for the planned repository for spent nuclear fuel in south-east Sweden.

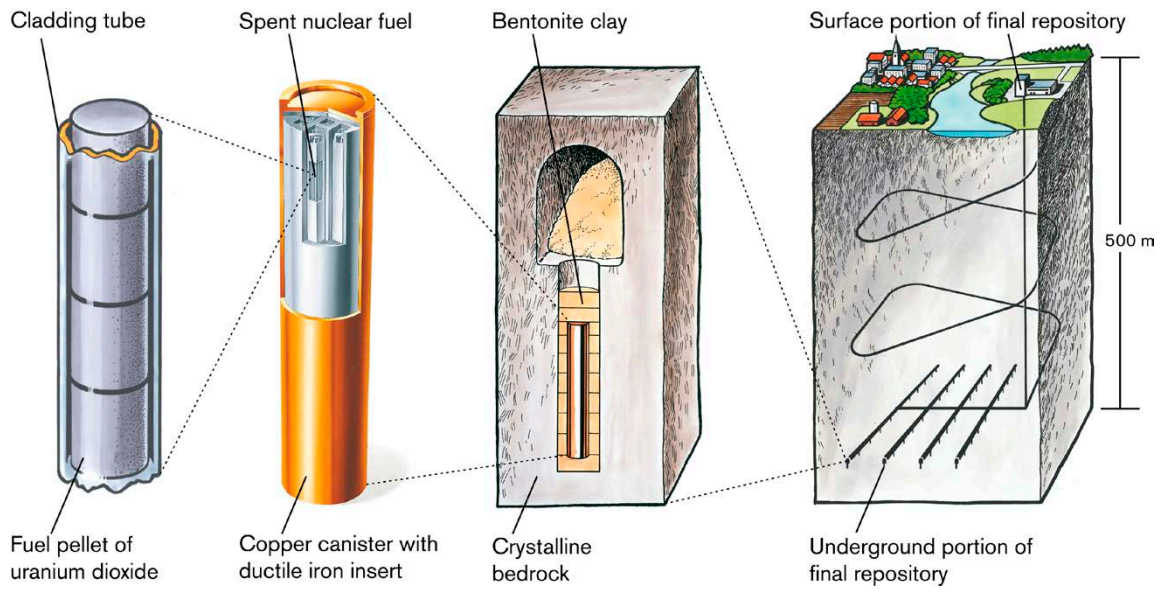


Figure 1-3. Multi-barrier concept for the Spent Nuclear Fuel Repository.



Figure 1-4. 3D-illustration of the planned facility for spent nuclear fuel.

1.2 Purpose of the rock mechanics methodology report

In the process of planning and designing the different facilities at Forsmark, SKB will produce a thorough and detailed description of all relevant rock mechanics conditions at the whole Forsmark site, including both the volumes for the spent nuclear fuel repository (SFK) and for the short-lived radioactive waste repository (SFR). Such a Site Descriptive Model, named SDM-Site (Glamheden et al. 2007, SKB 2008), was created for Forsmark in a first version, with focus on the volume for the spent nuclear fuel repository, at the completion of the investigation phase. A site description of the rock volume for the extension of SFR was presented in a separated report (SKB 2013).

The main purpose of this report is to summarize the rock mechanics methodology that will be applied in the next version of Forsmark site description, and later applied and developed in future site descriptions. Most of the methodology applied previously, which followed strategies summarized in Andersson et al. (2002) will be retained. However, in this new strategy report, the methodology that has been continuously evolving and improving during years, will be presented comprehensively and all new parameters to be included in the coming models will be listed accordingly.

Since facilities such as the planned spent nuclear fuel repository are unlike most other rock constructions there is a need to have a specific assessment and documentation of the methods that will be applied. A spent nuclear fuel repository differs in several ways from most other rock engineering projects in terms of the acting rock mechanics processes, in particular the great depth involved, the temperature loads exerted by the waste and the long-term perspectives, but also in terms of the extra ordinary requirements regarding traceability in the methods and analyses applied and the safety analyses procedures.

In Chapter 2 the expected mechanical processes that will take place in and around the facilities are briefly described. Some main concepts and important nomenclature used are introduced and defined. This chapter also summarizes the rock mechanics concerns, from the point of view of the long-term safety assessment, and how they motivate collection of the different mechanical parameters required.

In the subsequent Chapters 3 through 8, the methodology for each parameter required to characterize in situ rock stresses, intact rock, fractures, and rock mass properties is presented. Particular attention is given to methods and concepts that are new compared to the previous strategy reports for rock mechanics modelling (Hakami et al. 2002, Röshoff et al. 2002, Staub et al. 2002).

2 Rock mechanics concepts and nomenclature

Rock mechanics analysis in general may be summarized as the study of a system which consists of a certain number of components with certain surrounding initial and boundary conditions (Figure 2-1). This is the starting point of the process to be analysed. Stable initial conditions are assumed such that the system is at equilibrium at this stage (i.e., all forces and moments acting upon the system are balanced). Then some perturbation takes place due to the activity to be studied. The perturbation may be of different nature, often this is a mechanical perturbation, e.g. the excavation of a tunnel. But the perturbation may as well be an incoming wave, a change of water pressure in the fractures or a temperature change.

The prediction of the changes in the system, due to the perturbations, is the aim of all rock mechanics analysis, and many components must be described to get the right initial status for a certain rock mechanics system, as is illustrated in Figure 2-1. To determine what parameters are needed the expected perturbations must be known and how the situation can be simplified and described such that only the relevant and significant parameters are included.

In this Chapter 2 the aim is to give the motivation behind the primary data and parameters to be included in the models for the rock mechanics discipline, and to briefly explain how these parameters appear in the analyses of different mechanisms which are part of the layout, design and safety assessment for a deep repository of spent nuclear fuel.

First the Section 2.1 gives some general background to rock mechanics analysis and explains what the most expected situations are for SKB applications. In the following sections particular concepts and nomenclature of importance are explained, “Excavation damage zone” (Section 2.3) and “Spalling” (Section 2.4).

It is important to agree on what, in SKB framework, is meant by different terms and how these rock mechanics processes will play a role in the safety assessment of the repository. This Chapter 2 is aimed at presenting the reasons and motivation to efforts needed to collect the data required for each rock mechanics parameter in the future SDM, and therefore a summary of the rock mechanics concerns for the safety assessment is given in Section 2.5.

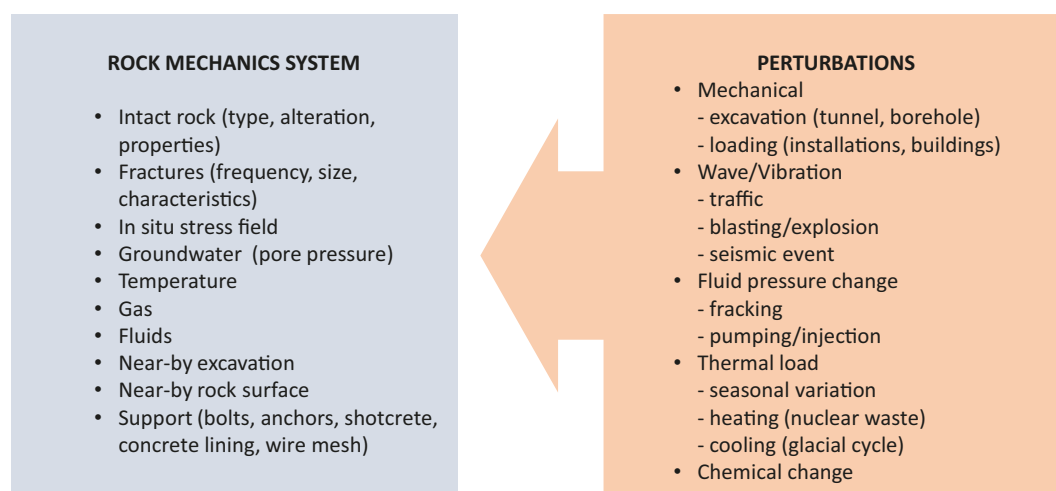


Figure 2-1. The general components of a rock mechanics analysis consist of a system where loads are initially in equilibrium and the subsequent analysis of the effects of perturbations.

2.1 Rock mechanics engineering and failure modes

Rock mechanics response and rock mass instability modes in general depend both on the rock mass fracturing state (i.e. in situ fracture network, see Section 2.6.1) and the relation between in situ stress and intact rock properties, which is illustrated in Figure 2-2. From what is known from previous descriptions of Forsmark area (SKB 2008) the deposition area is expected to be in the lower left or middle square categories in Figure 2-2, with fairly high stresses and quite few natural open fractures. Therefore, brittle failure around the openings is to be expected, *if* stresses are high enough. The extent of the brittle failure zone, away from the excavation boundary, depends on the stress level and on the bedrock properties.

The repository will be accessed by both vertical shafts and a ramp, which means that the lower stress situation is expected for the excavations closer to the rock surface. There, the failure mode is better described by the upper middle square in Figure 2-2, i.e. falling or sliding of blocks and wedges. Low stress may also occur in some part of the excavated boundaries at repository depth, as a result of the excavations, the so-called secondary stress field, which can give a mix of failure modes. Furthermore, some sections of the excavations of the facility may pass through deformation zones and in these locations the rock mass behaviour may be closer to the middle right square of Figure 2-2.

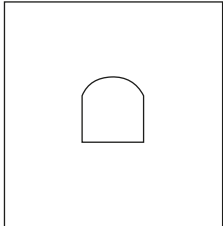
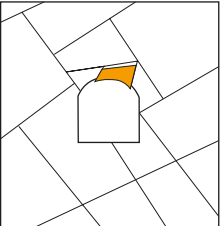
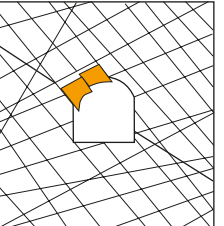
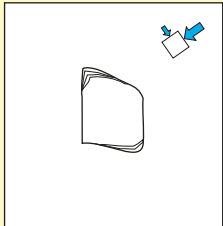
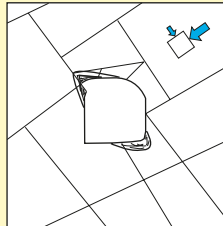
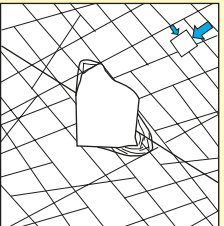
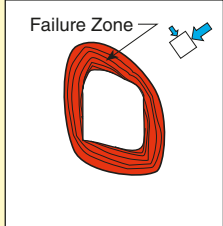
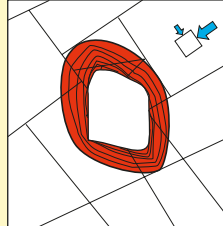
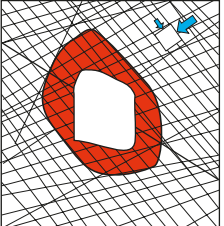
	Massive ($GSI > 75$)	Moderately Fractured ($50 > GSI > 75$)	Highly Fractured ($GSI < 50$)	
Low In-Situ Stress ($\sigma_1 / \sigma_c < 0.15$)	 Linear elastic response.	 Falling or sliding of blocks and wedges.	 Unravelling of blocks from the excavation surface.	$D_I < 0.4$ (± 0.1)
Intermediate In-Situ Stress ($0.15 > \sigma_1 / \sigma_c > 0.4$)	 Brittle failure adjacent to excavation boundary.	 Localized brittle failure of intact rock and movement of blocks.	 Localized brittle failure of intact rock and unravelling along discontinuities.	0.4 (± 0.1) $> D_I < 1.1$ (± 0.1)
High In-Situ Stress ($\sigma_1 / \sigma_c > 0.4$)	 Failure Zone Brittle failure around the excavation.	 Brittle failure of intact rock around the excavation and movement of blocks.	 Squeezing and swelling rocks. Elastic/plastic continuum.	$D_I > 1.1$ (± 0.1)

Figure 2-2. Modes of tunnel instability as a function of rock mass quality index (RMR) and the ratio of stress-to-strength around the tunnel (Andersson and Söderhäll 2001) (For notation details go to the source reference).

A division into the rock quality classes may be made, as shown in Figure 2-2, based on the empirical index RMR (Bieniawski 1989). Similarly a division into typical modes has been made using the index GSI (Hoek and Brown 1997), which is illustrated in Figure 2-3. The two figures show how the different combinations of rock conditions, i.e., in situ stress and fracturing, is expected to result in quite different response and instability patterns.

To enable discussion and prediction of the behaviour and all the types of failure modes that are possible in the repository, the rock must be described in a comprehensive way. The description will include the properties of the intact rock and the fracture properties separately, as well as the properties of the “rock mass”, which is the intact rock and fracture network together at a larger scale (Section 2.6.1 and 7.1).

The main basis for a reliable rock mechanics property description is a good geological understanding, including tectonics (the dynamics of structural geology) and seismological aspects. The quality of any rock mechanics description and subsequent predictions will rely on the correct division into rock domains and fracture domains, and the deformation zone modelling. This division is obtained from the deterministic geological modelling part of the site description, and an updated methodology for geological description is presented in DGMM (Hermanson and Petersson 2022). The properties within each domain will be described using stochastic methods which will be explained in Section 2.6.

Furthermore, the changing thermal load situation in the repository, because of the heat generated by the spent nuclear fuel, means that also the thermal properties of the bedrock at all scales must be described. The corresponding updated methodology for the thermal properties is, however, described in a separate methodology report, THPM1 (Back and Sundberg 2022).

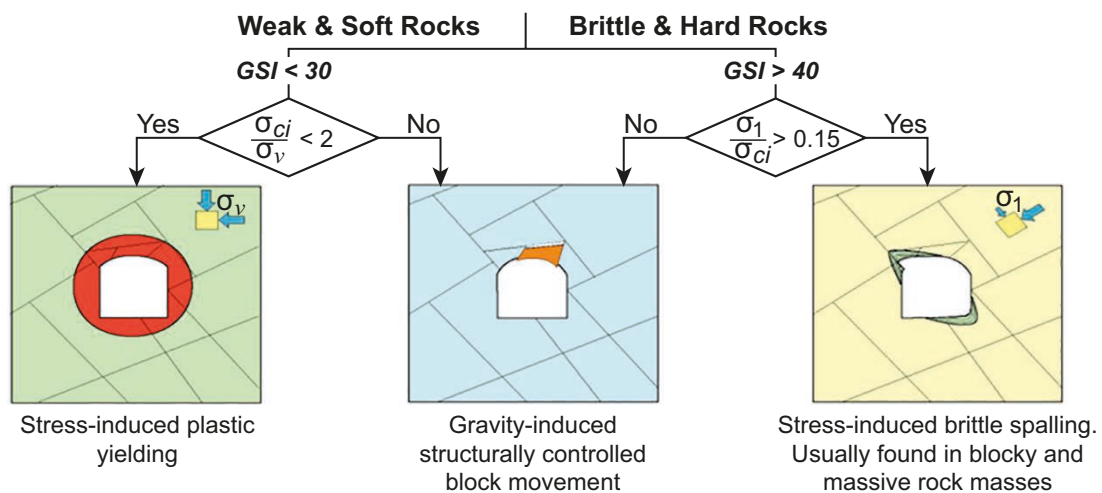


Figure 2-3. Instability modes based on rock quality (GSI), intact rock strength and stress level (Martin et al. 2003).

2.2 Scale aspects in rock mechanics

Any modelling will consider a certain scale, and for SKB purposes a nomenclature for different applicable scales has been developed to enable consistent terminology. These scales are qualitatively described and illustrated in Figure 2-4 and Table 2-1.

Depending on the discipline, different scales are more relevant than others. Rock mechanics modelling has been performed on all scales, from the modelling of tectonic stresses to the simulation of micro-mechanics processes in small rock samples. Table 2-2 is presented here to summarize and illustrate the variety of analyses and different scales that exists for rock mechanics modelling, giving a few examples of studies focused on issues explicitly related to the spent nuclear fuel repository. This wide range of objectives and scales is a characteristic that makes it necessary to use different modelling approaches for different purposes. As a consequence, a wide range of different property parameters are necessary to enable a complete rock mechanics site description.

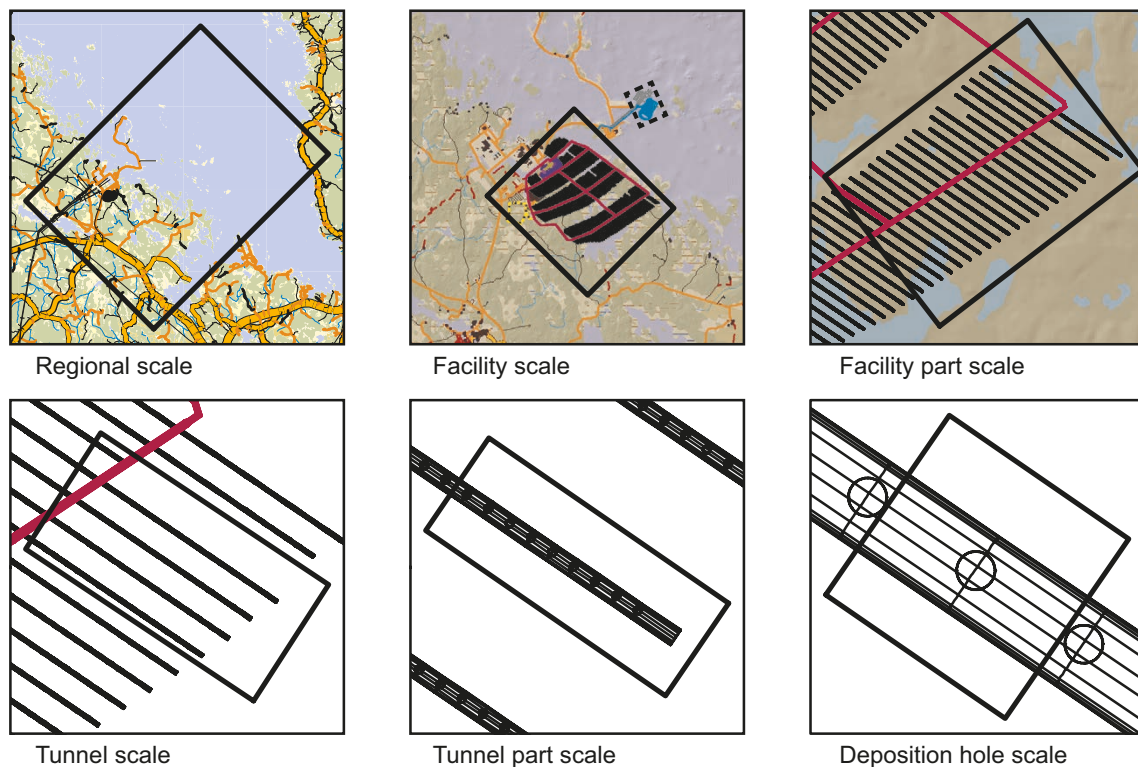


Figure 2-4. Illustration of model scales of radioactive wastes disposal facilities in the Forsmark area that may be found in the development of site descriptive models and site analyses.

Table 2-1. Model scales applicable to detailed site investigations in the Forsmark area. Modified from Winberg (2017).

Model scale	Approximate model dimensions
Continental scale	
National scale	1 500 km × 300 km × 5 km
Larger regional scale	50 km × 30 km × 2 km
Regional scale	165 km ² × 2.1 km
Facility scale	7 km ² × 1.2 km
Facility part scale	0.5 km × 0.9 km × 0.1 km
Tunnel scale	10 m × 15 m × 300 m
Tunnel part scale	20 m × 30 m × 40 m
Deposition hole scale	10 m × 15 m × 20 m
Excavation Damage Zone scale – Borehole scale	10 – 100 cm

Table 2-2. Modelling volumes/scales for quantitative modelling as defined in Table 2-1 and examples of rock mechanics modelling studies performed at different model scales.

Model scale	Example application	Numerical tool	Reference
Larger regional	Earthquake simulation	3DEC	(Hökmark et al. 2019)
	Glaciation load modelling		(Hökmark et al. 2010) (Lönnqvist and Hökmark 2015)
Regional	In situ stress field	3DEC	(Hakami et al. 2002) (Hakala et al. 2019)
Facility	T-M-modelling	FLAC ^{3D}	(Hakami and Olofsson 2000)
	DFN based rock mass properties	PyRockMassTool	(Davy et al. 2018) (Darcel et al. 2018) (Darcel et al. 2021)
Tunnel	Tunnel, long-term stability	3DEC	(Mas Ivars et al. 2014)
Tunnel part	LVDT-cell data analysis	FLAC ^{3D}	(Hakala et al. 2003, 2013)
	EDZ study	UDEC/3DEC	(Jonsson et al. 2009)
	Excavation induced fracture displacement	3DEC	(Mas Ivars et al. 2015)
Deposition hole scale	APSE (Äspö Pillar Stability Experiment) T-M model	Code_Bright	(Andersson 2007)
	APSE, Continuum/Discontinuum model	3DEC	(Mas Ivars 2020)
Borehole/ core scale	Spalling	PFC ^{2D}	(Potyondy and Cundall 2004)
		UDEC	(Lan et al. 2010)
	Fracture shear modelling	PFC ^{2D}	(Ríos Bayona 2019) (Ríos Bayona 2022) (Valli et al. 2016)
		3DEC	(Hakala 1999)
Ring dinking, Core dinking	FLAC ^{3D} 3DEC	(Sjöberg et al. 2007)	

2.3 Definition of excavation damage zone concepts

Within rock engineering it is common to refer to excavation damage or an excavation influenced zone, but these terms and similar others may have slightly different meaning, depending on the author and the application. The excavation damage zone is an important volume to be understood, as explained in the previous section, and therefore the concept and the terminology chosen to be used within the SKB site-descriptive modelling work is presented in the following paragraphs (see also Figure 2-5):

Excavation damage zone (EDZ) – The volume of rock around an excavation in which *new fractures have been created*, or sealed fractures have opened up, due to the excavation. A sealed fracture is a fracture with a developed tensile strength due to strong infilling material. A propagation of an existing fracture is also counted as a new fracture.

The EDZ may be caused by blasting *or* drilling *or* mechanical excavation *or* due to damage induced by redistribution of in situ stresses (or often a combination of these processes). The depth of EDZ will thus be largely dependent of the excavation method, the in situ stress field, the shape and orientation of the excavation and the fractures in the near-field with respect to the in situ stress field and the bedrock properties. The EDZ may also to some extent be time-dependent, i.e., the EDZ may develop progressively (and most often irreversibly) during some time after the excavation. The damage caused by additional thermal loading *after* excavation and deposition of nuclear waste is normally *not* included in the concept of EDZ. Read more about EDZ in Section 2.3.1

Spalling – The certain type of excavation damage that is caused by high in situ stresses, resulting in failure of *intact rock* at the excavation surface, is called spalling. If rock stresses are high enough spalling will occur around the excavation no matter the type, shape (cross section) or scale of the excavation. The additional spalling that may be caused by thermal loading *after* the excavation is normally not considered a part of the EDZ but should rather be denoted *thermal spalling*. Read more about spalling in Section 2.4.

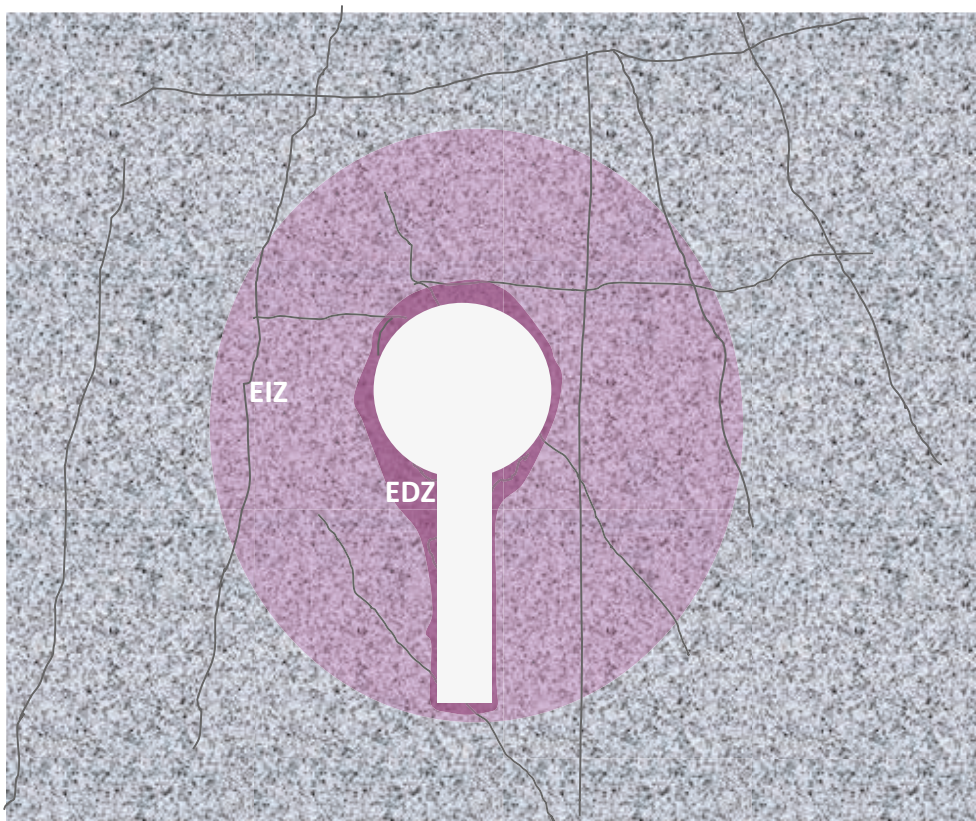


Figure 2-5. The Excavation Influenced Zone, EIZ, is the larger pink volume within which the natural fractures have opened or closed due to the excavation. The EIZ includes the much thinner Excavation Damage Zone, EDZ, which is defined as the volume where new fractures have been created or existing fractures propagated, due to the excavation. (See text.)

Excavation influenced zone (EIZ) – The volume of rock around an excavation in which the *pre-existing fractures* in the rock have experienced *movement* (opening, closure or shearing), due to the excavation process. (The EDZ thus becomes the inner part of the EIZ). In this influenced zone the fracture hydraulic conductivity, and hence the rock mass conductivity, may have decreased or increased due to the excavation, and it is conductivity change that is of main importance for the repository (Ericsson et al. 2015). Read more about the EIZ in Section 2.3.2.

None of the defined volumes, EIZ or EDZ, are expected to be evenly distributed around the periphery of an excavated rock cavern or tunnel. On the contrary, the geometric configuration of the fracture system, anisotropy in the “intact” rock properties, excavation geometry, blasting charge pattern and the anisotropic stress field will result in the EDZ and EIZ having clearly different depth at different points around the excavation.

2.3.1 EDZ – Excavation Damage Zone

Several researchers have studied the damage due to excavation in some respect. The nomenclature and definitions used have been similar but slightly different. Perras and Diederichs (2016) used the definitions shown in Figure 2-6. In comparison to the definition previously given in Figure 2-5 the three inner zones of Figure 2-6 can be regarded as a more detailed description or subdivision of the EDZ. For SKB purposes there is no absolute need for a more detailed separation of the damage zone because this zone is expected to be quite limited all together, and it is also indistinct and hard to separate the zone with fractures created by “construction” from natural fractures or those created by other types of loading.

Posiva selects the same division into EDZ and EIZ as in Figure 2-5 (Follin et al. 2021), and another example is Walton et al. (2015) who also uses the term Excavation Damage Zone. In the work by Ericsson et al. (2015) the term EDZ has however been defined as the volume in which “the hydromechanical and geochemical modifications induce significant changes in flow and transport properties”. In this research study the term “EDZ” was separated from the “EdZ”, the latter being excavation disturbed zone. These two definitions were mainly focusing on the hydraulic properties, but the formation of new fractures will induce significant changes in flow and transport properties, so in this sense the two different EDZ definitions (the one in Ericsson et al. (2015) and the one in Figure 2-5) are not in conflict. The EdZ in Ericsson et al. (2015) is closer to what is in Figure 2-5 denoted EIZ (see next section).

A comprehensive summary of the character of the EDZ and the factors influencing EDZ, in the context of spent nuclear fuel repository, was made by Hudson et al. (2008), see Figure 2-7. It is notable that, apart from safety analysis, the EDZ concept is of importance to several rock engineering issues that are major parts of the design and construction process for the repository, such as the selection of methods for excavation and the geometry of excavations.

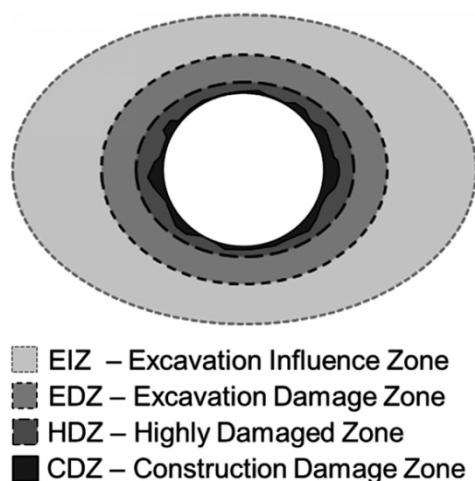


Figure 2-6. Definition of different damage zones around an excavated opening, according to Perras and Diederichs (2016).

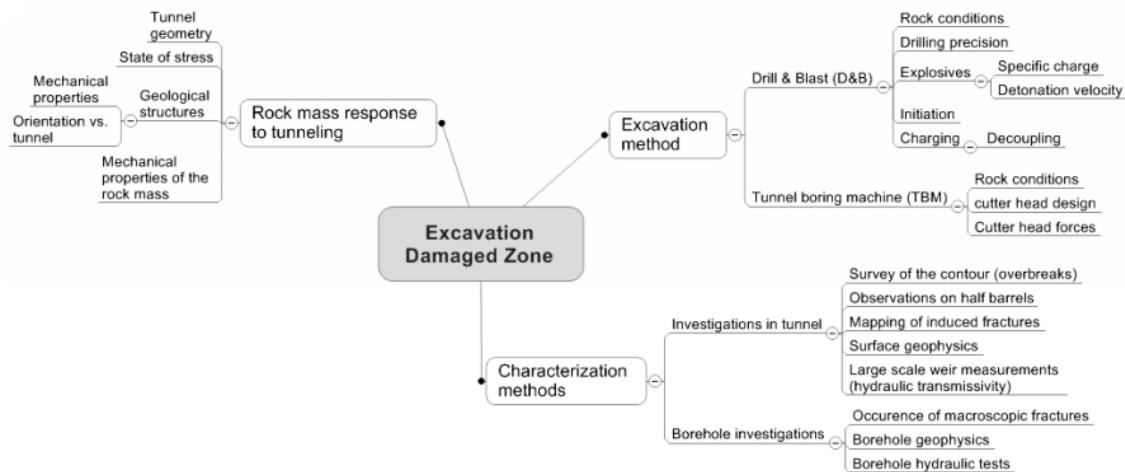


Figure 2-7. Summary of factors relating EDZ to the rock mass response to tunnelling, the excavation method and the characterization methods. (Hudson et al. 2008).

2.3.2 EIZ – Excavation Influence Zone

As presented above, the term EIZ is preferred (over EdZ) because the latter is easily confused with the EDZ and also the notation “influenced” in EIZ properly explains its meaning. Excavation influenced zone, using the definition given above, is a zone which has a larger volume than the damage zone, because even the rock which is not really damaged will, elastically or non-elastically, respond to the changes in stresses that will inevitably come with any excavated underground opening. In particular, for the future spent nuclear fuel repository located at large depth, the *in situ* stress magnitudes will be significant and thus the changes close to the excavation considerable. The new rock surfaces created during excavation will have zero stresses in the direction normal to the surface, and the stress field will be influenced to a distance about three times the radius out from the excavation wall, assuming linear and homogeneous behaviour. Depending on the fracture orientation with respect to the stress field in the EIZ, the fracture will close, open or shear because of the excavation. Normally fractures at large depth in hard brittle rock have a high stiffness, such that the movements to be expected here are very small. Nonetheless, the movement may cause measurable effects on groundwater flow and transport in the EIZ.

Although practically quite challenging, a comprehensive experiment was carried out in Äspö Hard Rock Laboratory to specifically study the hydraulic properties of EDZ and EIZ (Ericsson et al. 2015, 2018). Direct hydraulic measurements were conducted in boreholes drilled in the floor of a drill and blast tunnel, with saturated conditions. The results from this experiment called RESKONTR are extensive, including also geophysical studies of different kinds. The example results shown in Figure 2-8 provide good evidence that the coupling between section transmissivity (sealed off sections) and EDZ does exist. Comparing the probability plot result from section at 0–10 cm distance (from the excavation boundary surface) to the results from 60 cm to the end of the boreholes reveals that the slopes of the probability curves are much steeper at 60 cm distance, i.e., the transmissivity is not so varied and is also never as high as it is close to the surface. The highest transmissivity at 60 cm distance to the end of borehole was 10^{-8} m²/s while it was 10^{-4} m²/s at 0–10 cm distance, i.e., four orders of magnitude larger. A consistent and gradual trend can also be seen for the sections between 10 and 60 cm distance. Figure 2-8 further demonstrates how the EDZ and hydraulic conditions are dependent on the blasting performed (compare column charge and bottom charge results).

Since the transmissivity governs the ground water flow and solute transport from the deposition hole up to the biosphere, transmissivity in the bedrock close to the excavations is one of the factors that determine the long-term safety. This is the reason why understanding and predicting the EIZ in general, but the EDZ in particular, is subject to major attention in the SKB safety assessment.

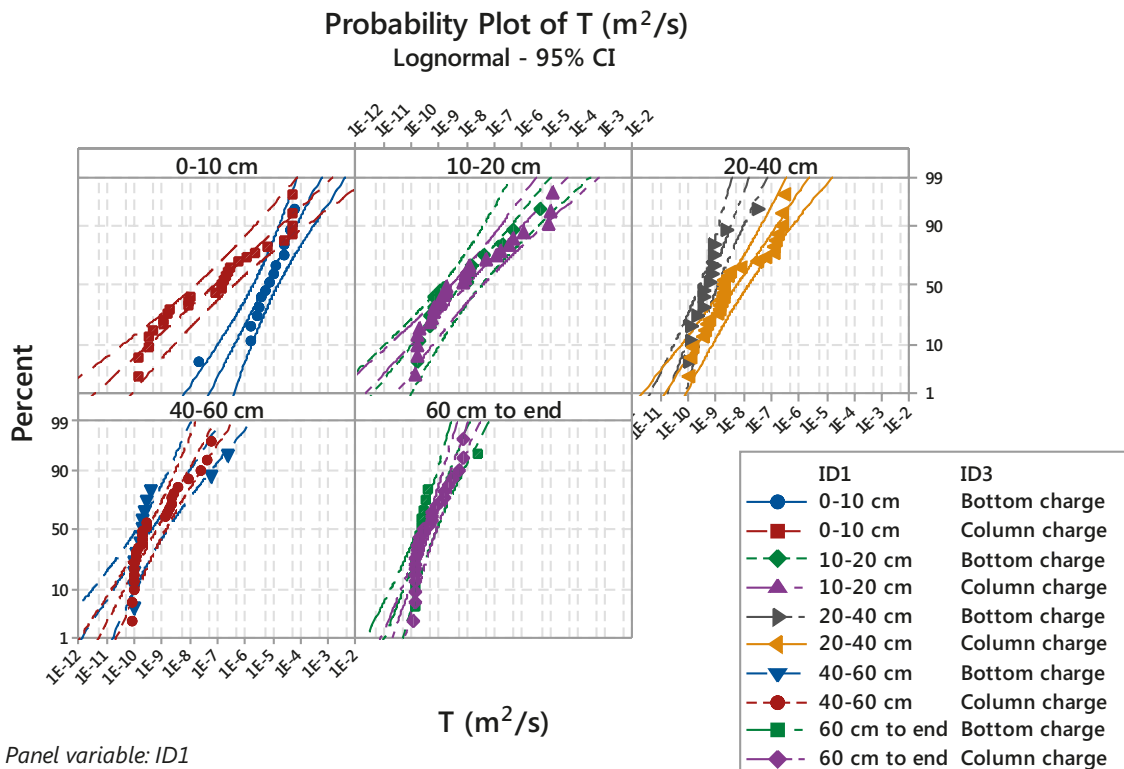


Figure 2-8. Probability plots of the interpreted transmissivity values from hydraulic test conducted in the different sections, at different distances from the floor of the excavation, of the influenced zone around the excavation. Also note the differences between bottom charge and column charge. Figure from Ericsson et al. (2015).

The excavation damage or influence zone should not be confused with the concept called “skin effect”, although the skin effect is also referring to the influence from an excavation. The term “skin effect” is only used with reference to flow studies, not purely mechanical studies, and it is a term used for the often-observed phenomenon that the flow into a tunnel is less than what would be expected only based on the permeability measured in boreholes at the same location.

Kröhn and Lanyon (2016) summarize the different processes that could be the explanation of this permeability reduction, the skin effect, as being one or possibly a combination of the following:

- a) Mechanical processes related to excavation/drilling: stress redistribution and shear, mechanical clogging.
- b) Hydraulic and multi-phase flow processes: degassing, desaturation, turbulent flow in channels.
- c) Effects of heterogeneity and scaling: channel connectivity.
- d) Other flow, chemical, biological or coupled Thermo-Hydro-Mechanical (THM) processes. E.g. fracture closure due to thermal expansion or long-term clogging due to chemical disequilibrium.

It may be noted that two of these processes are mechanical in nature, and this further underline the need for an increased knowledge and prediction capability regarding the excavation influence zone. It also demonstrates well how interconnected the different geosciences often are and the level of complexity of the processes that must be understood to explain a seemingly simple observation as decreasing inflow into a tunnel. Figure 2-9 shows the example from the access tunnel to SFR in Forsmark where the inflow has decreased from the time the tunnel was built until now, and the explanation to the observation is still under discussion.

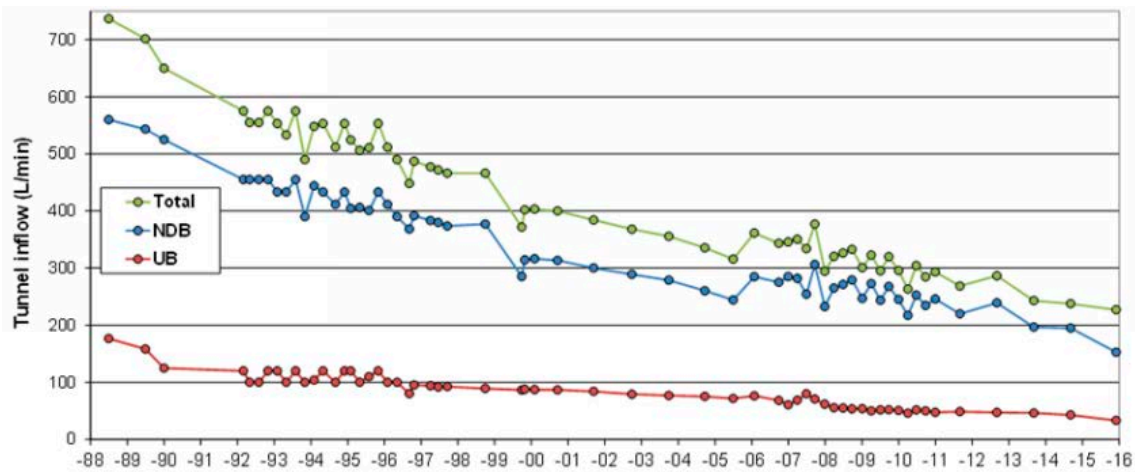


Figure 2-9. Decline in inflow to the SFR from first operation to 2016. NDB: inflow to access tunnel and lower construction tunnel. UB: inflow to rock caverns and other tunnels. (Kröhn and Lanyon 2016).

Another study exemplifying the complexity of the processes in the excavation influence zone is the study by Mas Ivars (2020). In this study, the stress change due to the excavation was analysed, using the actual excavated geometries and some mapped fractures. The stress redistribution and the consequent fracture displacements induced by the excavation of a destressing slot were simulated and could be compared to what was actually observed and measured at the site (Mas Ivars 2005). The results demonstrate the fact that the natural fractures intersecting the excavation will be dominating the “picture” and the properties in the excavation influence zone, and that influence from excavation cannot be neglected. This type of analyses requires a complete set of rock mechanics parameters: estimation of the stress field, the rock mass stiffness, the fracture stiffness and strength and the hydro-mechanical properties of the fractures.

2.4 Spalling

2.4.1 Observations of spalling

Spalling is a phenomenon that has been observed around openings of different sizes and located in different geological settings. Fairly close to the Forsmark conditions, and of particular interest, is the spalling observed at the Canadian underground rock laboratory, URL. At the URL the fracture frequency was extremely low in the area of experiments, and the stress levels at about 420 m depth, the level of the Mine-by Experiment, were high enough to produce a consistent spalling along a test tunnel. The final shape of the tunnel when the tunnel opening had attained a stable shape can be seen in Figure 2-10. Note that the spalling will take place on opposite sides, in the roof and the floor, since the horizontal stress magnitudes are much higher than the vertical stress and the spalling conditions therefore arise in those two opposite sides. The typical spalling process is illustrated further in Figure 2-11 with the photo of one of the created rock fragments, also from the URL. The diameter of the Mine-by Experiment tunnel was 3.5 m.

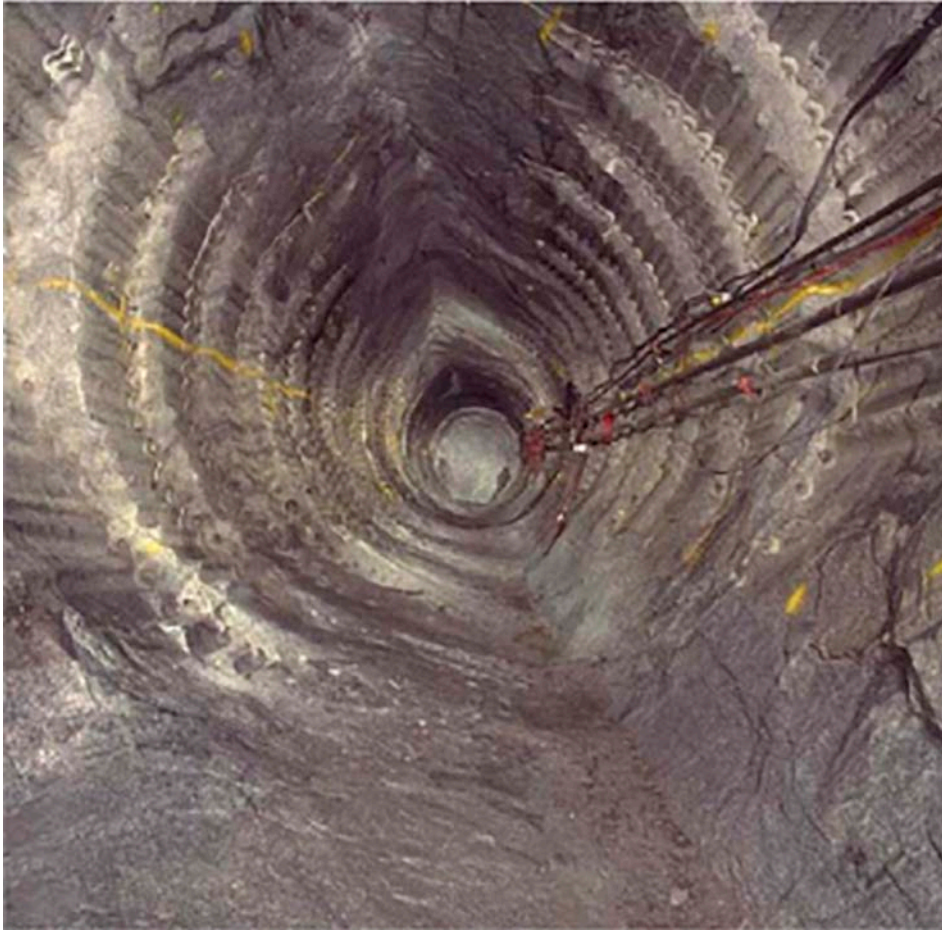


Figure 2-10. Mine-by Experiment test tunnel at AECL underground research laboratory (URL) showing final V-shaped spalled notches in the crown and invert. The tunnel theoretical diameter is 3.5 m (Read 2004).

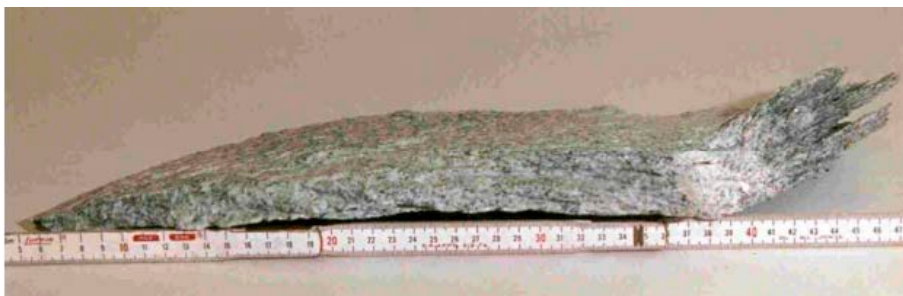


Figure 2-11. Typical slab of rock detached from the Mine-by Experiment tunnel crown during failure process. Note the curved shape of the slab (Read 2004). The high compressive stresses form, in a consistent direction due to the in situ stress, initiates the cracks and they propagate to form the slabs, one after the other until a stable shape of the opening is obtained.

The next example of spalling, shown in Figure 2-12, is from the Äspö Pillar Stability Experiment (APSE) at the SKB Äspö Hard Rock Laboratory (Andersson 2007). This involves a vertical borehole with smaller diameter (1.75 m) compared to the Mine-by Experiment tunnel at the URL. In this experiment the layout was designed to achieve as high stresses as possible using two vertical boreholes drilled separated by a short distance giving a highly stressed pillar between the holes. The stress in the pillar was still not high enough to produce extensive spalling except close to the tunnel floor. When heating the area of the pillar and the borehole, the stress increased to a level that caused spalling also deeper down in the borehole walls, cf Figure 2-12.

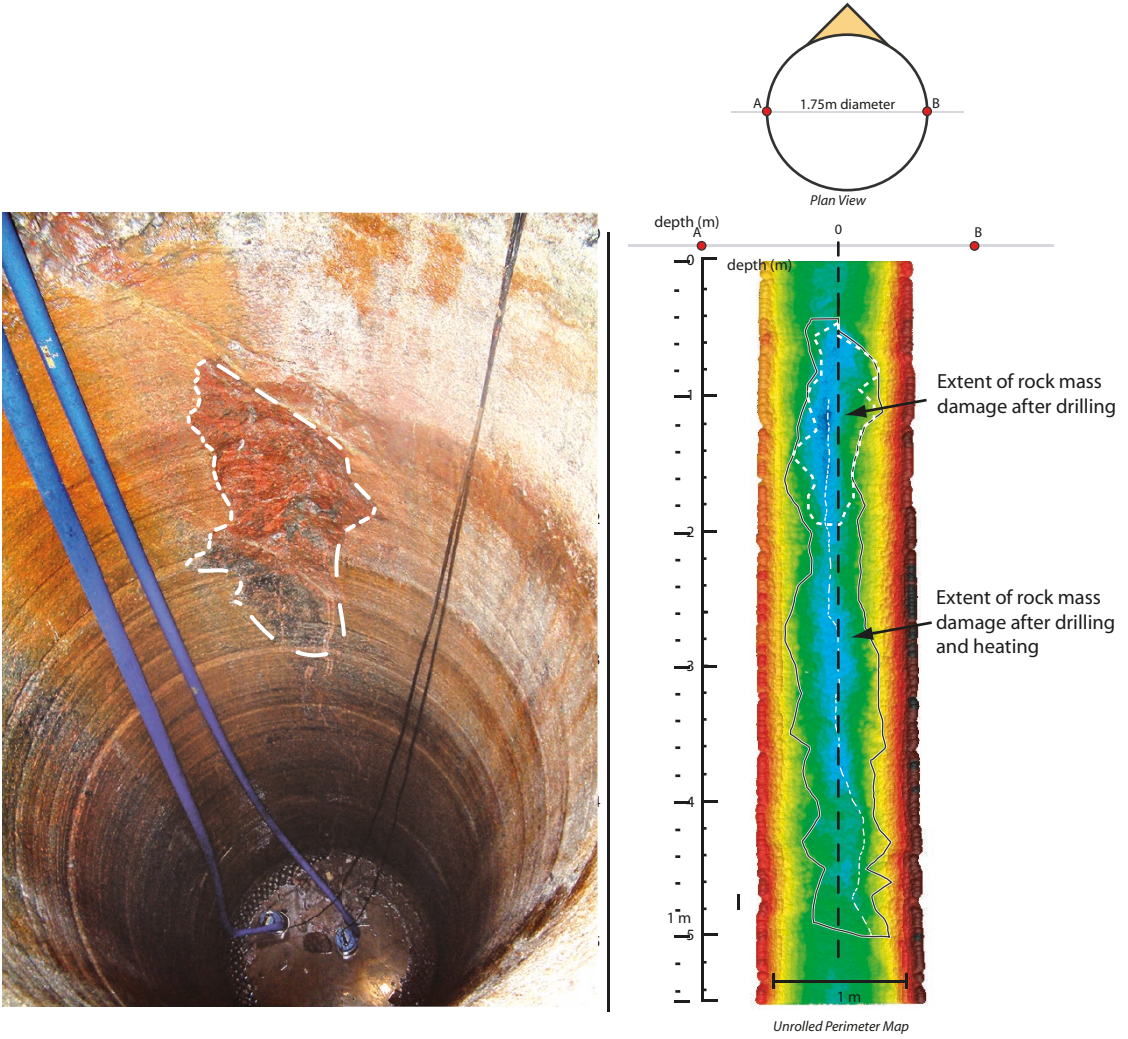


Figure 2-12. Photograph of APSE experiment borehole wall. The rock volume that yielded during the excavation is marked with white dotted line. The total yielded area after heating, derived from laser scanning of the wall, is shown to the right. The spalled area increased down about 5 m in the vertically oriented borehole (Andersson 2007).

The following two examples in Figure 2-13 are boreholes also from the URL but smaller in diameter (1.24 m and 0.6 m). It may be noted that the spalled volume also becomes smaller, and that the depth of spalling is less, while the ratio between the spalling depth and the diameter of excavations is roughly the same. A common phenomenon observed, when vertical boreholes are drilled from a tunnel floor with high stresses, is that the spalling starts to occur at a short distance from the floor and stops at a certain depth from the tunnel floor because the stress concentration caused by the tunnel disappears (Figure 2-14). The reason for not having spalling in the very beginning of the hole is probably that the stresses are already released in the floor due to previous excavation damage and movements close to the excavation.

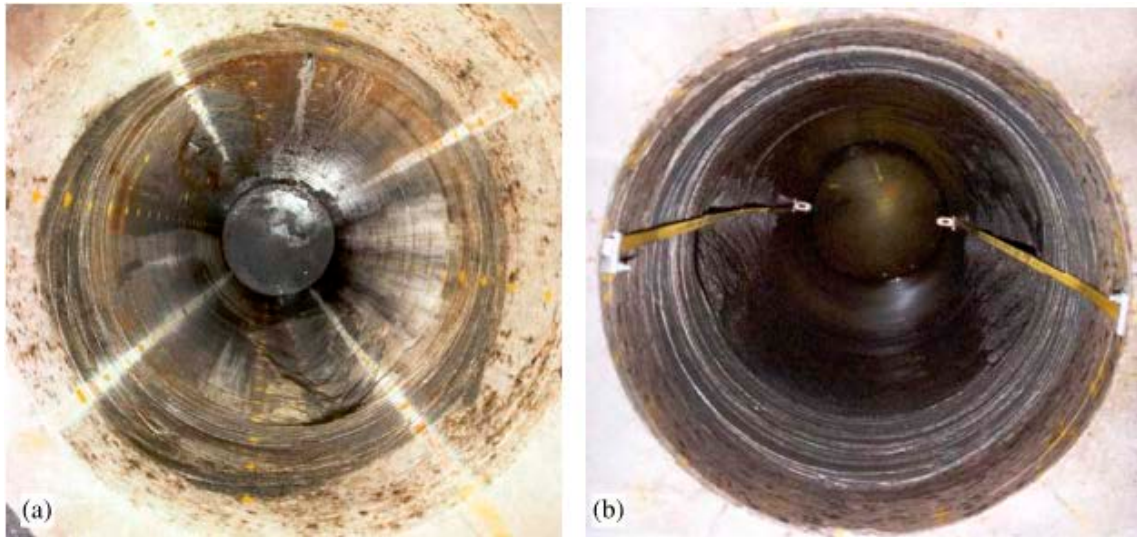


Figure 2-13. Spalling in a borehole of 1.24 m diameter (left) and in a borehole with 600 mm diameter. Both from the AECL underground research laboratory, URL (Read 2004).

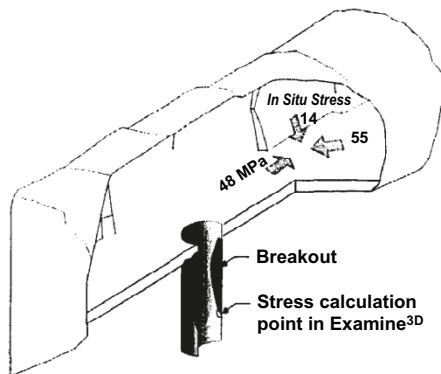


Figure 2-14. Illustration of the three-dimensional geometry used to calculate the stress at the initiation of failure in the borehole wall. Such boreholes of different diameters were drilled in the floor of tunnels at the URL (Read and Martin 1996).

The Counterforce Applied to Prevent Spalling project, CAPS (Glamheden et al. 2010), was conducted by SKB at the Äspö Hard Rock Laboratory at a similar diameter. Spalling was induced in several ca 490 mm diameter boreholes, this time using heaters inside the boreholes to increase the stress field. The result from one of the holes is shown in Figure 2-15, with one photo from either side of the same borehole. It is remarkable how similar the spalling appearance is on the two opposite sides. The UCS of the rock in the test area has a mean value of 227 MPa (span 170–294 MPa) and the stress calculated to prevail at failure was around 120 MPa.

The next example of spalling observation is from a laboratory experiment directly aimed at understanding spalling in hard brittle rock conducted by Jacobsson et al. (2018). The rock type tested was Äspö diorite sampled at Äspö Hard Rock Laboratory. The geometry of the axially loaded sample is seen in Figure 2-16. The rock surface that was intended to fail was located in the centre of the concave surface with a 225 mm curve radius that was machined out of a large cylindrical core sample. This laboratory experiment would thus correspond to an in situ borehole test with a 450 mm diameter borehole. The size and the typical shape of the spalled fragments that were induced in this experiment are shown in Figure 2-17.

Spalling failure can also occur in smaller diameter boreholes, but these rock failures (or fallouts) are normally called boreholes breakouts. The breakouts can be used in the stress modelling. This is developed further in Section 3.2.3.

If stress levels at hole wall failure for these different examples with different scales are compiled, the result is the diagram in Figure 2-18. In this diagram, modified from Read (2004), showing URL results, the results from the three SKB studies are added. There is a general agreement between results showing that the spalling stress level (i.e., the ratio of stress at spalling to the UCS of the rock type) decreases with hole size from the laboratory/borehole scale to the size of deposition holes. The newly added SKB data fit well with URL results. The results of Figure 2-18 are sufficient to demonstrate that the scale is a factor that should be part of the prediction for spalling. Compared with the previous strategy for site description, the strategy of this updated methodology is to also include some quantitative measures to help explaining the scale effect and further supporting the prediction of spalling around deposition tunnels and deposition holes.



Figure 2-15. Example of spalling developed in a ca 490 mm diameter borehole in an experiment (CAPS) with applied thermal loading at the Äspö Hard Rock Laboratory. The two photographs are from the same borehole showing the two opposite sides of the hole. This occurrence is typical for the spalling phenomenon because the stress increase develops on both sides of the created opening, with the orientation depending on the direction of the major stress (Glamheden et al. 2010).

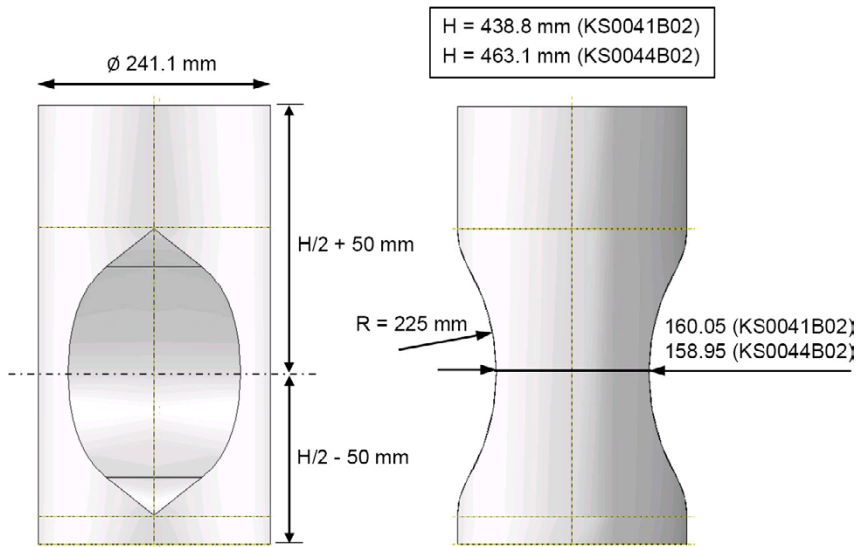


Figure 2-16. The sample set up for compression laboratory test of large sample in hard rock for spalling studies. The rock type was Åspö Diorite (Jacobsson et al. 2018).

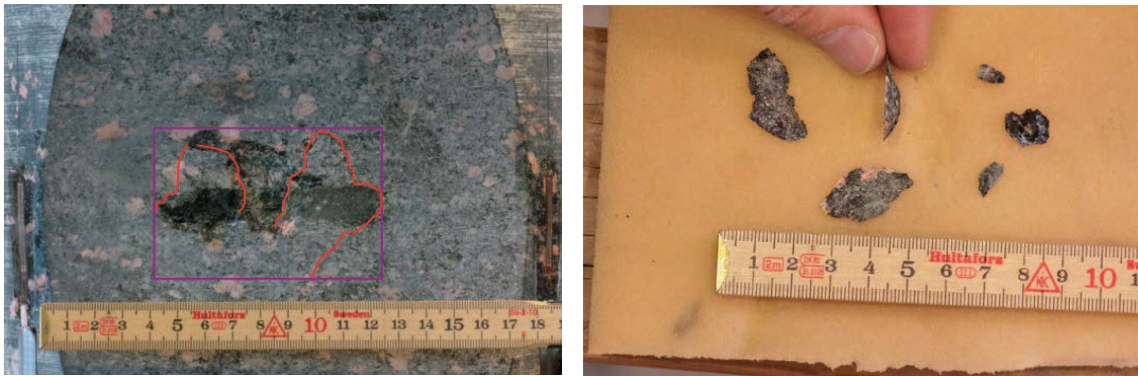


Figure 2-17. Photo of the failed surface of the load experiment shown in Figure 2-16. The pieces that have fallen of the surface are seen to the right (Jacobsson et al. 2018).

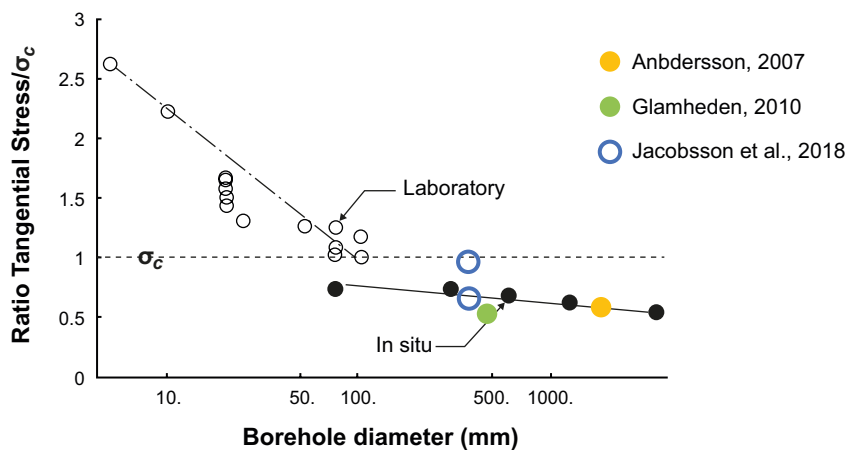


Figure 2-18. Ratio of the calculated tangential stress to σ_c (= UCS) at which spalling/breakout initiates for various borehole diameters. The white symbols are results on Lac du Bonnet granite from laboratory (URL) and the black symbols are from the same rock but in situ experiments. The approximately added (in this report) coloured symbols are from SKB laboratory and field scale results. (Note that the x-axis has log-scale) Based on figure from Read and Martin (1996).

2.4.2 Theoretical models for spalling

Spalling is a mechanism where intact stiff rock around an excavated opening fails, i.e., new fractures are created, and spalling is therefore a certain kind of excavation damage zone (EDZ). Spalling involves fractures created by high rock stresses (i.e. not associated with blasting) and natural fractures are not primarily involved in this phenomenon. Corkum et al. (2012) has explained a way to conceptually model the changes in the rock mass when it is fracturing due to spalling using a continuum modelling approach, as illustrated in Figure 2-19. The spalling process, taking place in an intact rock volume, starts with minor fracture initiation, and these tensile fractures will later coalesce while the rock loses its tensile strength, and this can be modelled as a loss of cohesion in the Mohr-Coulomb material model. When the fractures are all connected the only strength in the rock volume comes from the friction on the fracture planes when they are shearing under a certain normal load.

Saceanu et al. (2022) uses the fracture mechanics approach to analyse spalling. In their work the fractures are represented discretely using smooth parametric surfaces and their growth is evaluated at each fracture tip separately. The three modal stress intensity factors are calculated, which represent the energy necessary to deform the crack, and they determine the extent and orientation of growth at the tips of every fracture. In their model, multiple fractures of different sizes and evolving shapes grow along the paths determined by the local stress state at their tips, with growth being influenced by the stress distribution. The finite element method is used to compute the deformation in the system, considering the physical properties of both the intact rock and the fracture surfaces. The modelling approach was validated by comparing simulated fracture patterns against those observed in the AECL Underground Rock Laboratory Mine-By Tunnel Experiment (Figure 2-20).

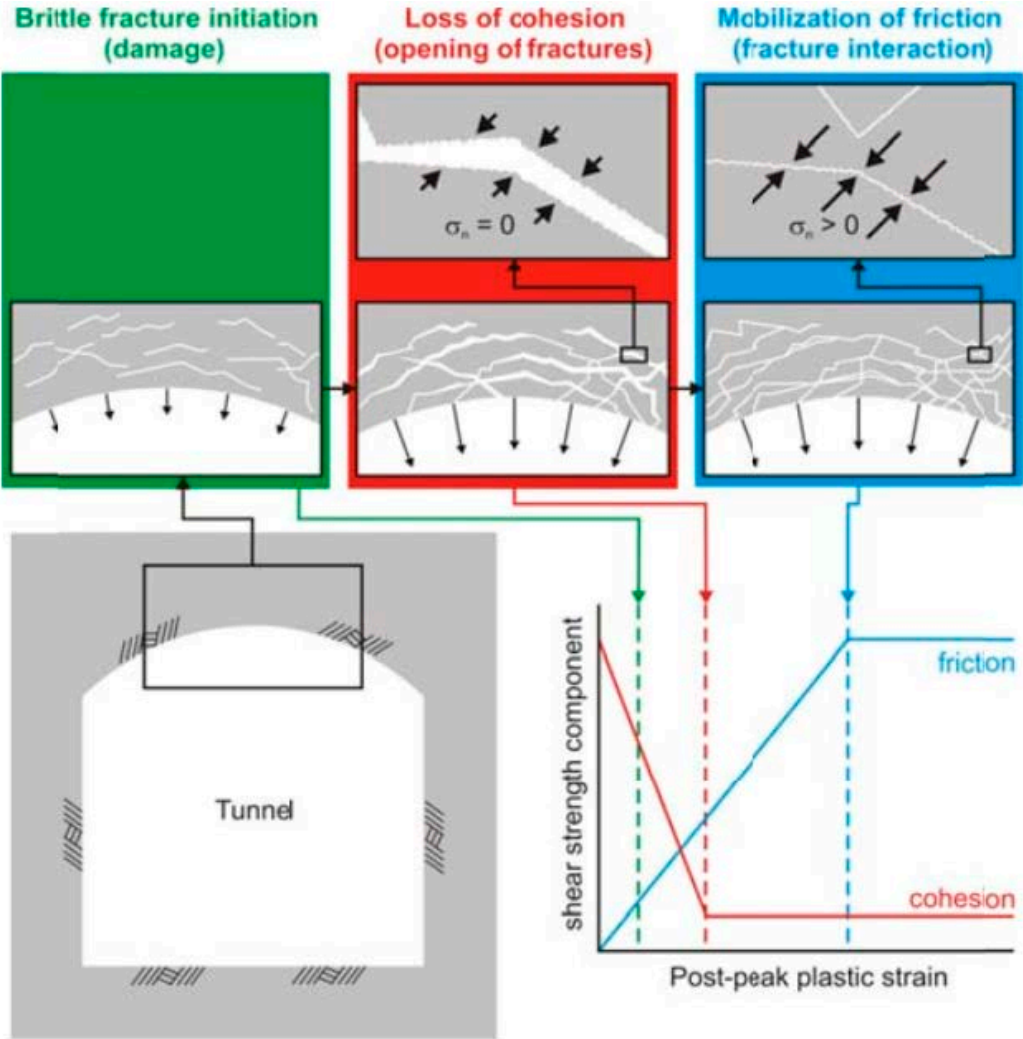


Figure 2-19. Illustration of a model for the process of spalling, where the behaviour is first governed by cohesion loss and thereafter the by mobilization of friction. (Corkum et al. 2012).

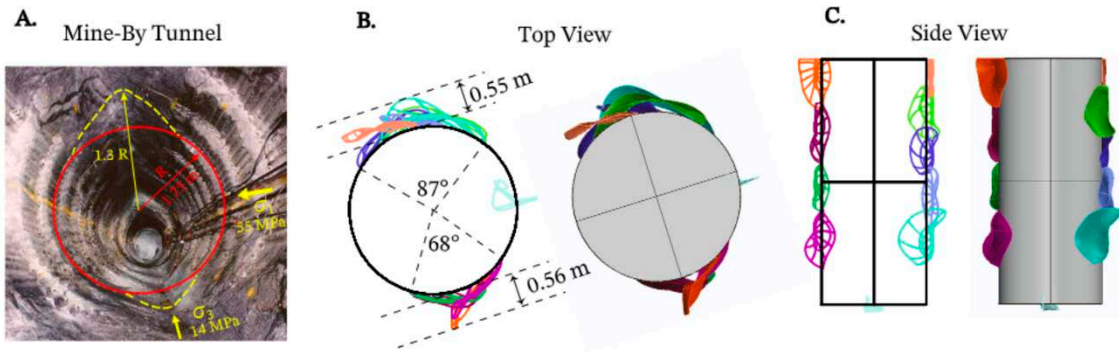


Figure 2-20. A numerical simulation of the Mine-by Experiment (described in Section 2.4.1) using a fracture mechanics approach. a) Photo of actual tunnel. b) Results from simulation with the propagated fractures in the numerical model. c) The same result in side view where the non-planar shape of fractures due to their re-orientation during propagation can be noted (Saceanu et al. 2022).

Another way of numerically analysing the spalling phenomena is to directly mimic the microstructure of the material and applying a discontinuum numerical model. In such models the rock is considered as a composite material with bonded grains of different minerals, for example (Potyondy and Cundall 2004) using PFC (Particle Flow Code, (Itasca 2017 or Lan et al. 2010) using UDEC (Universal Discrete Element Code, (Itasca 2016)). In these models the failure mainly takes place in the weaker bonds between the stronger grains. To find the most appropriate numerical material model for a certain rock type they must be calibrated against laboratory results such as those from a uniaxial compressive strength test, see example in Figure 2-21 from Lan et al. (2010).

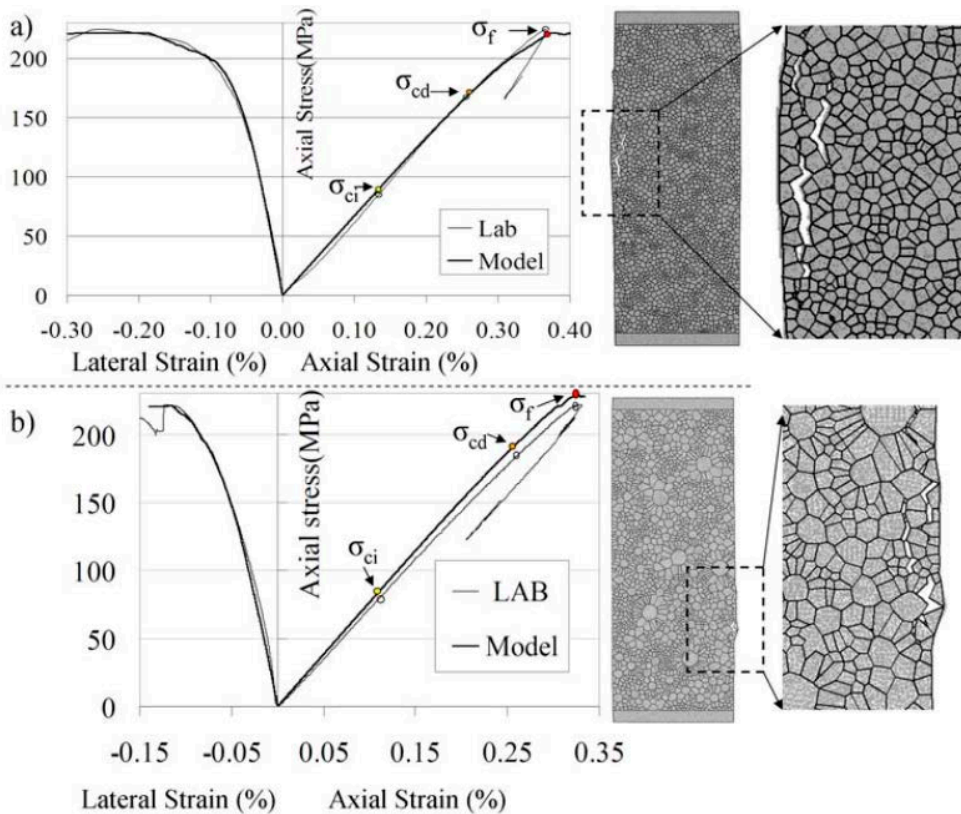


Figure 2-21. Calibrated stress strain response from GBM-UDEC modelling together with lab test data for (a) Lac de Bonnet granite and (b) Aspö Diorite. The drawings on the right show the damage pattern of the 2D discontinuum model specimen (Lan et al. 2010).

In terms of material models and theoretical prediction tools for the spalling phenomenon there is still no single obvious approach or strategy, since there is scarcity of data to validate the failure models, even if different attempts have been made. The SKB strategy for the safety assessment has so far been to mainly rely on empirical correlations between direct observations of spalling at a larger scale and measured laboratory strength on corresponding rock core samples, combined with estimates of prevailing stresses at the time of observed spalling. Examples of observations of spalling were given in Section 2.4.1 and a closer account of the factors involved in empirical spalling predictions is given in Section 2.4.3.

2.4.3 Strategies for improved spalling prediction

As already understood from previous sections the prediction of spalling in deposition holes and deposition tunnels is not a simple task. It is not possible to directly study the actual situation that SKB want to predict in full scale field experiments; at least not until the construction is down at the repository level. However, there is a desire to make design plans and predictions earlier, with a minimized uncertainty.

Prediction of spalling in the repository excavations will depend on three circumstances where the laboratory rock test situation differs from the real situation: (1) core samples are cylinders while excavations are holes, (2) the scale of laboratory samples is centimetres while the scale of excavations are metres and (3) the time scale of laboratory tests is minutes while the time before deposition holes are filled with canister and buffer material is years (and many thousands of years if the whole period after canister and buffer emplacement is considered).

With regards to the first circumstance, the fracturing in the rock occurs close to a surface of different shape, in the case of laboratory sample and hole, respectively. The former failing surface is convex, and the latter is concave. This induces different confinement situations for the two cases and the mechanism and strength of these different rock surfaces will not be the same. A small hole in a loaded rock block will be stronger than a small loaded cylindrical sample having the same diameter as the hole. At least this seems to be true for the smaller diameter cases that have been studied in laboratories (Figure 2-18). For small diameter cases the grain size is similar to the scale of the failing area and it is reasonable that the grains will strongly influence and inhibit the overall failure process for these cases. Nordlund et al. (2014) showed that the thermally spalled chips created in their laboratory experiments were typically of the same thickness as the rock type grain size, which is understandable since the grain boundaries are generally weaker than the grains of the rock.

A second factor to be understood is therefore the scale effect on strength. In the future site description, the plan is to include also some estimates of the size effects on the strength parameters. This will support any prediction or analysis where the starting point is observations at different scales (see also Section 2.6.2).

Figure 2-22 presents three of the factors that are involved in explaining different stress levels at the onset of spalling, for different situations. In the scheme examples are given for small- and large-scale loading on cylindrical sample shape (convex surface) and rock with holes (concave surface). The different situations further involve short or long-time scales. Naturally, there are cases in between these as well and the amount of data available varies greatly between rock types and sites. Some situations are almost impossible to study in laboratory experiments, for example large scale cylindrical sample loading at short time scale. In the literature there are some examples of ca 200 mm diameter samples, but for strong rock the total load needed to initiate failure is too high for the loading machines. In field tests the natural load can be used but the drawback of in situ tests is that the actual load is not well known and has often to be calculated based on different assumptions.

In Figure 2-23 a scheme based on Figure 2-22 illustrates how predictions of spalling strength are often based on small scale laboratory data such as UCS. To obtain the spalling strength in any other case than the laboratory test itself, UCS is often multiplied with some given factor. (Note that the quantified factors given in the figure are indicative judgements only.) The red arrow is the approach taken in the current safety assessment (using the crack initiation stress described as a factor of the UCS for large-scale long-term spalling strength). The spalling strength for a large-scale excavation is estimated to be about 57 % of the UCS, due to the summed-up influence of shape, scale and time differences between the situations. This factor is chosen based on experimental results at URL Mine-by Experiment and Äspö Pillar Stability Experiment at Äspö Hard Rock Laboratory (Martin 2005).

	Minutes		> Days	
cm scale	 Cylinder Uniaxial compressive laboratory tests	 Hole Borehole breakouts in field or hollow sample laboratory tests	 Cylinder Laboratory creep tests	 Hole Long term stability of boreholes in field
m scale	 Cylinder (Large sample laboratory tests) Excavation of rock pillars, immediate effects	 Hole (Large hole laboratory tests) Tunnel and shaft excavations, immediate effects	 Cylinder Long term rock pillar stability (e.g. in room and pillar mines)	 Hole Long term shaft, tunnel and deposition hole stability

Figure 2-22. Summary of main factors involved in spalling prediction. The SDM will describe the standard test data that represent the upper left situation while the situation that is to be predicted is described in the lower right corner. (In this diagram assuming homogeneous rock without open or sealed fractures. In a real case this may not be valid since such inhomogeneities further contribute to the complexity of the prediction. The irregular geometry of the rock surface in real excavations is also a factor to consider).

	Minutes		> Days	
cm scale	 Cylinder UCS = 1	 Hole X = ca 1.3	 Cylinder X = ca 0.8	 Hole X = ca 1
m scale	 Cylinder X = ca 0.8	 Hole X = ca 1	 Cylinder X = ca 0.5	 Hole X = ca 0.6

Figure 2-23. Scheme, based on Figure 2-22, illustrating how the empirical spalling strength prediction is based on small scale laboratory data such as UCS. To arrive at the spalling strength estimates for the other cases the UCS should be multiplied with the factor X given. Note that the factor numbers are here indicative judgements only.

When analysing the strength for large scale excavations it is important to recognize the influence of the boundary geometry. In the diagram it is only included in the difference in size but, in the real case, the large “hole” of a tunnel size also does not have the same perfectly smooth periphery as a drill hole. This issue was pointed out by Cai and Kaiser (2014) and they also performed numerical analyses to demonstrate how important it is that oversimplified geometries do not mislead our interpretations or the understanding of rock strength parameters (Figure 2-24). By including the irregularities of the periphery of the opening, the peak yielding strength of the rock does not have to be lower than $0.8 \times \text{UCS}$ to match the observed spalling at the URL Mine-by Experiment, while the same type of analyses with smooth excavation periphery give an “apparent strength” of about $0.65 \times \text{UCS}$ (Cai and Kaiser 2014).

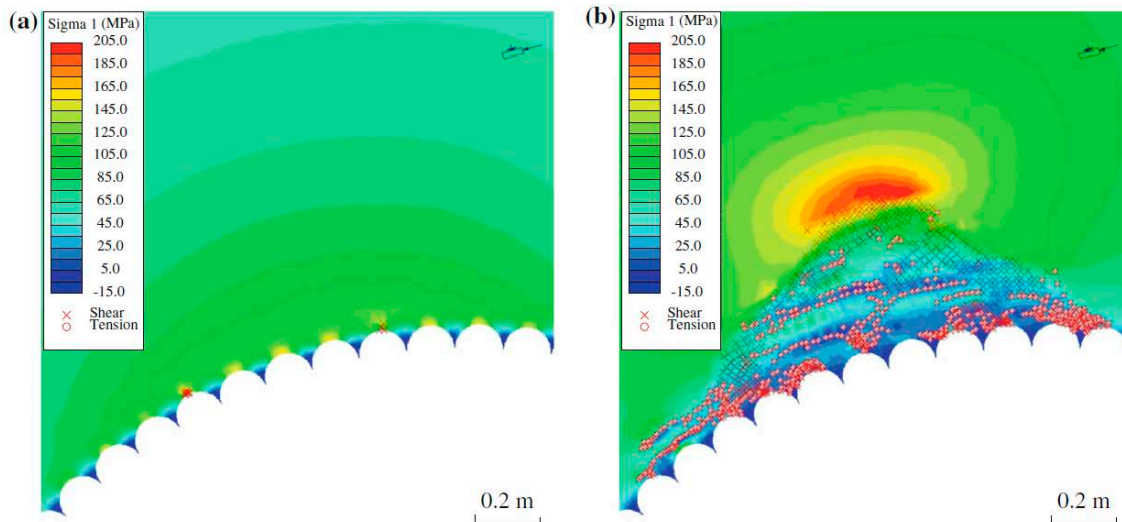


Figure 2-24. Result from numerical simulation of case with uneven tunnel periphery (figure shows only a part of the model at the failing area in the roof). a) Stage of simulation when the first yielded elements appear due to the “stress raisers” (boundary irregularities). b) Later stage when the spalling process has continued until a wedge-shaped yielded area is developed. The confined part directly inside the wedge can sustain high maximum principal stress up to the peak rock strength assigned, about 175 MPa (Cai and Kaiser 2014).

If, in coming safety analyses, it is possible to arrive at a comparable spalling prediction using several different model paths (in the Figure 2-23 diagram) this would clearly increase the certainty of the prediction. This may be achieved by using additional site knowledge and improved process understanding, giving improved empirical and theoretical relations. Therefore, the strategy is to try to further investigate both the scale effect, and time dependency for the main intact rock type at the Forsmark site. The properties and predicted occurrence of inhomogeneities, such as sealed fractures and weaker rock types (amphibolite primarily) will be included in the rock mechanics description. Further, the influence of actual excavation shape (periphery irregularities) will be considered when the potential for spalling for different types of excavations is analysed.

2.5 Rock mechanics concerns in the safety assessment

Within the safety assessment work, SKB has identified all Features, Events and Processes (FEPs) that are of relevance for future containment (SKB 2011). Two of the time-dependent factors included in the “SR-Site FEP chart” (Figure 2-25), which summarizes the most important processes, are direct rock mechanics factors, namely “Rock stresses” and “Fracture structure in host rock”. These factors are connected to the requirement that the buffer and the canister is not allowed to be damaged by a large shear displacement across the deposition hole. These factors also impact the host rock fracture structure with potential consequence on the transmissivity of the entire fracture network and thereby on the groundwater flow and transport properties of the geosphere barrier at different scales and time phases.

This emphasizes the importance of rock mechanics description with respect to the safety assessment. However, rock mechanics is also of main importance for design issues related to the repository, such as repository layout and choice of excavation methods.

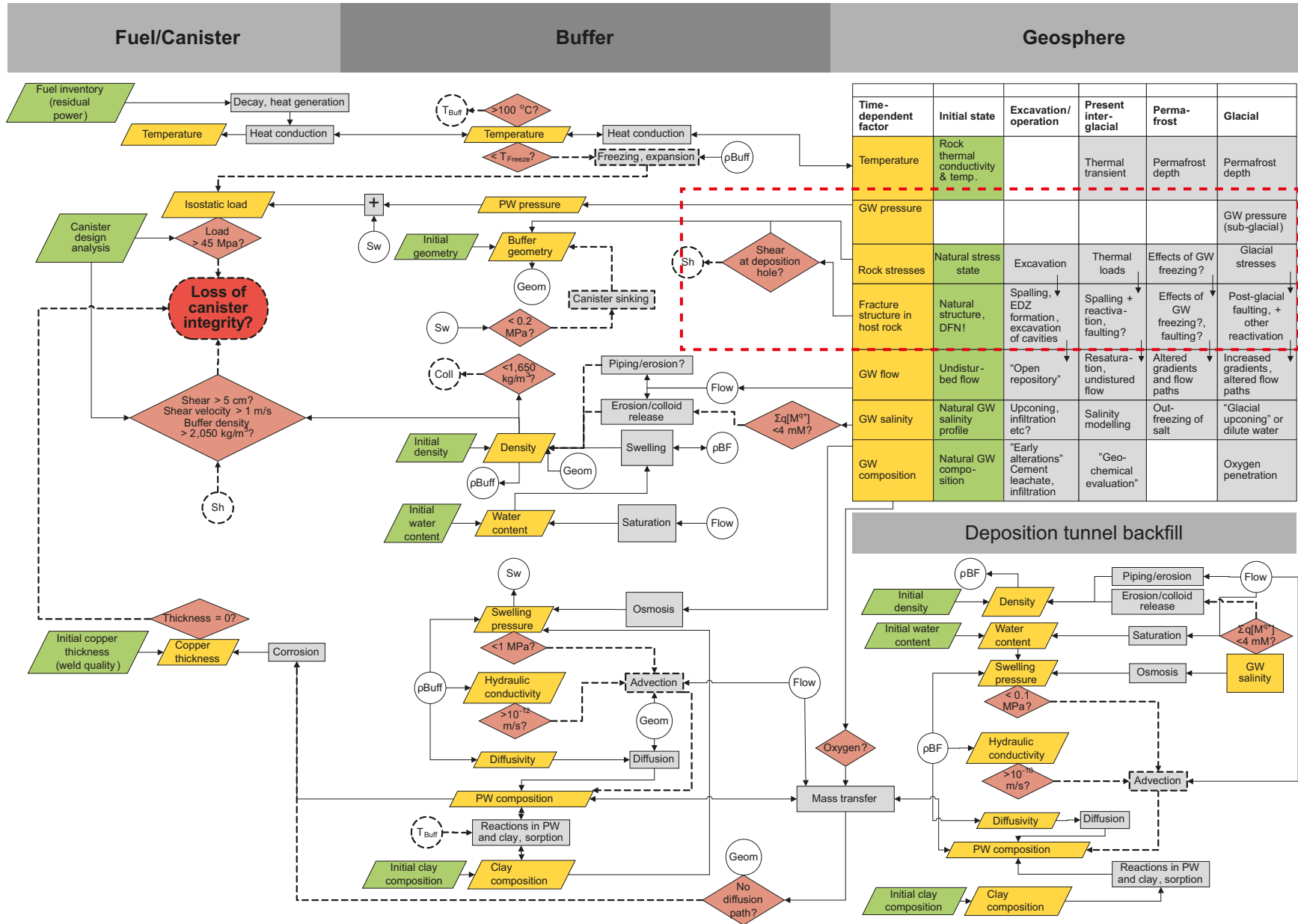


Figure 2-25. The SR-Site FEP chart (Features, Events and Processes), covering factors of relevance for containment (SKB 2011). The rock mechanics factors are here marked with the red dashed box.

The main four rock mechanics concerns, with respect to the long-term safety, may be summarized as shown in Figure 2-26. These four main concerns must be analysed as a part of the safety assessment and the analyses need the different parameters that are indicated in the diagram. These analysis requirements justify the parameter list included in this report, and the planned methodology for each group of property parameters will be presented in subsequent Chapters 3 to 7.

The four safety concerns in Figure 2-26 are explained briefly in the following paragraphs:

Concern A) – EDZ – Excavation Damage Zone

Depending on the in situ stress magnitude and orientation, a damage zone may develop around the deposition tunnel and the deposition holes, where the main mechanism expected to cause damage is spalling. The amount of expected spalling can be estimated if the strength properties of the intact rock are known (see further Section 2.4.3). The extent of EDZ is of importance for the estimation of hydraulic properties in the rock adjacent to the excavations, which is input to radionuclide transport calculations. Future safety assessment analyses will assume that EDZs have certain maximum transmissivities in order to comply with any potential requirement in this regard. In the deposition tunnels the EDZ could develop around the periphery with direction and extent depending on tunnel shape, stress magnitude and orientation with respect to the tunnel, inhomogeneities, etc. The extent of the EDZ will depend also on the excavation method, i.e., drill and blast or mechanical excavation and for the thermal spalling the extent depends on the thermal load from the spent fuel.

Spalling in deposition holes is expected to take place during the heated period *after* canister emplacement. However, initial spalling, i.e., spalling *before* the canister emplacement, is also of concern with respect to geometry requirements for the buffer emplacement in deposition holes (see Concern B). If, on the other hand, the in situ stress magnitudes turn out to be low or moderate, the EDZ concern becomes of minor significance for both deposition tunnels and deposition holes.

Concern B) – Deposition hole wall geometry

The excavation around the deposited canister should fulfil certain requirements concerning the total volume of the opening, such that the bentonite buffer will expand to a limited extent and keep the designed properties. Therefore, the probability for wedge or fragment fallouts from the deposition hole wall before the canister emplacement, due to fractures intersecting the borehole (or due to spalling), should be predicted. This analysis requires knowledge of rock stress and, in particular, a model for the fracture intensity and fracture network, and an estimation of fracture strength. If detailed analyses are performed, parameters describing the intact rock and the surrounding rock mass may also be required. For the assessment of this concern the sealed fractures must not be overlooked since the frequency for sealed fractures will most probably be higher than that of the open fractures (Section 6.1).

Concern C) – Fracture displacement

If the repository volume is subjected to a major seismic event a large fracture intersecting a deposition hole may shear. The shear can also be a result of thermal loading taking place when the heat generating canisters are deposited. To ascertain that the canister is not damaged, not even in the very long-term perspective, analyses are performed to estimate the maximum possible shear. The current safety criterion is that for intersecting fractures the maximum accumulated fracture shear should not exceed 5 cm (SKB 2010). These analyses require all the different categories of parameters, in particular the rock mass properties. This type of analyses is consequently made to support the decision of what type of fracture should be allowed to intersect a deposition borehole. This will affect the total number of available analysis for deposition holes.

Concern D) – Hydro-mechanical (H-M) effects in the geological barrier

The fourth concern is that the stress field in the area of the repository is such that the hydraulic conditions are influenced in a negative way. Here it should be remembered that it is the long-term period that is involved in the safety assessments and the time-period includes for example the next ice-age. When the hydraulic conductivity and the potential flow and transport from repository to the biosphere is to be predicted, the hydro-mechanical effects on the water bearing fractures must also be included. Further, the movement expected due to the thermal expansion of the rock mass surrounding the repository may also induce hydro-mechanical effects. The most critical factor for this rock mechanics concern, as for the other concerns, is, however, the in situ stress field. The stress magnitude is the key factor for most rock mechanics processes.

Long term safety concern	A) EDZ - Spalling	B) Wall geometry	C) Fracture shear	D) H-M effects
Rock mechanics parameters required				
In situ stress Chapter 3 	◆	◆	◆	◆
Intact rock properties Chapter 4 	◆	◆		
Single fracture properties Chapter 5 and 6 		◆	◆	◆
Rock mass properties Chapter 7 		◆	◆	◆

Figure 2-26. Summary of the main rock mechanics concerns with respect to long term safety. The different concerns require different key parameters for the safety assessment. See text for description of the safety concerns. The strategy for arriving at each parameter group will be presented in the following chapters of this report.

Apart from safety assessment requirements, the parameters of the rock mechanics site description will also be utilized in the design process of the repository. Different rock conditions may demand different excavation techniques and different reinforcement. The rock conditions will also influence the space accessible for deposition hole location and hence the cost for the repository construction.

2.6 Rock mass properties descriptors

The term “rock mass” is equivalent to the complex material that consists of intact rock and fractures together (ca 10–100 m scale).

In the former site model description stage (Glamheden et al. 2007), the rock mass descriptors were carried out using mostly empirical indices. The empirical indices for rock mass quality classification were introduced in the 1960s and aimed to establish standards to evaluate the rock mass quality for rock engineering, and directly from field data or core logging information. This approach is fast and useful for design purposes and will continue to be applied without major changes at the Forsmark site (see also Section 7.3).

More recent development during the last decade has been made in the area of the rock mechanics theoretical approach, with the aim to understand the mechanical processes in more detail and to allow calculation and prediction of large-scale properties, starting from the properties of the intact rock and fracture network components. This fracture systems approach is introduced in the following section. The particular application for derivation of rock mass mechanical parameters is presented in Section 7.1.

2.6.1 Fracture systems as Discrete Fracture Network models

Since the early stages of the site investigation programs and the formal safety assessment “SKB 91” (SKB 1992), the natural fracture system of the geosphere is identified as a key component for understanding structural geology, rock mechanics, hydrogeology, hydrogeochemistry and solute transport. Hence, the common description of brittle structures i.e., fractures and fracture zones, their properties, and representation in Discrete Fracture Network (DFN) models constitutes a cornerstone for site description, disposal facility construction and safety assessment.

All the stages – data collection, conceptual model development, use for applications – for building a unified methodology for a DFN description of the natural fracture system are presented in the methodology report DFNMM1 (Selroos et al. 2022). The principles developed in there are outlined below.

DFNMM1 (Selroos et al. 2022) uses the following definition: “The term DFN modelling defines how a fractured rock mass (the natural fracture system) can be equivalently and quantitatively represented as a population of individual, *fracture-like*, idealized tabular objects, including their geometrical and physical properties. The generic term fracture refers to these idealized objects (which cover a broad range and size of geological fractures). In the modelling process, the geometry of the individual fractures is first determined, as a basis for the definition of their individual hydraulic and mechanical properties and for the determination of the properties of the population of fractures (the DFN), as a whole.”

In practice, this involves the determination of specific range of properties (Munier 2004, Milnes 2006), defined by fracture or over the population of fractures (the DFN). First, each fracture of a DFN has a geometrical definition, with a location, size, shape and orientation (dip and strike angles), as given by the spatial density distribution of the whole population, including the size, shape and orientation distributions. Each fracture is also potentially characterized by more detailed in-plane descriptions of variations of fracture apertures coupled to surface morphology, e.g. the presence of voids/asperities, contact areas, roughness and undulations of surfaces, infilling mineralogy, alteration. All these characteristics contribute to define the fracture mechanical properties and hydraulic or hydromechanical properties (see Sections 4.5 and Chapter 6).

The fracture density distribution model (as defined in Chapter 6 in DFNMM1 (Selroos et al. 2022) refers to the most general definition of a DFN recipe. It embraces declinations of the model as an ensemble of fracture orientation sets (whose simplest expression is reduced to the numbers of sets, j_n , in the Q_{bas} index) or size scale dependency (Bonnet et al. 2001) to define the relative density evolution between “large” and “small” fractures at different modelling scales.

A typical DFN representation at a given model scale (Figure 2-4) combines deterministic, semi-deterministic and stochastic fractures. For some large-scale structural features, the above-mentioned fracture properties can be described deterministically based on an integration of geophysical, surface-based boreholes, outcrop, monitoring, and underground characterisation. However, for most fractures in the volume of interest it is not possible to determine more than a small fraction of the properties and their spatial distributions, if at all. Hence, they are described in terms of probability distributions, with statistical models and correlation structures derived from observations.

As a complement to the general DFN framework, simple quantitative metrics are also used to characterise DFN model and fracture systems. This includes, for instance, the total fracture surface area per unit volume of rock mass (commonly noted P_{32} following the notation introduced by Dershowitz and Herda (1992)) or of the total fracture equivalent volume (where each fracture contributes as its size to the cube, thus with the dimension of a volume) per unit volume of rock mass (known as the DFN percolation parameter, a quantity representative of the connectivity level of a DFN).

Hence, the DFN modelling methodology provides the recipe for creating a numerical system of fracture objects, leading to a synthetic rock mass representation where both discrete fractures and embedded rock matrix mechanical properties are combined. The DFN representation is the model representation of a fractured rock volume that is often considered to be the closest to the reality. However, a complete (site-scale) DFN representation in a numerical model potentially requires huge computational resources and therefore it is often necessary to partially or fully upscale a DFN-based rock mass model to a fully or partially upscaled Equivalent Continuous model.

The type of input data required to build the DFN models already exist in the SKB data acquisition guidelines. The basic data are the fractures mapped in the drill holes/cores, percussion drilled holes and on surface outcrops and the surfaces of underground openings. During the excavation of shafts, ramp tunnel and caverns of the planned repository, additional site-specific fracture network data will be collected from pilot holes and from the roof and walls of excavations giving further support to the DFN model for the site.

2.6.2 Fracture size range selection for modelling applications

Depending on the modelling application, a specific fracture size range or category may be critical for a model at hand. This makes also the issue of the mechanical and hydromechanical properties dependence with a given fracture category absolutely critical.

For the determination of equivalent rock mass mechanical properties, it is appropriate to integrate the multiscale range of fracture sizes together with the adequate mechanical parameters size dependency. On the other hand, for calculation of maximum potential shear on fractures intersecting the repository, the fractures that are critical are the very large ones, with diameters larger than 50 m (e.g. Hökmark et al. 2019).

3 In situ stress

3.1 Modelling approach

The overall approach to arrive at a model for the in situ stress is basically retained from that applied for SDM-Site. However, new developments have been made during the last ten years both regarding the measurement methods, numerical modelling and the theoretical background for results interpretation, integration and presentation. In Figure 3-1 the flowchart illustrates the different steps of the process. The grey part represents the collection of data from the site, the blue part is the input from other disciplines of the site descriptive model, the orange steps represent the theoretical analysis of potential stress models, and the green box is the final model chosen to describe the expected stress field, i.e., the aim of the activities. In the following each step of the approach is shortly described.

- a) Stress measurements have been performed, and additional measurements will be performed using different methods during construction of the repository. The different methods give slightly different information, and they have different advantages and weaknesses (See Section 3.2).
- b) In situ stress measurements are difficult to perform. Therefore, the next step is quality control of the measurement data. Only the data with acceptable quality will be used.
- c) The measurements result in a data point cloud, which constitutes the available site-specific information. The available information will be scarce, compared to the large rock volume of interest, and therefore modelling is needed to establish the basis for predictions at locations between measurements.
- d) The geological modelling results in a deformation zone (DZ) model, which gives the geometry of the zones, and a “fracture domain” model, which describes the rock between deformation zones. Possibly there may be some alternative models because of alternative interpretation of geological information and uncertainty.
- e) The loading history is not known in detail, but the understanding of previous loads can be simplified and simulated, and alternative load scenarios can be studied. A regional load situation is simulated by either assigning certain stresses to act on the boundaries of the numerical models or by forcing the model boundaries to displace in a predefined way. To enable the possibility to find the best fitting model(s), different load scenarios should be considered. The model cases can simulate different magnitude ratios between the vertical and horizontal stresses (different stress regimes), different stress gradients and different orientations of the model stress field.
- f) The mechanical properties of the deformation zones, to be used in the stress modelling, are estimated following the methodology presented in Chapter 7. The influence of the deformation zones and their geometries on the stress field clearly depends on what mechanical properties are assigned to those zones.
- g) The aim of the numerical modelling that includes the DZs is to assess the expected large-scale variation in stress due to the DZs inside the local scale model. This modelling step is performed with a discontinuum numerical modelling tool, such as 3DEC (Itasca 2020), and this work will be described further in Section 3.3.
- h) A discrete fracture network model (DFN) is an outcome of the geological and DFN modelling that describes the statistical distributions for the expected fracture network DFNMM1 (Selroos et al. 2022). The DFN consists of the “background” fractures in the rock mass between the deterministically modelled deformation zones.
- i) The fractures of the DFN have fracture properties that may be estimated based on another output from rock mechanics description (see Section 4.5). The properties can be different for different fracture sets and will be dependent on the normal stress level.
- j) The variation of the stress field at a smaller scale, due to the presence of fractures of different sizes (i.e., from facility part scale to deposition hole scale), can be estimated numerically using the DFN, the fracture properties and the intact matrix rock properties as input. This variation may exist superimposed on the large-scale variation. The approach for such analyses is indicated in Section 3.4.

- k) The combination of the large-scale deformation zone influence modelling and the small-scale stress variation modelling, results in several alternative stress models. By using spans of realistic input parameters, these model alternatives would be almost equally probable if there were no site-specific information. This is why measurement results are crucial for establishing a prediction with a desired level of certainty.
- l) The last step in the modelling approach is to compare the numerical model stresses with the available measurements and to try to find the model with the best fit to measurement results.

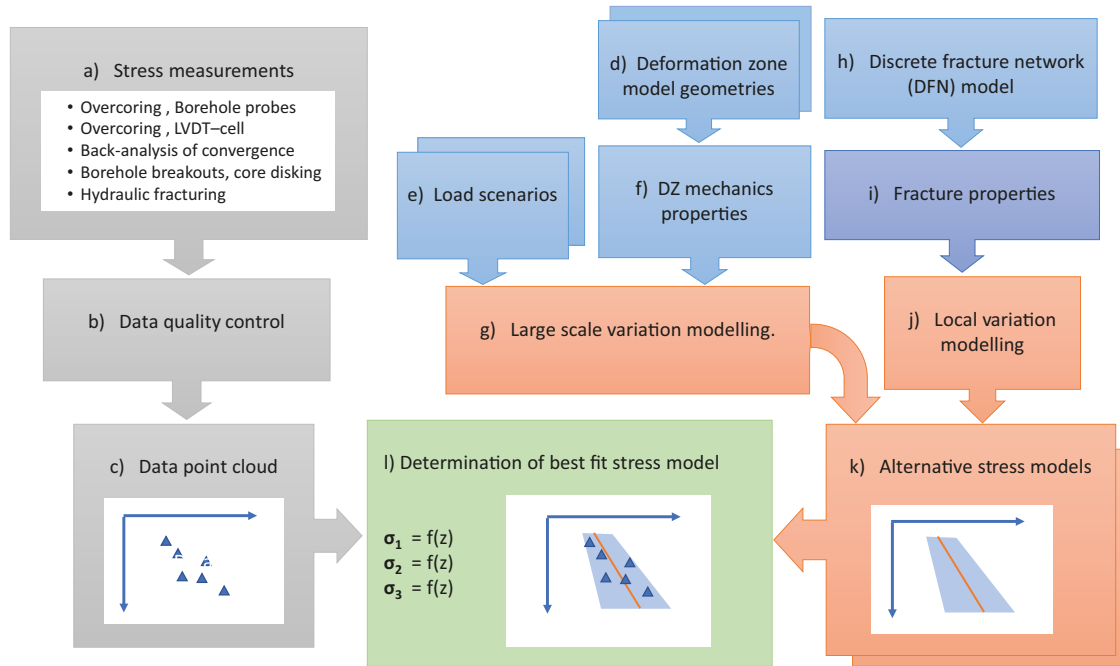


Figure 3-1. Modelling approach for the in situ stress model. Grey = collection of data from the site; Blue = input from other parts of the site description; Orange = theoretical analysis of the potential alternative stress fields; Green = Model choice for the site description.

3.2 Measurement methods

Two “direct” stress measurement methods were applied during the SDM-Site investigations to some extent: 1) Overcoring techniques imply measurement of the expansion of the rock when the in situ stress around the rock is released. 2) Hydraulic methods are based on measurement of the water pressure when a section of a borehole is pressurized, until the rock around the borehole is fractured and the fracture is opened or until a pre-existing fracture is reopened.

3.2.1 Overcoring methods

The overcoring instrument Borre Probe was previously used in the surface based site investigations and the results are summarized in SDM-Site (SKB 2008). The instrument is described for example in Hakala et al. (2003), also discussing in detail the various difficulties and possibilities in connection with the interpretation of overcoring results. During recent years the overcoring techniques (several suppliers) have been developed and refined, with added number of gauges and other improvements. These new probes, not yet utilized in Forsmark, often require 96 mm diameter boreholes.

Due to the difficulties and limitations of conventional small diameter overcoring measurements, a new technology was developed, with the support of SKB, since around 2003. This overcoring method uses mechanical LVDT (Linear Variable Differential Transducer) units in a cell to measure the displacements and is thus not dependent on in situ gluing procedures. The main limitation of this LVDT-cell is that it works in short boreholes from an excavation wall (Figure 3-2). The LVDT-cell will be used during the excavation of access tunnels or shafts, and it is thus not until the construction stage that the results from these measurements will be included in the stress modelling. The method description for the LVDT-cell is found in Hakala (2022).

The principle for the LVDT-cell measurements is shown in Figure 3-2 and Figure 3-3. The method is more robust than those based on traditional borehole instruments since the boreholes are short and the diameters of the holes are larger (the pilot hole is 127 mm and the overcoring is about 200 mm). However, in high stress areas the hollow rock cylinder created by the overcoring may easily break into rings, so called ring dinking as shown in Figure 3-4. Therefore, a sidecoring technique was added in which the stress release is achieved with a large diameter hole on the *side* of the pilot hole with the LVDT-cell. In areas where higher stress is expected sidecoring may be used instead of overcoring (Figure 3-5 and Figure 3-6). The in situ stress at the measurement location can be solved by numerical inversion using the results of the LVDT-cell measurements around the three-dimensional tunnel section. Because the inversion technique relies on knowing the exact location of the measurements and the geometry profile of the tunnel, modern survey techniques such as Lidar or photogrammetric technology should be used (Hakala et al. 2013).

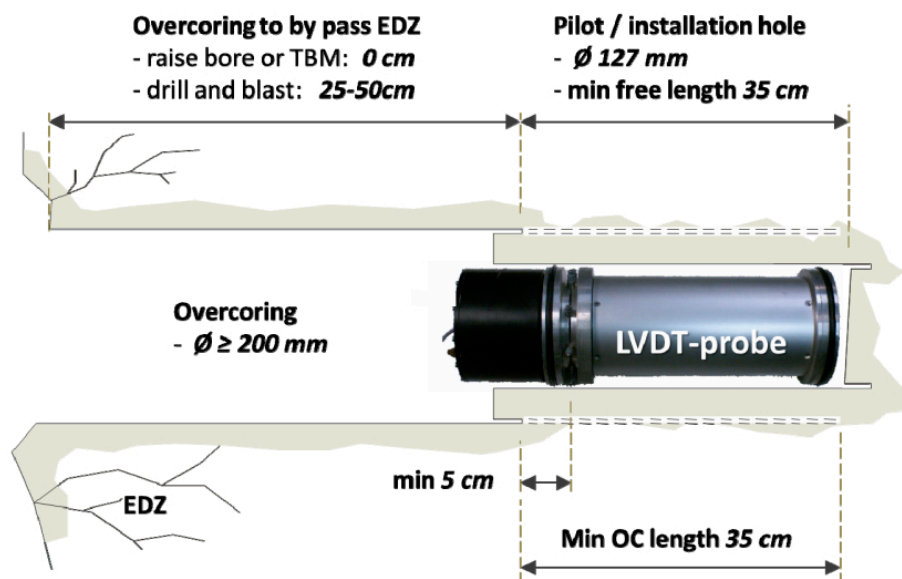


Figure 3-2. The LVDT-cell with suggested drilling and installation depths (Hakala et al. 2013).



Figure 3-3. The LVDT-cell is installed inside the pilot hole just before overcoring in the Äspö hard rock laboratory TBM-tunnel (at about 450 m depth). The drill bit was marked every 50 mm for manual coring advance recording (Hakala et al. 2013).



Figure 3-4. Ring dishing of a cylinder of Äspö diorite during overcoring of LVDT-cell. The inner diameter is 127 mm and the outer 200 mm (Hakala et al. 2013).

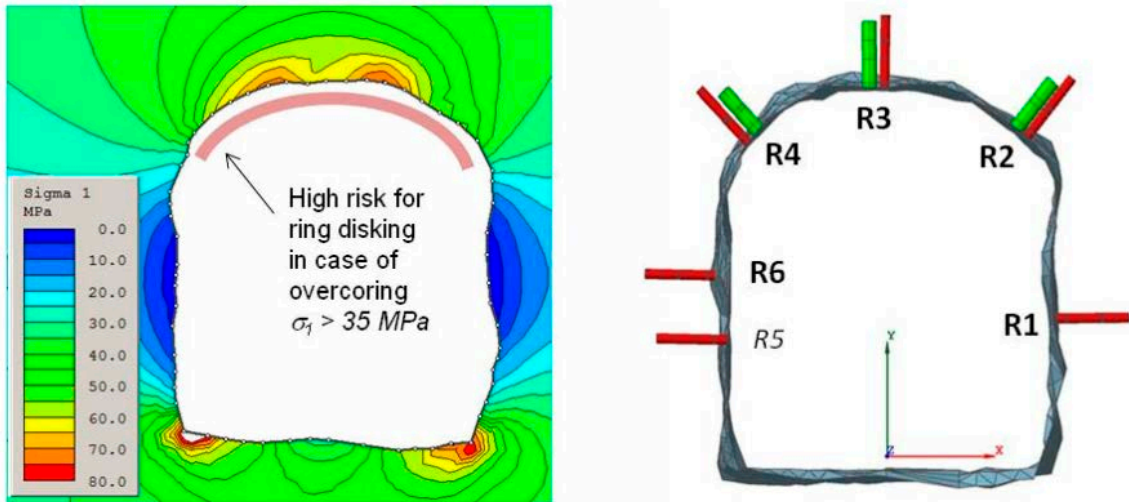


Figure 3-5. Estimate for ring disking potential (left) and the used LVDT-cell hole types and locations around the drill-and-blast tunnel. The pilot holes for the LVDT-cell are red and the side coring holes are green (Hakala et al. 2013).

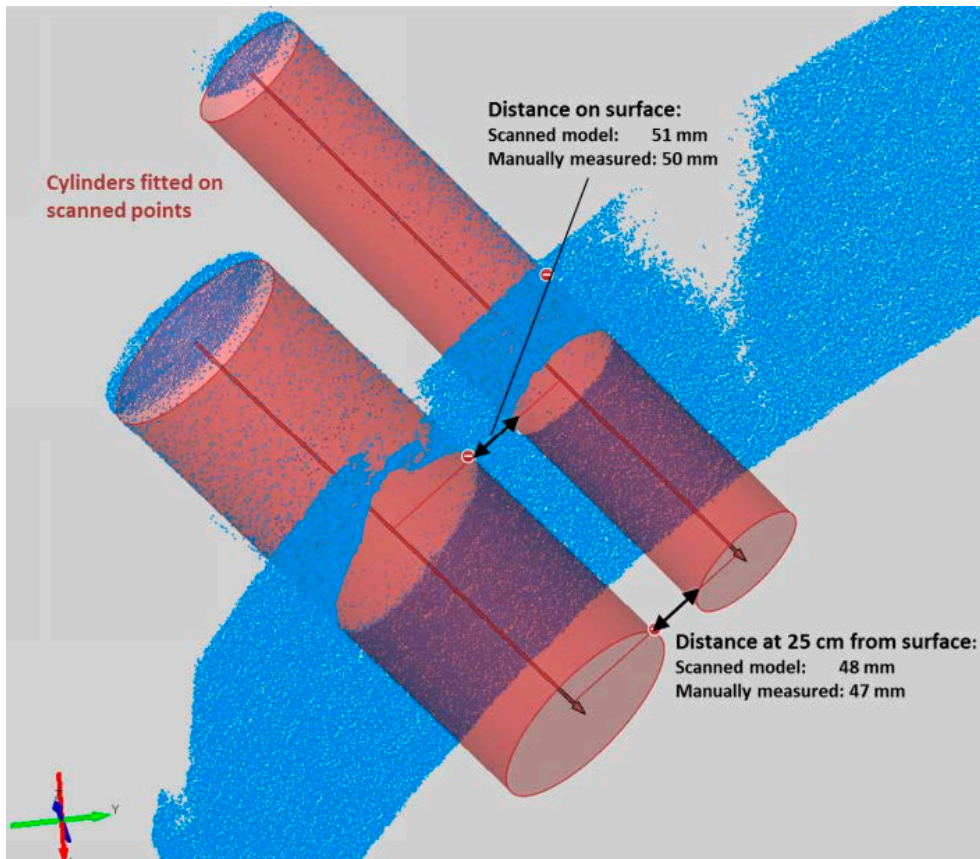


Figure 3-6. Laser scanner points (blue) are used to carefully measure the location of the pilot hole, side-coring borehole and the excavation rock surfaces. A numerical model is built to analyse deformation in the corresponding points and to find a model that fits well to the measurements (Hakala et al. 2013).

3.2.2 Hydraulic test methods

In the preceding surface-based site investigations in Forsmark, and the associated SDM-Site, a few hydraulic fracturing (HF) and hydraulic tests on pre-existing fractures (HTPF) results were included (SKB 2008). These data will obviously remain in the data set for the next stress modelling stage. However, the previous stress modelling demonstrated difficulties to find accordance between the interpreted stress magnitudes from hydraulic measurements and overcoring measurements.

In the future investigations some further field test with hydraulic measurement techniques might be performed. In addition to the traditional hydraulic fracturing procedures, the idea is to add some identification technique for the induced fracture orientation at a certain distance from the borehole. The orientation of the induced and propagated hydraulic fracture would give valuable indication of the stress regime, i.e., whether the minor horizontal stress or the vertical stress is the lowest at different depths. The stress regime is in turn of importance for hydro-mechanical rock mass modelling, deformation zone and fracture stability analyses (see Section 3.6).

However, during the excavation of the repository the strategy for stress modelling is to mainly rely on direct measurement data from overcoring techniques (probably including 96 mm diameter borehole probes). The need for complementary hydraulic tests at repository level will be evaluated based on the results and the uncertainty of stress modelling based on the other stress measurement techniques.

3.2.3 Breakout observations

Borehole breakout observations from televiewer logging in boreholes, and from mapping in shafts, can be used to determine the orientation of the stress field. This approach has been used in the most recent site description for Forsmark, modelling stage 2.3 (Glamheden et al. 2008), and the summary of borehole breakouts of different classes is shown in Table 3-1. It may be noted that the total amount is in the order of 2 % of summed-up borehole length for full “classical” breakouts but is more common, about 10 % for “micro-fallouts”. Both types of observations can be used to determine the direction of the major principal stress, because the breakouts develop and are observed in the borehole wall at two opposite sides, and the direction that is perpendicular to this plane is the major stress direction. Previous site modelling showed that both, breakouts and micro-fallouts, give consistent results in terms of orientation and they agree well (Figure 3-7 and Figure 3-8). Any additional available acoustic televiewer data from subvertical cored boreholes, for example from vertical shafts, will be analysed for breakouts and micro-fallouts and the data compilation updated using the same methodology.

Table 3-1. Summary of the breakout length by breakout class for investigation boreholes included in SDM-Site (Glamheden et al. 2008).

Borehole name	Survey length [m]	Length [m]				Total length [m]
		Borehole breakouts (BB)	Micro-fallout (MF)	Washout (WO)	Keyseat (KS)	
KFM01A	1000	18.4	278.1	4.8	0.8	302.1
KFM01B	480	23.5	118.5	0.8	70.7	213.5
KFM02A	979	55.2	91.7	4.4	2.5	153.8
KFM03A	989	21.2	81.6	1.0	0.2	104.0
KFM03B	83	0.2	30.7	1.2	0.0	32.1
KFM04A	984	30.8	70.6	1.0	2.4	104.8
KFM05A	990	23.0	47.8	7.8	1.0	79.6
KFM06A	933	6.7	8.2	1.0	0.8	16.7
KFM07C	512	26.5	178.0	2.9	0.3	207.7
KFM08A ¹⁾	886	2.2	3.5	3.0	0.1	8.8
KFM08A ²⁾	886	2.2	104.9	3.0	0.3	110.4
KFM08C	840	9.2	23.7	–	0.1	33.0
KFM09A	781	16.4	55.0	3.8	–	75.2
KFM09B	598	4.2	49.4	3.2	–	56.8
Total [m]	10055	237.5	1138.2	34.9	79.1	1489.7
% of surveyed length		2.4	11.3	0.35	0.79	14.8

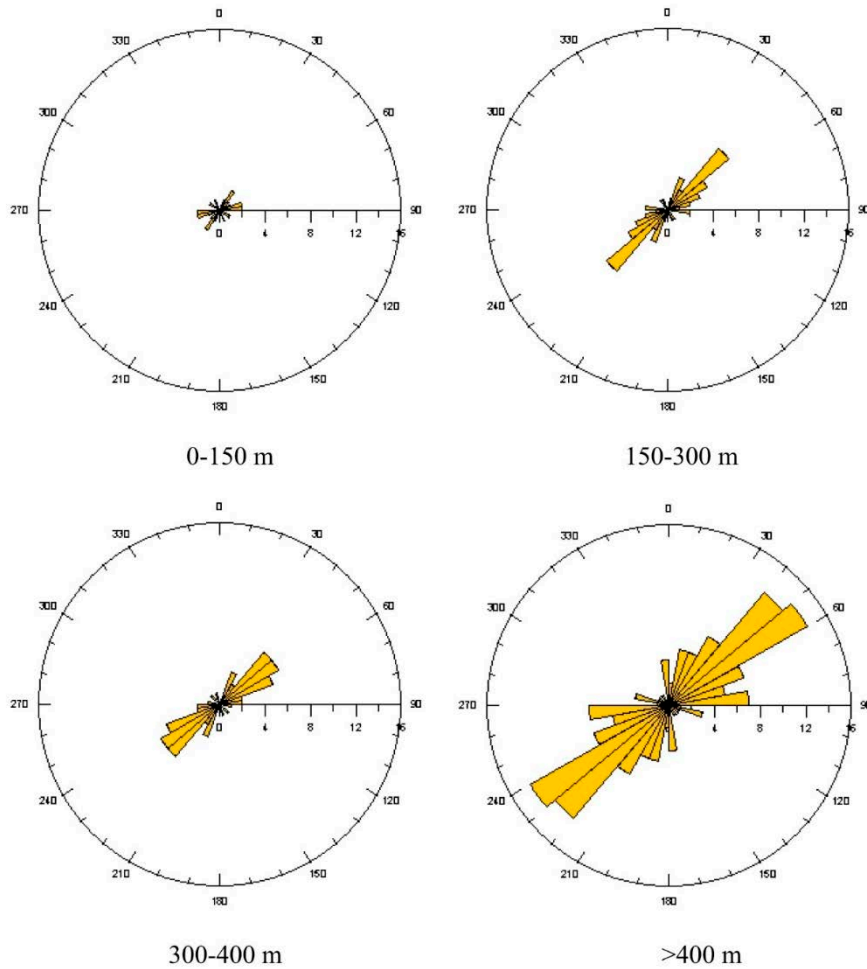


Figure 3-7. Rose diagram showing the orientation of the “classical” breakouts at different depth in boreholes KFM01A, KFM01B, KFM02A, KFM03A, KFM04A, KFM05A, KFM06A, KFM07C, KFM08A, KFM09A and KFM09B. The number of breakouts is 11 in the interval 0–150 m, 27 between 150–300 m, 29 between 300–400 m and 75 for depths > 400 m (Glamheden et al. 2008).

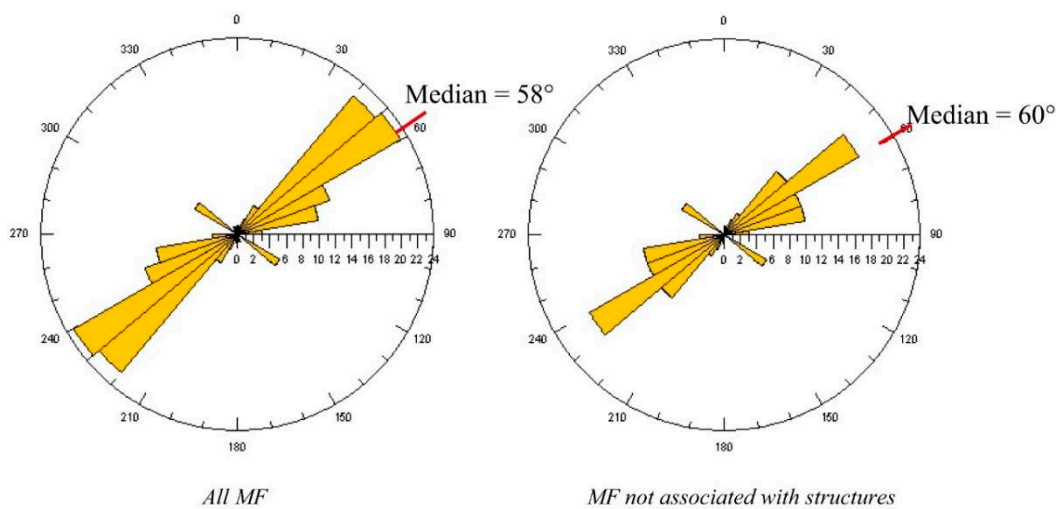


Figure 3-8. Rose diagram showing the orientation of the micro-fallouts (MF) in boreholes KFM01A, KFM02A, KFM03A, KFM04A, KFM05A, KFM06A, KFM07C, KFM08A, KFM08C, KFM09A and KFM09B. In the left rose diagram all MF (85 micro-fallouts) are shown and in the right diagram only MF not associated with structures are shown (64 micro-fallouts) (Glamheden et al. 2008).

Breakouts may also be *induced* using heat inside boreholes, with the objective to use the small spalls caused by the temperature expansion to similarly find the orientation of the rock stress at the actual borehole section. The method of induced thermal spalling (denoted SLITS) is described in Hakami (2011).

Breakout observations can also be used as an indication of the spalling probability and relative occurrence in the different rock types. If breakouts occur in small diameter boreholes, some type of rock failure should also be expected to occur in larger diameter boreholes or excavations (Figure 2-18). And since the subject of spalling and EDZ in tunnels and deposition holes is of main interest for planning and prediction, the breakout investigations and results are valuable in the site description (see also Section 2.4).

Observations in the larger scale shafts and tunnels during excavation can also be used as an indication of the in situ stress field. One example is shown in Figure 3-9 where fractures were mapped in the vertical shaft at the URL. After passing a regional deformation zone the walls of the vertical shaft started to show zones of both longer and shorter fractures and some breakouts, as a result of the increased in situ stresses (Figure 3-10). A change in fracture occurrence in boreholes or shafts is a clear, although qualitative, indicator of change in stress conditions or a change in the rock strength conditions.

In the case of the Canadian URL, in correspondence with the damage mapped in the vertical shaft, the horizontal tunnels at depth later showed consistent spalling, even in rock material which was unaltered and fresh (Martino and Chandler 2004) (see figures in the spalling Section 2.4). The reason for collecting detailed direct observations of breakout and fracture occurrences in boreholes, as well as any larger excavation, is that they give valuable indications also when direct stress measurements are not performed or are not applicable.

In places where breakouts have been observed and accurately measured, the stress situation may also be estimated *quantitatively* by using material models and theoretical modelling of the breakout failure process (Gerolymatou 2019). This approach has not yet been attempted within the framework of SKB site investigations at Forsmark, since the amount of breakout is limited, and the size of breakouts has been small in slim investigation boreholes.

3.2.4 Core dinking and ring dinking

In a similar way to borehole breakouts, core dinking gives indirect information regarding the stress state. Core dinking is recorded specifically during core mapping and the occurrence should be compiled and analysed as a part of site description. So far, the boreholes in Forsmark have shown very limited core dinking, but some short dinking has occurred in each investigation borehole. Examples of occurrences from Forsmark and Äspö Hard Rock Laboratory are given in Figure 3-11 and Figure 3-12, respectively.

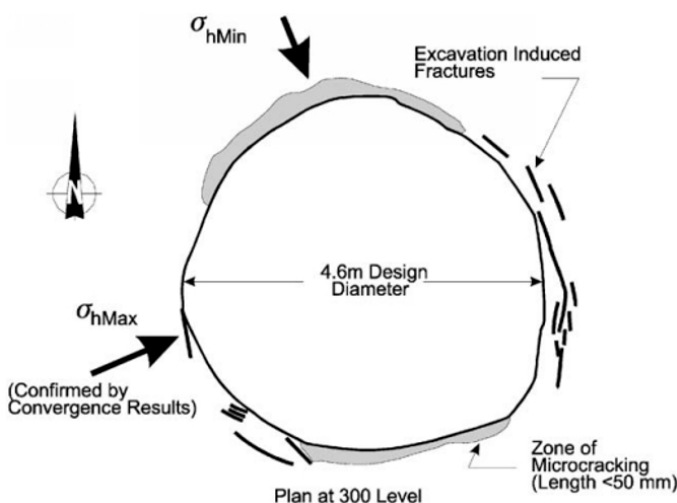


Figure 3-9. Pattern of damage mapped around the vertical shaft at the 300 m level at AECL Underground Research Laboratory, URL. The zone of microcracking is in the direction of the minor principal stress direction (Martino and Chandler 2004).

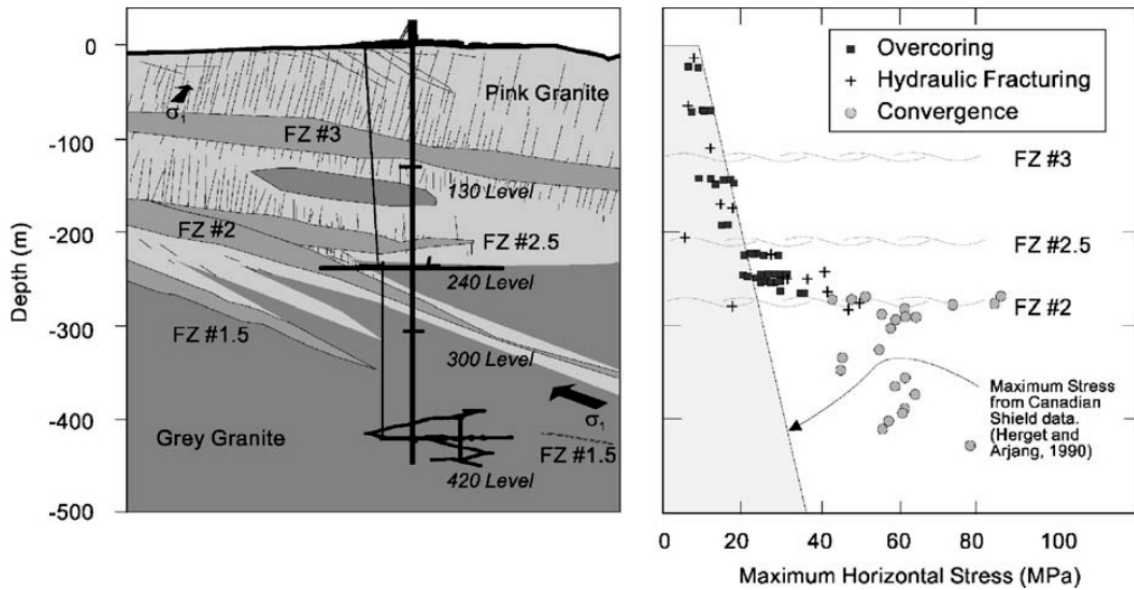


Figure 3-10. Geology and the stress measurement results at the URL (Martino and Chandler 2004).



Figure 3-11. Example of core diskings observed on drill core from borehole KFM26 at about 100 m depth, Forsmark site. These core diskings fractures have not all propagated through the whole core, the fractures to the left (white lines) are still connected at the centre of core.



Figure 3-12. Example of core diskings at the TASQ tunnel site in Äspö Hard Rock Laboratory, from a borehole in a point where stresses were elevated due to the excavations (Sjöberg et al. 2007).

The explanation to a core dishing occurrence in a certain isolated section may be that the stress is locally higher but probably more often the reason is that the strength of the rock is lower at this location. The core dishing could possibly also be influenced by the heat and forces generated during drilling operation, but there is no documented knowledge to support this.

Hakala (1999) has performed numerical analyses of core dishing. Consequently core dishing has been used to estimate the in situ stress at the Hästhölm and Olkiluoto sites in Finland (Hakala 2000, Ask 2011, Posiva 2012). To make such analyses the important inputs are the tensile strength and Poisson's ratio of the rock and careful observations of the core dishing occurrence, such as the shape of the induced fracture. Further, the stress regime in the area, i.e. the relation between principal stress components, must be assumed. Sjöberg et al. (2005) used the approach of Hakala (2000) on the data available at Forsmark at the time.

Another illustrative example of the core dishing mechanism is given by the numerical analysis result in Figure 3-13 made by Wu et al. (2018). A bonded particle material model is used and the black lines in the figures indicate the location of bond breakage between particles. These results demonstrate how the stress field will determine not only if the dishing occurs or not but also how the fracturing process and the fracturing shape will differ depending on the stress field. For some cases a fracture is only created along the boundaries of the core.

Based on data from URL, Lim (2013) studied the core dishing phenomenon frequently observed in this underground laboratory due to the high stresses. The photo in Figure 3-14 from Lim and Martin (2010) is an illustrative example of how the thickness of disks is dependent on the stress magnitudes. The drill core in the figure is drilled from the excavation wall where the stresses are more elevated and passes towards lower stresses at larger distance from the tunnel. In this case the rock material is quite homogeneous and correspondingly there is a consistent occurrence of the dishing phenomenon. At places where the rock type changes a change in the occurrence or in the disk thickness is to be expected, which is also what has been observed.

Lim (2013) correlated the results from overcoring stress data with the dishing occurrence at URL and established a model for predicting the core dishing and the so-called ring dishing. Ring dishing occurs at locations where overcoring stress measurements are performed and rock rings are formed due to the tensile stresses that result from the destressing during overcoring (one example was shown in Figure 3-4). A lower stress (about 40 % lower) is needed to cause the *ring* dishing compared to what is needed to cause full *core* dishing (Figure 3-15). This is a finding that could be useful in Forsmark where ring dishing has been observed (e.g. Sjöberg et al. 2005), and additional ring dishing may be observed also in future investigations.

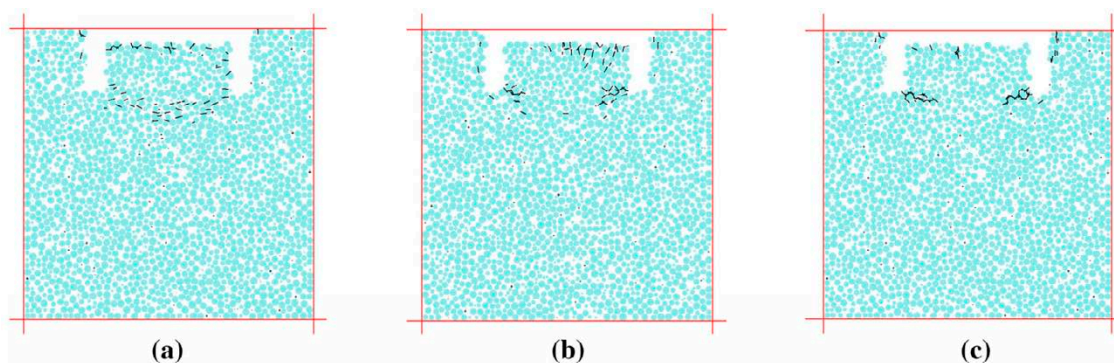


Figure 3-13. Simulation of core dishing fracturing. The blue dots are particles of the rock model material, and the black lines indicate broken particle bonds. Results are from models with different surrounding stress and the difference in outcome illustrates the effect of stress field on the dishing: a) $\sigma_x = 20$ MPa, $\sigma_y = 40$ MPa, $\sigma_z = 10$ MPa. b) $\sigma_x = 40$ MPa, $\sigma_y = 10$ MPa, $\sigma_z = 20$ MPa. c) $\sigma_x = 10$ MPa, $\sigma_y = 20$ MPa, $\sigma_z = 40$ MPa (z is the drill hole direction) (Wu et al. 2018).

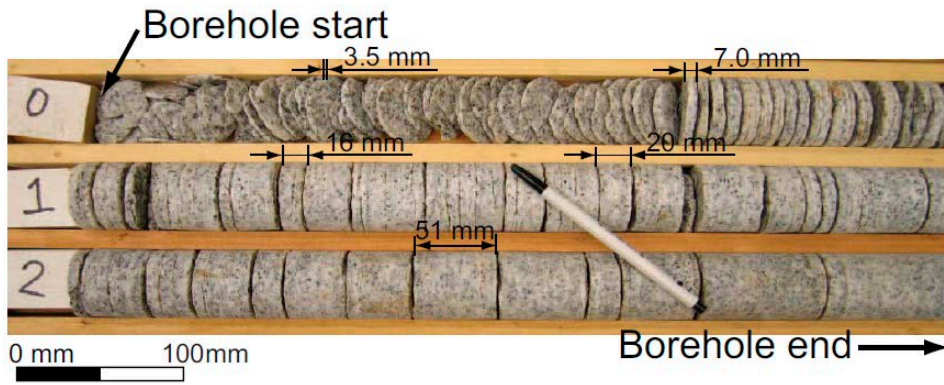


Figure 3-14. Typical core diking from a borehole at 420 level of URL, Canada. The core diameter is 45 mm and the total length of the core is 2.54 m (Lim and Martin 2010). Note how the distance between fractures increase as the borehole gets further out from the tunnel wall where stresses get lower.

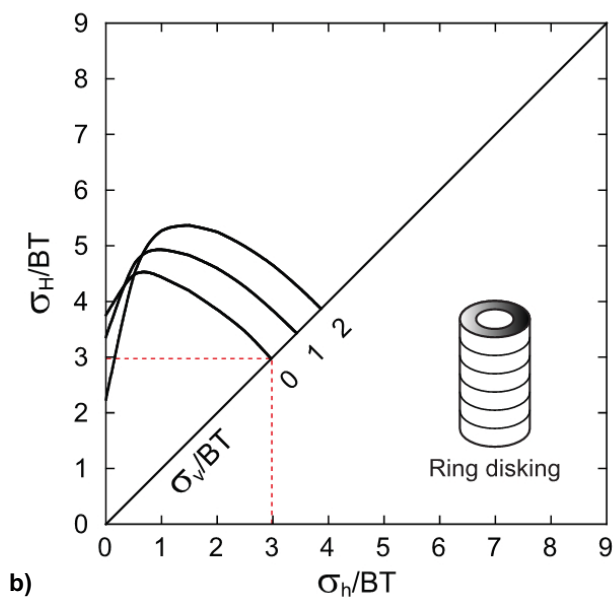
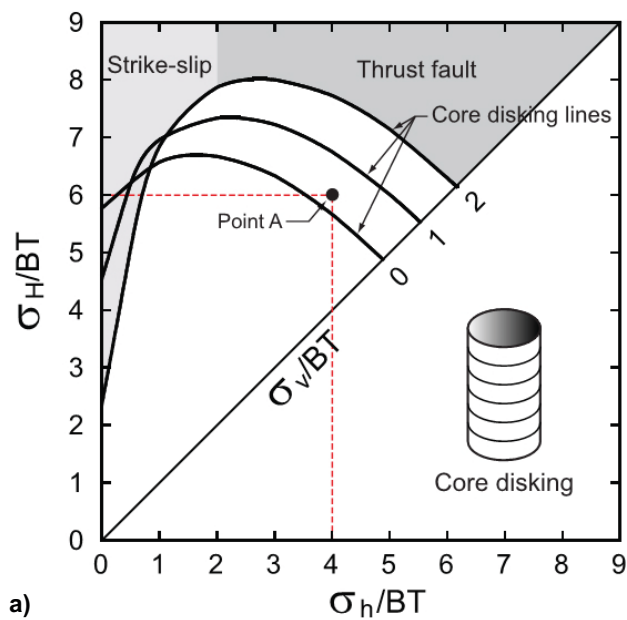


Figure 3-15. The model for determining the stress criterion for a) core diking and b) ring diking (Lim 2013). (BT = Brazilian test = Indirect tensile strength., ITS).

The strategy for use of the diskings phenomenon as part of the stress modelling is that they can help set estimates of lower and upper stress limits. For example, if, as in KFM07C, *ring* diskings is mapped at several locations with various lithologies (Figure 3-16), the diagram in Figure 3-15 suggests that the maximum horizontal stress should have a value higher than the tensile strength times about 4. This means that the major horizontal stress is at least about $4 \times 10 \text{ MPa} = 40 \text{ MPa}$ in a point with ring diskings in granite to granodiorite, at least 28 MPa at a pegmatite and at least 8 MPa in amphibolite (assuming the very lowest measured tensile strength 2 MPa for amphibolite (Table 4-1)).

Also a few sections of pegmatite have shown *core* diskings. These indicate, following the models by Lim (2013), that horizontal stresses should be at least about $6.5 \times 5 = 32.5 \text{ MPa}$ (assuming the pegmatite has a minimum of 5 MPa tensile strength; the actual strength at the point is not known). This is a result that is realistic, and at least roughly fits with the results from the close overcoring measurements.

At the same point where the ring diskings in KFM07C with rock type 101057 was observed there was *no core* diskings observed, and this means that the actual maximum stress is *lower* than the about 78 MPa ($6.5 \times 13 \text{ MPa}$) which is needed to induce core diskings, following the core diskings model of Lim (2013), Figure 3-15. This is a very high stress level, and it is therefore predicted that no consistent core diskings should occur, in this most common rock type, even at very large depths. Some weakness or rock type variation, resulting in lower tensile strength, is needed to give rise to core diskings. It seems that out of the core diskings occurrences so far observed in the investigation boreholes several have been at pegmatite or amphibolite locations. However, no updated detailed diskings analysis has been performed after Sjöberg et al. (2005). The correlation between diskings occurrence and rock type properties and property variations will be further analysed in future stress modelling.

3.2.5 Co-visualisation of borehole stress measurement results

The different stress measurements and observations are presented together with geological logging for each borehole (see WellCAD diagram example in Figure 3-16). This is done to provide an overview of the total available stress data set but also to simplify identification of possible correlations between the stress related data and changes in rock types, structures or depth. This type of diagram is not a new methodology but will be retained and applied for any additional borehole to be included in the coming site descriptive modelling work.

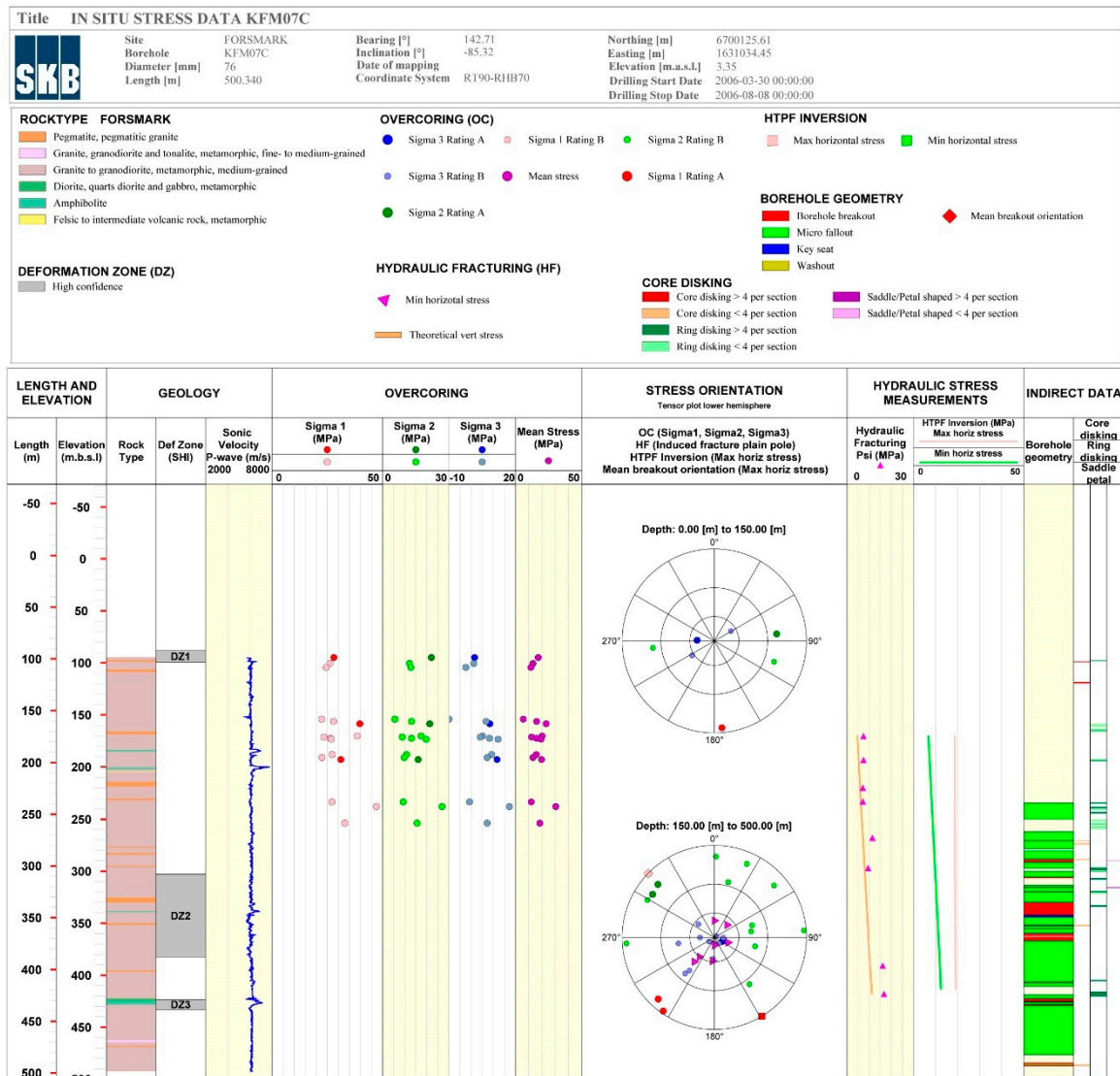


Figure 3-16. Example of a WellCAD diagram for a borehole (KFM07C) at the Forsmark site, showing geological data together with direct and indirect measurement results of the state of stress (Glamheden et al. 2007).

3.3 Stress modelling – large scale

Deformation zones have clearly lower strength than the surrounding rock mass, and therefore the stress field will be influenced to some extent by their presence. The amount of influence is not a simple task to analyse because both the detailed geometries of the deformation zones and the actual tectonic loads that are, and have been, acting on the area are unknown. Use of numerical modelling is one way to analyse the potential influence of these structures, and this methodology has been used previously in Forsmark site descriptive modelling but is most recently applied by Hakala et al. (2019).

In the study by Hakala et al. (2019) the most recent official deformation zone model of the Forsmark area (Stephens and Simeonov 2015) was used as geometrical input, and the influence of undulating (as interpreted) instead of planar zones was one of the issues addressed (in Phase 1). The general features of the 3DEC model are shown in Figure 3-17. Different alternative model cases were studied concerning the methodology for application of boundary thrust, deformation zone properties, orientation of tectonic thrust, target stress magnitudes and effect of pore pressure (in Phase 2). The Figure 3-18 and Figure 3-19 together with Table 3-2 and Table 3-3 exemplify how a numerical study with different cases, reflecting the uncertainty in actual conditions, can be performed.

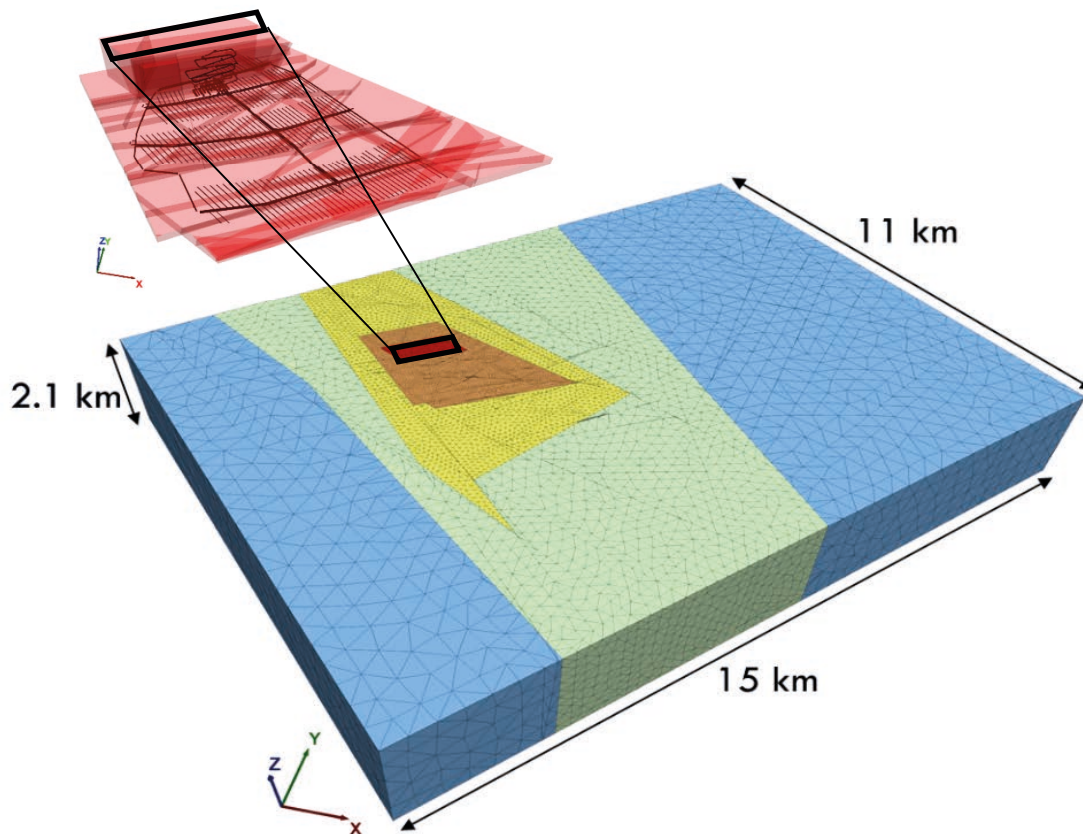


Figure 3-17. Example of how a numerical model (3DEC) simulating the volume encompassing the underground facility at Forsmark. The mesh size of the numerical model decreases closer to the facility where a detailed stress prediction is desired (Hakala et al. 2019).

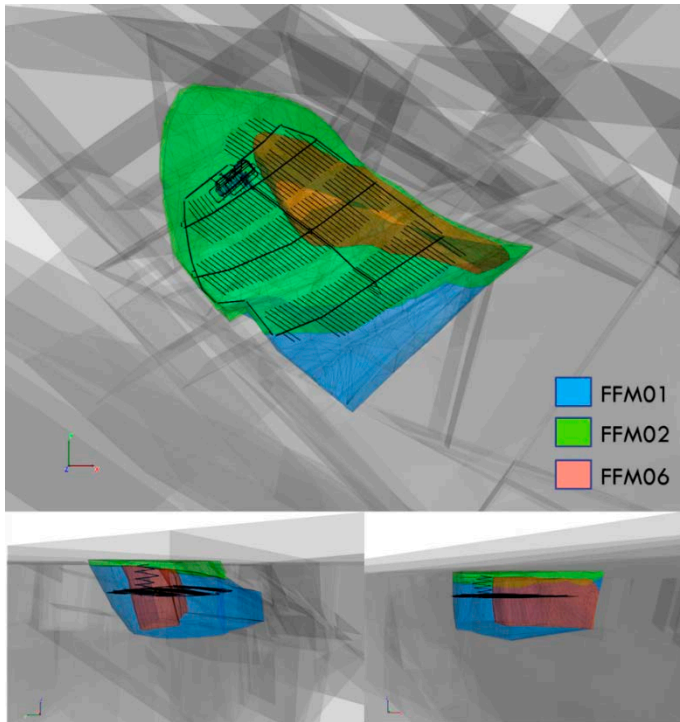


Figure 3-18. Fracture domains surrounding the facilities included with different properties in the numerical model made to study the influence on stress field. From Hakala et al. (2019).

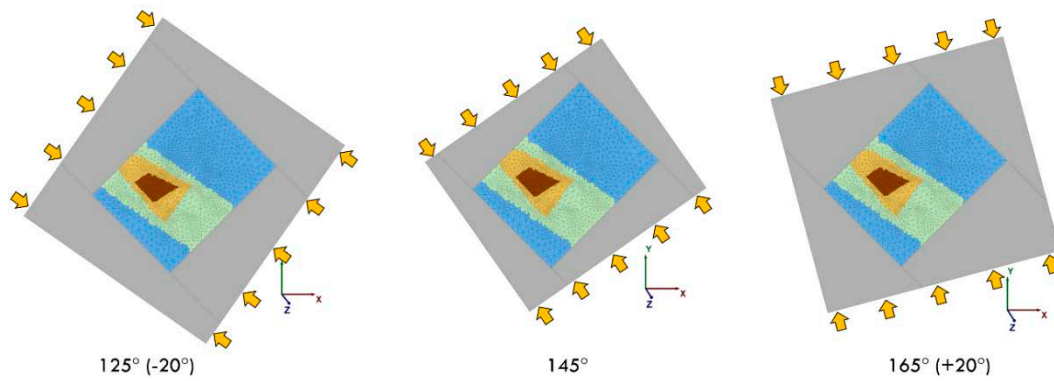


Figure 3-19. The varying major thrust orientations used in the numerical simulations (Hakala et al. 2019).

Table 3-2. Parameter values and calculation conditions for the different cases analysed in Phase 2 of the study by Hakala et al. (2019). The differences of a certain case, compared to Case 2-1, are highlighted in orange (Hakala et al. 2019).

Case	Boundary thrust for <i>in situ</i> stress target: Martin 2007 at 400 m level*	Deformation parameter values			Excess glacial pore pressure	After glacial stress adjustment
		Name	phi (°)	c (MPa)		
Case 2-1	z-gradient	All except Singö Singö (ZFMWNNW0001)	36 31.5	0.7 0.4	90 %	N
Case 2-2	z-gradient	All except Singö Singö (ZFMWNNW0001)	36 31.5	0.7 0.4	90 %	N
Case 2-3	z-gradient σ_H, σ_h trends +20°	All except Singö Singö (ZFMWNNW0001)	36 31.5	0.7 0.4	98 %	N
Case 2-4	z-gradient σ_H, σ_h trends -20°	All except Singö Singö (ZFMWNNW0001)	36 31.5	0.7 0.4	98 %	N
Case 2-5	z-gradient	All except Singö Singö (ZFMWNNW0001)	20 20	0.3 0.3	98 %	N
Case 2-6	z-gradient σ_H, σ_h trends -20°	All except Singö Singö (ZFMWNNW0001)	20 20	0.3 0.3	98 %	N
Case 2-7	constant	All except Singö Singö (ZFMWNNW0001)	36 31.5	0.7 0.4	98 %	Y σ_2 reduced
Case 2-8	constant σ_H, σ_h trends -20°	All except Singö Singö (ZFMWNNW0001)	36 31.5	0.7 0.4	98 %	Y σ_2 reduced
Case 2-9	constant	All except Singö Singö (ZFMWNNW0001)	20 20	0.3 0.3	98 %	Y σ_2 reduced
Case 2-10	constant σ_H, σ_h trends -20°	All except Singö Singö (ZFMWNNW0001)	20 20	0.3 0.3	98 %	Y σ_2 reduced
Case 2-11	constant, OC high	All except Singö Singö (ZFMWNNW0001)	36 31.5	0.7 0.4	98 %	Y σ_2 reduced
Case 2-12	constant, OC high σ_H, σ_h trends -20°	All except Singö Singö (ZFMWNNW0001)	36 31.5	0.7 0.4	98 %	Y σ_2 reduced
Case 2-13	constant, OC high	All except Singö Singö (ZFMWNNW0001)	20 20	0.3 0.3	98 %	Y σ_2 reduced
Case 2-14	constant, OC high σ_H, σ_h trends -20°	All except Singö Singö (ZFMWNNW0001)	20 20	0.3 0.3	98 %	Y σ_2 reduced

* Cases 2-11 to 2-14 have a higher target stress state magnitude but are otherwise equivalent to Cases 2-7 to 2-10.

Table 3-3. Applied thrust for Phase 2 simulation cases (Hakala et al. 2019).

Cases	Orientation	Velocity (m/model time step)
2-1 to 2-6	$\sigma_H = \sigma_1$	$2.14 + z \times 2e-3$
	$\sigma_h = \sigma_2$	$0.706 + z \times 9.5805e-4$
2-7 to 2-10	$\sigma_H = \sigma_1$	4.2
	$\sigma_h = \sigma_2$	1.75
2-11 to 2-14	$\sigma_H = \sigma_1$	4.2
	$\sigma_h = \sigma_2$	1.95

z = depth in metres.

The output of the numerical stress modelling is the calculated stress field in the whole volume and the influence of the deformation zones and varying properties are visualized with contour plots. Examples of results comparing undulating and planar deformation zones are shown in Figure 3-20 and Figure 3-21. The deformation zone with low-angle dip crops out on ground surface and, as expected, this zone will shear from horizontal compression and the stresses vary clearly across this zone. But, as can be noted in the diagrams, even minor zones induce a stress variation over a horizontal section.

This modelling does not include the small-scale variation that can be expected due to the smaller scale fracturing. To describe this variation specific modelling must be performed at a different scale.

Using a defined ranking system, the fit for each model case, between stresses in the model and available measurement data, was compared, see example of this in Figure 3-22. The Case 2-3 with basic material parameter values and +20 degrees rotated thrust resulted in the best score. This model should thus be considered the best prediction of the stress situation.

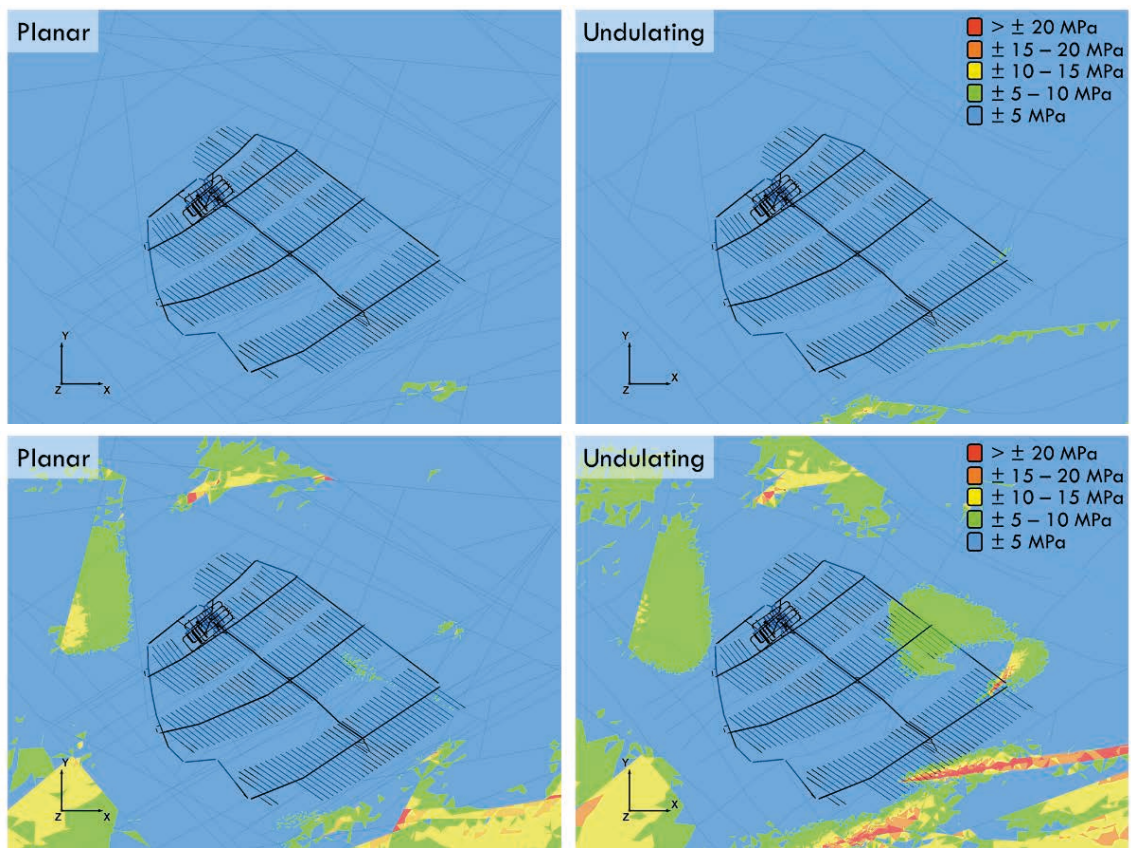


Figure 3-20. Example of results (Phase 1) showing the change in σ_1 magnitude (compared to boundary stresses), in a horizontal section at repository level, Case 1-1 (above) and Case 1-3 (below). The difference between Case 1-1 and Case 1-3 is that the latter has lower friction angle (20 compared to 36) and lower cohesion (0.3 compared to 0.7 MPa) which gives a larger variability within the volume. The deformation zone geometry in the target area is simulated planar in the left cases and undulating (as interpreted) in the right cases. The undulating deformation zone cases gives more variation in stress magnitude (Hakala et al. 2019).

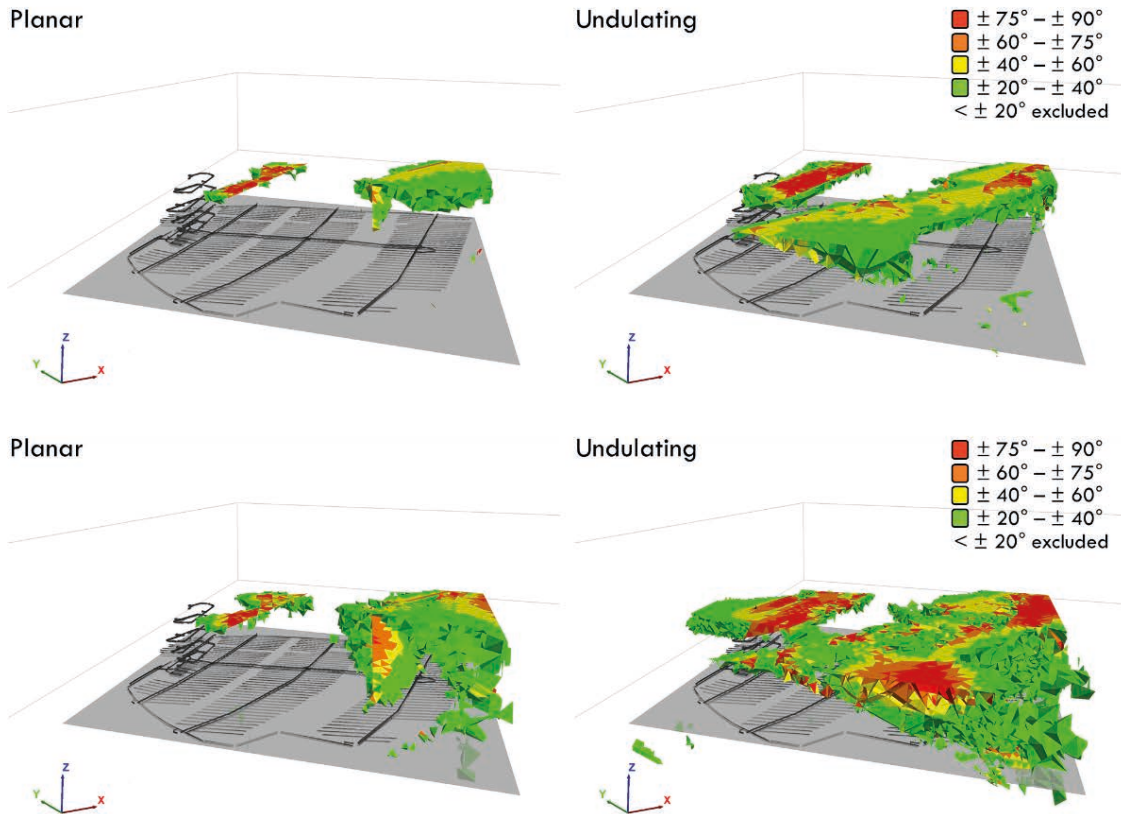


Figure 3-21. Change in σ_1 trend, 3D-view with repository, Case 1-1 (above) and Case 1-3 (below). In a similar way as for the magnitudes, the largest variation in stress orientation is noticed for the cases with undulating deformation zones and lower strength properties on the zones. Some areas closer to the model surface get a clear influence in stress orientation from the deformation zones that have sheared due to the load applied to the model (Hakala et al. 2019).

Case	Sum of ranking values for;		
	$\sigma_1 + \sigma_2$	σ_1	σ_2
Case 2-1	1.1	0.2	0.9
Case 2-2	1.1	0.3	0.8
Case 2-3	0.9	0.1	0.7
Case 2-4	1.0	0.2	0.7
Case 2-5	1.0	0.3	0.6
Case 2-6	1.0	0.4	0.5
Case 2-7	1.7	0.3	1.3
Case 2-8	1.6	0.4	1.2
Case 2-9	1.4	0.4	1.0
Case 2-10	1.5	0.7	0.8

Figure 3-22. Example of how the numerical result can be compared with measurement data to find the best fit stress model. Sum of goodness of fit ranking values for simulation Phase 2 cases, values are coloured from best (green) to worst (red). Table 3-2 describes the cases (Hakala et al. 2019).

3.4 Description of spatial variability in stress field

The actual in situ stress tensors are expected to show a certain variability in space, due to the fractures and structures in the rock mass. Therefore, there will be a need to describe the variability, also denoted heterogeneity, in the stress model results or when presenting the direct measurement results. Such statistical methodology is presented in Figueiredo (2019).

The methodology to quantitatively describe the spatial stress variation, in a mathematically correct way requires that the analyses should treat stresses as full tensors and not as magnitudes and orientations as non-correlated scalars. The same way to calculate mean stress conditions and to use the covariance matrix and the effective variance to describe the heterogeneity can be used for measurement data and for “data” sampled in discontinuum numerical models. The technique is presented and exemplified by the work of Figueiredo (2019), and constitutes an improvement compared to previous stress modelling.

The study by Figueiredo (2019) furthermore shows that the full tensorial approach needs to be applied to at least seven overcoring measurements in a volume with negligible depth gradient in order to obtain a reliable result.

3.5 Description of uncertainty in stress field

There are several sources of uncertainty in the stress models. Some stem from the scarcity in measurement data, i.e., the minute number and often long distances between measurement points, with some contribution also from the uncertainty in stress measurement methods as such. If the latter is first neglected and assuming that several overcoring measurement points are located in the same far-field stress regime, the Euclidian average of these measurements should be the best prediction for this general far-field stress field, and the variation around the mean at the separate points is a measure of the heterogeneity of the stress in this volume as discussed in the previous section. Some of the variability observed is expected to be true variability but some is also expected to be due to measurement error, and, since it is not possible to separate these two from each other, the format for the description of this total variation (from actual variation and from errors) will be as a calculated variance of the overcoring measurement data. Such description, while being fully tensorial, will include heterogeneity both in magnitude and in orientation. This methodology to describe the heterogeneity, further described by Figueiredo (2019), is different from that applied in the previous site description, which was only using uncorrelated scalars instead of tensorial analysis.

Since the uncertainty is closely linked to scarcity of measurement data, there may be a need for describing the uncertainty differently for different domains (and/or depth intervals) of the analysed rock volume. A division into a number of volumes with respect to the uncertainty is therefore foreseen. With such differentiation in the description, the selection of appropriate stresses in the design and safety assessment work in a certain volume of rock is facilitated. However, before the collection of additional measurement data during construction of the accesses, when the model is quite uncertain, one single stress uncertainty estimation for the whole model will probably be used.

The results on stress magnitudes from the *different measurement methods* applied in Forsmark (overcoring and hydraulic methods) do not agree well with each other, e.g. (Sjöberg et al. 2005, Martin 2007, Glamheden et al. 2008, Backers et al. 2014, SSM 2018), see Table 3-4. So far, no investigators attribute the noted differences to spatial variation in the in situ stress field. They all consider that the differences in results between methods can be explained by sources of error in one or the other applied method or interpretation. This means that the epistemic uncertainty is currently significant in the model for stress magnitudes. Epistemic uncertainty is best described with judgement of confidence in qualitative classes, i.e. in text and not as calculated numbers, in the same way as was made in SDM-Site (SKB 2008).

Continued efforts will be made by SKB during the coming site descriptive modelling work with the aim to decrease the uncertainty in the in situ stress field, by further measurements with different updated technologies, as was described in the Section 3.2.

Table 3-4. Stress magnitudes predicted for the Forsmark area as presented in the SDM-Site (SKB 2008). The depth below surface is z in metres. The values by Martin (2007) are based primarily on overcoring data while the values by Ask et al. (2007) are based on hydraulic fracturing and hydraulic testing of pre-existing fractures.

Depth (m)	Maximum horizontal stress (MPa)	Trend (°)	Minimum horizontal stress (MPa)	Trend (°)	Vertical stress (MPa)
Martin (2007)					
400	38.7 ± 5.8	145 ± 15	20.4 ± 4.0	55	10.6 ± 0.2
500	41.0 ± 6.2	145 ± 15	23.2 ± 4.6	55	13.2 ± 0.3
Ask et al. (2007)					
400	19.2 ± 0.7	124 ± 6	9.3 ± 1.1	34	10.4
500	22.7 ± 1.1	124 ± 6	10.2 ± 1.6	34	13.0

3.6 Stress models for hydro-mechanical analyses

One of the safety assessment objectives is to analyse the potential transport of radionuclides by the groundwater in the bedrock from the repository and up to the biosphere (SKB 2010). The groundwater flow will for the most part take place inside the connected voids (apertures) of the fractures and therefore the process and analyses are hydro-mechanical in character. It is well known that the stress field controls the fracture displacements, leading to aperture changes, and this means that a successful H-M modelling will require a relevant stress model and a model for the stress versus transmissivity coupling (see reviews by e.g. Fransson (2009) or Thörn (2015)).

Since some numerical flow models are discrete, i.e., calculating the actual flow *inside each* fracture separately, the stress acting over each fracture can be a required part of the analysis. This is the case in particular when the analyses concern scenarios with changing effective normal stress and shear stress, such as the glaciation scenario. See further about the hydro-mechanical properties of fractures in Sections 5.6.2 and 7.1.2.

4 Intact rock properties

4.1 Strength properties of intact rock

4.1.1 Compressive strength

Uniaxial compressive strength tests are performed on core samples from all occurring rock types of significance in the investigated area. The test methodology is described in SKB method description (SKB MD 190.001e), which follows the ISRM standards (ISRM 2014). In the next site description, any additional uniaxial compression strength test on intact rock will be performed and evaluated in the same way as for the previous SDM, i.e. in accordance with Section 3.2.1 in Glamheden et al. (2007). The uniaxial compressive test result is collected in the form of a full stress strain curve and the peak load value, the uniaxial compressive strength (UCS), is used as the main descriptive parameter (Figure 4-1, see also Section 4.1.2 and 4.2). Note that all laboratory strength testing on intact rock, following the method description, should be performed on saturated samples. The influence on the strength of the degree of saturation and the salinity of the water was investigated in a limited study on rock samples from Äspö Hard Rock Laboratory by Jacobsson and Bäckström (2005). The saturated samples were about 10 % weaker than the dry samples. Natural formation water gave results in the same order as results from test using distilled water.

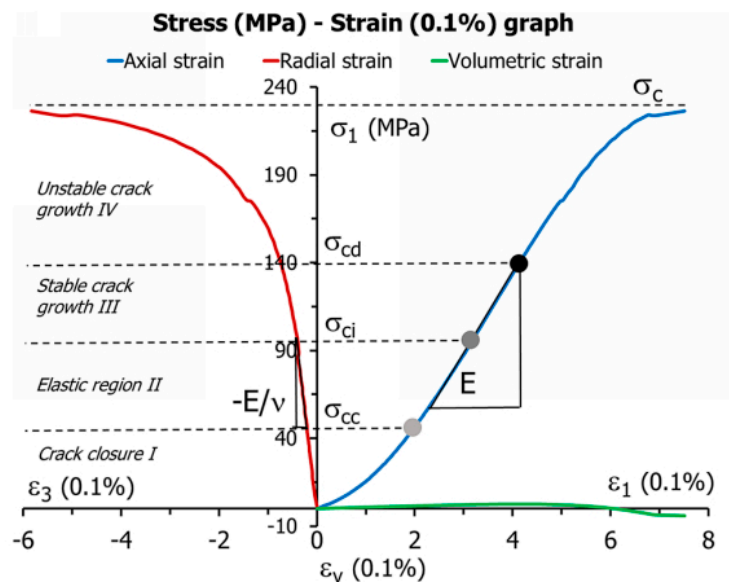


Figure 4-1. Stress-strain diagram obtained from a single uniaxial compressive strength (UCS) test. The UCS is defined as the peak stress value (σ_c). The graph also shows how crack initiation (σ_{ci}) stress, Young's modulus (E) and Poisson's ratio (ν) are determined (see following sections) (Quiñones et al. 2017).

To also determine the strength at different confined conditions, triaxial compressive tests have been performed in the laboratory, using the procedures ISRM (2014) described in SKB MD 190.003 following ISRM suggested methods. These results are the basis for determination of the Mohr-Coulomb and Hoek-Brown material model parameters, which is described in previous strategy reports (Staub et al. 2002) (Figure 4-2). It may be noted that the indirect tensile strength test gives higher tensile strength than that of Hoek-Brown that comes from the fit of the compressive strength test only. The tensile cut-off for the Hoek-Brown and Mohr-Coulomb failure models may be chosen independently with respect to indirect tensile strength data. These aspects must be considered by the user of the parameters, depending on the purpose of the modelling. This issue will be further elaborated in future model descriptions.

No change in the methodology for uniaxial and triaxial testing has been made. For updating the future rock mechanics descriptions, it is mainly additional testing that is foreseen, in order to have an appropriate number of samples for all main rock types occurring at the site.

4.1.2 Crack initiation stress

The crack initiation stress is determined when a uniaxial strength test (UCS) is performed, as part of the standard procedure and interpretation. Using the same laboratory compressive strength test results as for the peak strength (Figure 4-1) the point at which the cracking starts to increase is determined, Figure 4-3. The definition of crack initiation used is the peak point on a lateral strain versus stress curve, Figure 4-4. This parameter will be interpreted and included in the same way as in the previous SDM Site, i.e. Section 3.2.2 in Glamheden et al. (2007). The grouping of data for the descriptive model will be the same as for the peak compressive strength (UCS). Previous studies have shown a clearly evident correlation between the crack initiation stress and the peak strength, and therefore the strategy is to describe this parameter as a function of the UCS for each rock type separately. In Forsmark the performed site investigations show that the mean crack initiation stress for the different rock types is 50–54 % of the mean UCS value.

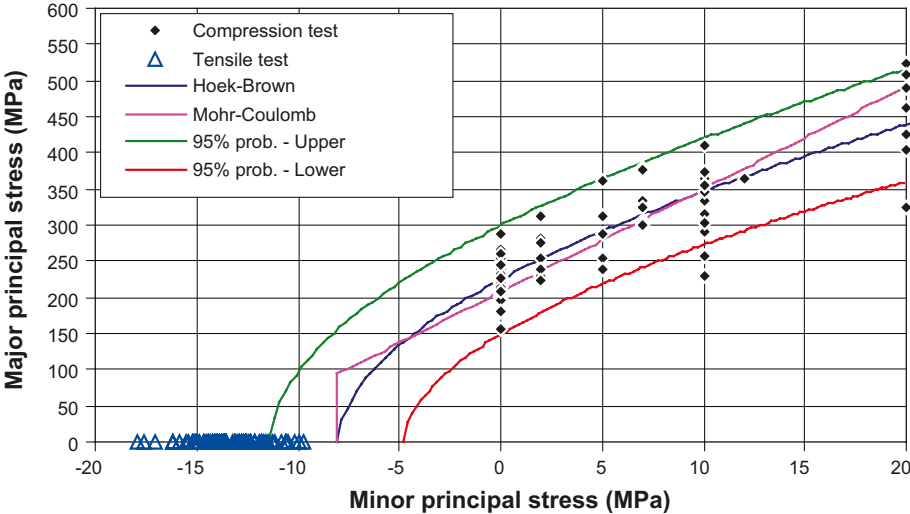


Figure 4-2. Example of how Hoek-Brown’s and Coulomb’s failure envelopes have been determined based on uniaxial and triaxial tests results for Granite to granodiorite (rock type 101057). The tensile strength data from indirect tensile strength tests (Brazilian tests) are also presented in this diagram, however not used for the determination of the failure envelopes (Glamheden et al. 2007).

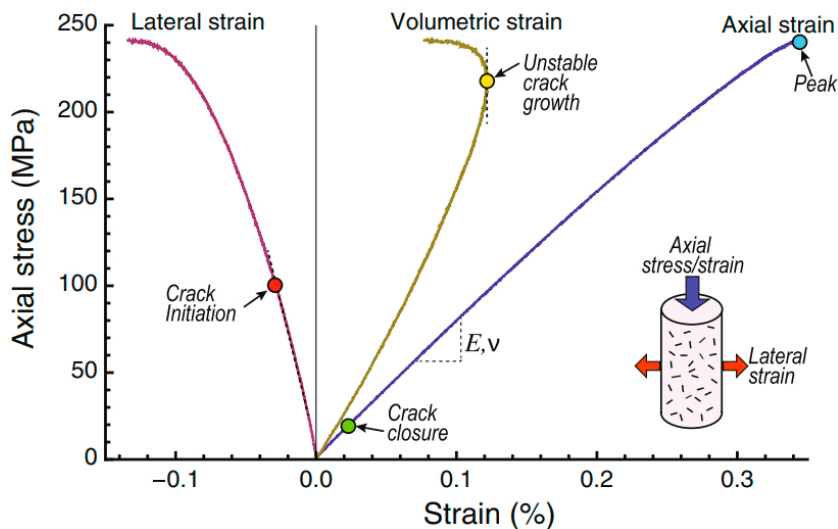


Figure 4-3. Typical stress-strain response in a uniaxial compressive test (Nicksiar and Martin 2012).

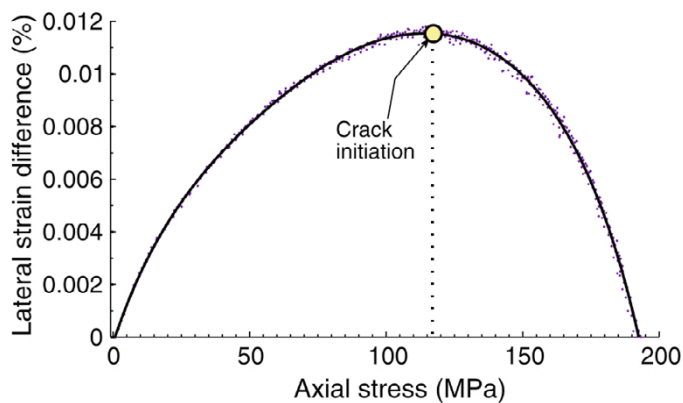


Figure 4-4. Definition of crack initiation stress parameter (Nicksiar and Martin 2012).

4.1.3 Tensile strength

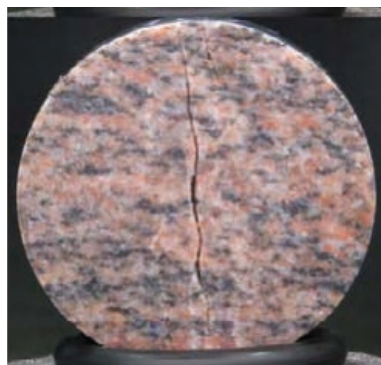
The tensile strength parameter is important for most of the mechanical processes that will be analysed, both for design purposes and in safety assessment. It has been used for example in the prediction of spalling.

The same laboratory methodology will be applied to determine the indirect tensile strength as previously applied. The methodology report for indirect tensile strength test (often called Brazilian test) is SKB MD 190.004e.

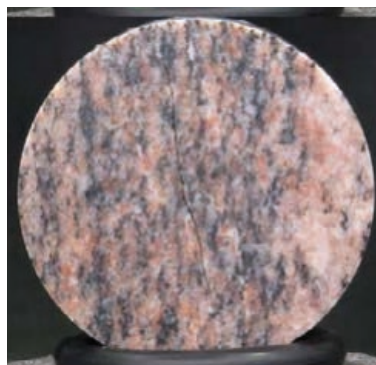
According to Perras and Diederichs (2014) the *indirect* tensile test overestimates the *true* tensile strength. To arrive at the true tensile strength the indirect results should be multiplied with a factor of 0.8–0.9 for igneous and metamorphic rock types. SKB has also performed some direct tensile tests and these results support the above noted magnitude in difference between direct and indirect measurements (Gorski et al. 2007). For the sake of convenience, the description will keep to the parameter indirect tensile strength, because this parameter is well established, and the test is much easier to perform. In the different applications where the tensile strength parameter is utilized, a reduction of the indirect tensile strength to the “true tensile strength” may be considered, depending on the analysis.

For the subordinate rock types at the site, where there is lack or scarcity in data, complementary tests are planned to be carried out to a limited extent, to give a more comprehensive description of the site. The rock types now foreseen to be additionally tested are amphibolite (Rock type ID 102017) and the albitized variant of granite to granodiorite (101057_104).

For some of the rock types the tensile strength dependency on orientation, i.e., the strength anisotropy may be included in the description. The orientation of tested samples is normally determined by the orientation of the drill core. However, when the foliation of the rock is oriented along the drill core axis, the anisotropy can be easily studied by loading the core “slices” in different directions. This direction with respect to the foliation is noted on foliated rock samples. Samples are also always photographed before and after testing. Examples of such photographs after loading in perpendicular direction to the foliation for granite to granodiorite (101057) and amphibolite (102017) are shown in Figure 4-5. As expected, the amphibolite is much weaker than the granite and also the strength is clearly lower when the compression is applied parallel to the foliation.



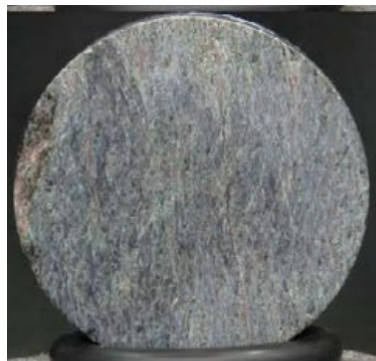
Tensile strength (MPa)
14.5



Tensile strength (MPa)
11.9



Tensile strength (MPa)
2.16



Tensile strength (MPa)
1.18

Figure 4-5. Example of results from indirect tensile strength test (Brazilian test). The upper two are samples of the most common Forsmark rock type, “granite to granodiorite” (101057) and the lower two are from the weakest rock type tested, amphibolite (102017). The left samples are oriented with the foliation perpendicular to the load direction and the right samples parallel to the load. The expected anisotropy typical for foliated rock types is seen in the strength results (Jacobsson and Sjöström 2019).

4.1.4 Fracture toughness

Fracture toughness is a mechanical property that quantifies the resistance of materials to the propagation of pre-existing fractures. The fracture toughness parameter will be used in the DFN methodology (DFNMM1, (Selroos et al. 2022)) in which the fractures are simulated including the propagation mechanism. Fracture toughness is further needed in all geomechanically based material models used to analyse rock mechanics strength and fracture propagation problems using the fracture mechanics approach. In the safety analysis these analyses will concern prediction of spalling and EDZ around deposition holes and deposition tunnels. The fracture toughness parameter may also become useful in the assessment of mechanical excavation techniques.

In SDM-Site the fracture toughness was not part of the presented parameters. However, this parameter will be added in the updated future site description. Laboratory testing of fracture toughness in Mode I, on samples from surface boulders at Forsmark has recently been performed, and further testing on samples from repository depth is planned. Figure 4-6 shows fracture toughness results from the literature for rocks with various strength. For Forsmark rock the tensile strength is typically about 11–17 MPa (Table 4-1) and, following the empirical relation in Figure 4-6 (a), the foreseen fracture toughness values would lie in the range 1.6–2.6 MPa m^{1/2}, and in the range 1.2–1.9 MPa m^{1/2} following the relation suggested in Figure 4-6 (b). The spread in test results underlying the empirical relations supports the suggested collection of direct site-specific data for the Mode I fracture toughness of the rock type at the future repository.

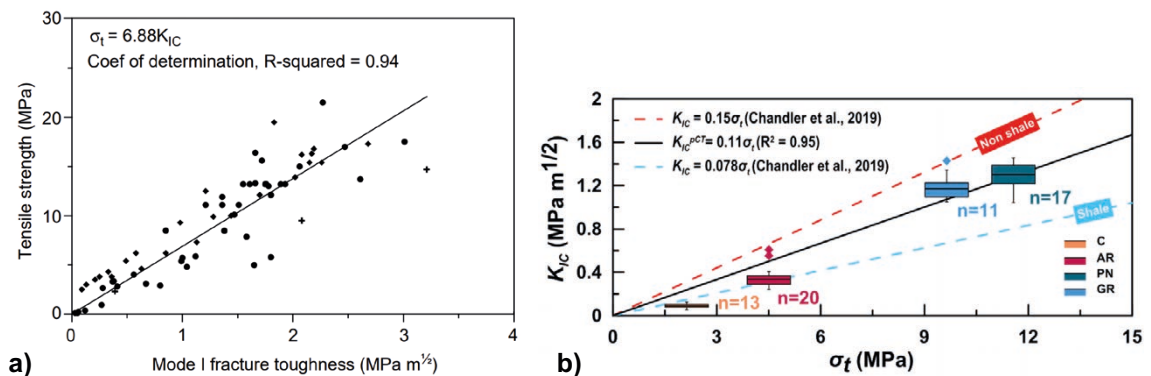


Figure 4-6. Empirical relation between fracture toughness and tensile strength of rock (straight line) together with test data from a) (Zhang 2002) and b) (Muñoz Ibáñez 2020).

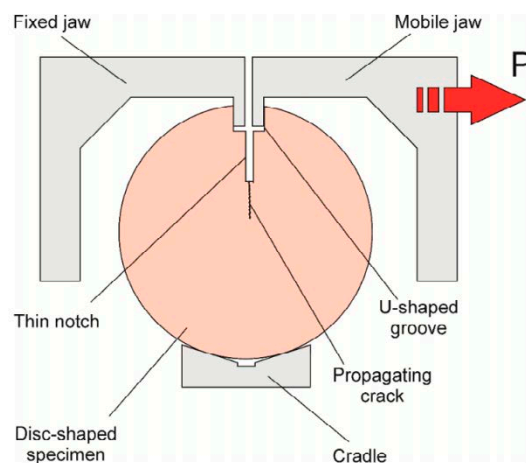


Figure 4-7. Experimental set-up of the pseudo-compact tension (pCT) test (Muñoz Ibáñez 2020).

There are several different laboratory testing methods to determine the Mode I fracture toughness. In the planned future tests the pseudo-compact tension (*p*CT) methodology recently developed will mainly be applied. Comparisons made between results from semi-circular bend (SCB) (ISRM 2014) and *p*CT are presented in Muñoz Ibáñez (2020) and Delgado-Martin et al. (2021) showing good agreement.

4.1.5 Cerchar Abrasivity Index – CAI

The CAI (Cerchar Abrasivity Index) is a laboratory test that is performed on broken surfaces of small rock core samples in order to assess the efficiency of mechanical excavation techniques, such as tunnel boring machines. The method measures the wear of the pick after scratching the surfaces with a specified length and load, Figure 4-8. The CAI test has so far been performed on a number of samples from Forsmark site and these results show a value of about five. The CAI values will be added to the SKB database (SICADA) and become part of the Site Description, as a new parameter. The methodology for the test follows the ISRM Suggested methods for CAI (Alber et al. 2013).

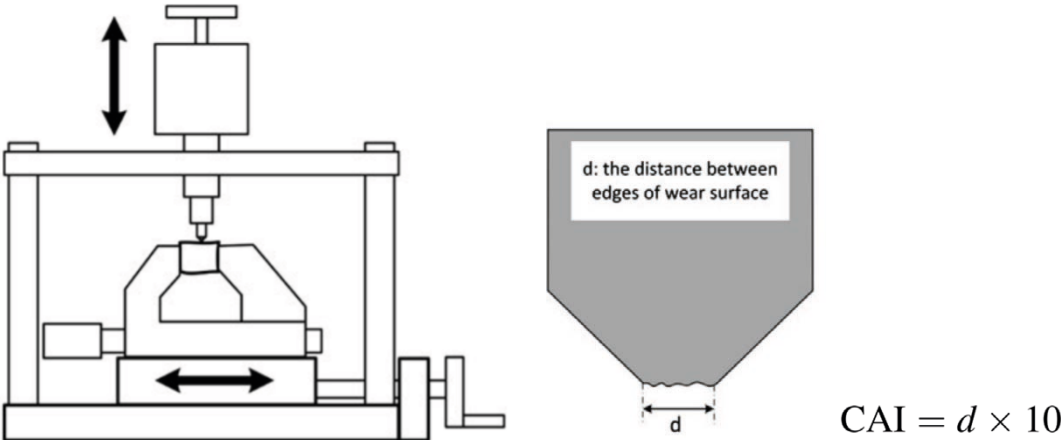


Figure 4-8. The Cerchar Abrasivity Index, CAI, is a test where the wear is measured after a specified scratching is performed on a fresh broken surface of the rock sample. Left: Example of one form of test apparatus. Middle: The wear *d*, in mm, is measured from a side view of the stylus tip after a 10 mm scratch. Five separate scratches are performed (Alber et al. 2013).

4.2 Deformation properties of intact rock

The deformation properties of the intact rock will be described using the Young's modulus and Poisson's ratio based on uniaxial compressive test results, in the same manner as in previous SDM (Glamheden et al. 2007, SKB 2008).

An example of results from SDM Site concerning deformation properties is shown in Figure 4-9. In these histograms the data for rock type 101057 is separated based on the fracture domains FFM01 and FFM06. In the latter domain the rock type is albitized and a clear influence on the Young's modulus and the Poisson's ration is evident. Similar differences were also noted in other mechanical properties.

Therefore, a change for the future description is that the albitized variant of rock type 101057 will be described separately, using a separate rock type identification (e.g. with the notation 101057_104 or 101057_Alb), and complementary laboratory testing will be performed to have a representative number of samples. According to SDM Site about 25 % of the planned repository rock volume has this albitized granite to granodiorite variant (albitized 101057) as the main rock type. Therefore, the importance of these rock type properties for the design, predictions and safety assessment need not be negligible. The strategy is to describe, and possibly understand and quantify, to what extent the degree of albitization influences the mechanical properties, since there will be a continuous range from very weak to strong albitization occurring in the repository volume (Stephens et al. 2007). Furthermore, the correlation between deformation and strength parameters and mineral composition for different variants of rock type 101057 will be analysed.

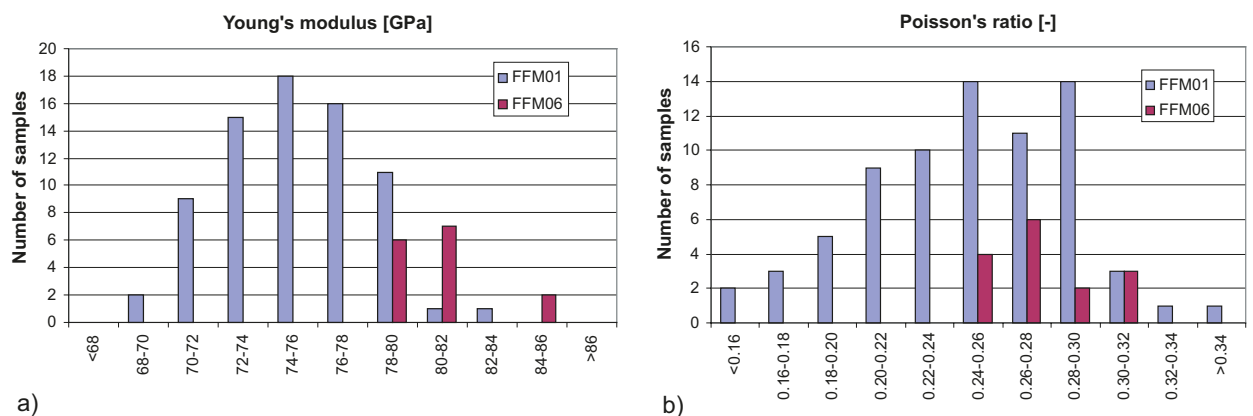


Figure 4-9. Frequency distribution of Young's modulus and Poisson's ratio (b) from uniaxial test on intact rock of rock type 101057 in two different fracture domains. In fracture domain FFM06 (corresponds to rock domain RFM045) the albitized variant of 101057 is dominating, and this explains the difference in the results compared to FFM01 (RFM029) (Glamheden et al. 2007).

4.3 Intact rock property parameter – Summary table

In general, the way to summarize and present the models for the intact rock property parameters will be made in the same way as previously done. Some minor changes are however proposed, as seen in Table 4-1 (which may be compared to Table 7-3 of SKB (2008)). The division is now made for the different rock types of the same ID, regardless of other characteristics and domains, and there is no specific description for intact rock inside or outside deformation zones. Depending on the potential variation or trends that could occur, based on sample borehole location or on degree of sample alteration for example, a refined division of rock types may become warranted. The numbers in the table are now taken from SKB (2008) but are only to be regarded as indicative and will be subject to reanalyses during future site description modelling based on the total available data inventory in the SKB database (SICADA). Empty fields are intended for the proposed new parameters.

Table 4-1. Summary table format, for deformation and strength properties for intact rock, suggested for descriptive models. Current values in table are from SKB (2008) or Glamheden et al. (2008). Empty cells are new suggested parameters.

Rock Type ID	101057	101057_104	101061	101058	101056	101051	102017
Parameters given as: Mean/Standard dev. Min–Max truncation ± Uncertainty %*	Granite to granodiorite, metamorphic No, or faint, albitization	Granite to granodiorite, metamorphic Medium to strong albitization	Pegmatite, pegmatitic granite	Granite, metamorphic, aplitic (albitized)	Granodiorite, metamorphic	Granodiorite to tonalite, metamorphic, fine- to medium- grained	Amphibolite
Number of uniaxial compressive tests	47	10	13	5	4	4	
Young's modulus (GPa)	76/3 69–83 ± 1 %	80/1 78–82 ± 1 %	74/4 69–80 ± 3 %	83/3 80–86 ± 3 %	77/3 73–81 ± 4 %	75 73–76	
Poisson's ratio	0.23/0.04 0.14–0.30 ± 4 %	0.29/0.02 0.26–0.31 ± 4 %	0.30/0.03 0.26–0.35 ± 5 %	0.27/0.03 0.25–0.31 ± 8 %	0.23/0.03 0.19–0.25 ± 11 %	0.29 0.28–0.29	
Uniaxial compressive strength, UCS (MPa)	226/29 157–289 ± 4 %	373/20 338–391 ± 3 %	214/32.8 158–266 ± 8 %	310/58 229–371 ± 16 %	236/12 222–249 ± 5 %	224 222–249	
Number of triaxial tests	44	0	5	0	0	0	
Cohesion in Mohr- Coulomb model (MPa)	28	–	33	–	–		
Friction angle in Mohr-Coulomb model (MPa)	60	–	56	–	–		
Constant m_i in Hoek- Brown model	28	–	18	–	–		
Number of indirect tensile tests	82	10	12	0	11	0	
Indirect tensile strength, ITS (MPa)	13/2 10–18 ± 2 %	15/1 13–17 ± 5 %	12/3 8–16 ± 9 %	–	18/1 17–20 ± 3 %		
Number of fracture toughness test							
Fracture toughness							
Number of CAI test							
Cerchar Abrasivity Index, CAI							

4.4 Scale effect in properties of intact rock

Many researchers have observed that there is an effect of sample size on results from compressive strength tests. At the same time most problems to be analysed concern rock blocks of sizes significantly larger than ordinary core sample size. For SKB both small and larger scales may be part of analysed issues. Therefore, to improve the description of intact rock in the SDM there is a desire to find a scaling law that is appropriate for the rock types in Forsmark (see also Figure 2-18 and Figure 2-22).

SKB has recently supported research work to study the influence on scale on the intact rock properties. This work is presented by Quiñones et al. (2017)) who have performed a series of laboratory test on Blanco Mera (Spain) granite samples of different sizes (Figure 4-10). In this work the USEL (unified size-effect law) model proposed by Masoumi et al. (2016) is applied on granite. This model incorporates both the *increase* in strength with size, and the *decrease* with size after a certain peak strength size is reached (see example results from the Blanco Mera granite in Figure 4-11). It may be noted that the size giving highest strength is the samples size SKB has used in the standard laboratory tests during site investigations (ca 53 mm core diameter).

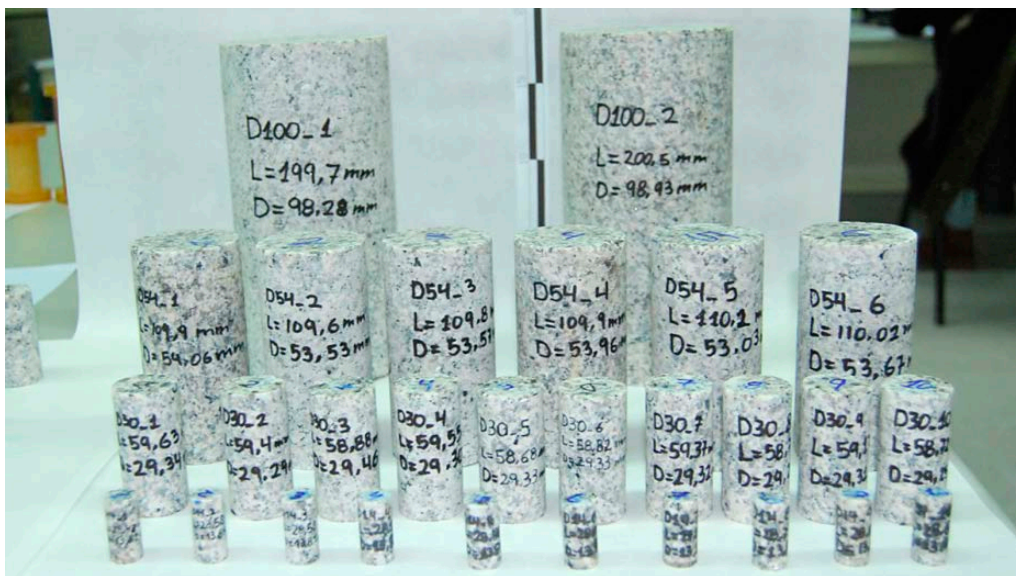


Figure 4-10. Set of Blanco Mera granite samples with diameter between 14 and 100 mm (Quiñones et al. 2017).

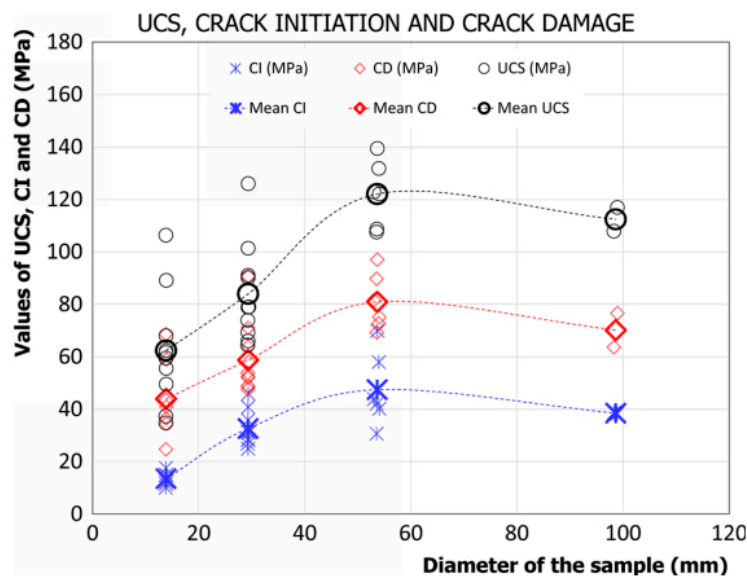


Figure 4-11. Results for CI, CD and UCS (Uniaxial Compressive Strength test) results for the different sample diameters tested (Figure 4-10) (Quiñones et al. 2017).

The same research group (Delgado-Martin et al. 2021) recently continued their studies on scale effects using samples from the two rock types in Forsmark, 101057 from rock domain RFM029 (samples shown in Figure 4-12) and 101058 from RFM045, which has provided site-specific data (Delgado-Martin et al. 2021). This is regarded important for the reliability of the intact rock description since the many mechanisms involved in rock strength are complex, and different rock types have shown different scale dependence behaviour (Quiñones et al. 2017).

The strategy in terms of the SDM is to present the parameter values statistics for the small standard laboratory scale samples (such as in previous description, see Table 4-1) with the scale dependence being described separately, for example using the USEL model parameters. This is considered the best way for the SDM since the scaling laws are still not well-established and because the appropriate property scale may be different in various future analyses.



Figure 4-12. Samples from rock type 101057 which is the most common rock type at Forsmark, dominating in domain RFM029. The smallest samples are 16 mm in diameter and the largest are 100 mm. b) The same samples as in a) but wet surfaces, which makes the grain size and typical foliated character of the rock type clearly visible.

4.5 Creep – Time dependent behaviour of intact rock

The final repository should keep its function for an extremely long time (ca 100 000 years), and it is therefore of relevance to consider also the time dependency in the description of rock mechanics properties. For the issue of long-term strength of intact crystalline rock, a special review was performed for SKB by Damjanac and Fairhurst (2010). This study examines the possibility that there is a strength threshold below which no time dependent decrease in strength occurs. Similarly, POSIVA performed a literature study on time dependency in the mechanical properties of crystalline rocks (Hagros et al. 2008).

While direct extrapolation for such long-time spans from a laboratory test is not possible (see Figure 4-13), the study by Damjanac and Fairhurst (2010) lends support to the proposed threshold strength concept from in situ measurement of current tectonic stress levels as well as analytical and numerical studies of the expected failure process on a grain level. Since it is stress corrosion at the crack tips that is thought to explain the time dependency, a condition for starting the corrosion is that some crack has first developed, and therefore the long-term strength, of a fully intact rock, should be equal to or greater than the crack initiation strength.

The conclusion from their study is that a long-term strength threshold does exist and that it is likely to be a significant proportion of the measured crack initiation stress, i.e., about 40–60 % of the UCS. They suggest that a realistic estimate of the time-independent strength should be 45 % of the standard laboratory uniaxial compressive strength, UCS.

Based on the results from Damjanac and Fairhurst (2010) it is judged that no additional model parameter is necessarily required apart from what is already chosen for intact rock. If the ultimate time-independent strength for the intact rock is to be part of any assessment, the uniaxial compressive strength (UCS, Section 4.1.1) and the crack initiation stress (σ_{ci} , Section 4.1.2) can be utilized as proposed by the authors.

A relevant aspect is that the UCS is determined following a standard procedure, which takes a few minutes under loading until it breaks. The ISRM standard prescribes the loading rate of about 60 MPa/minute (i.e., a constantly increasing axial load), which means that the UCS is a measure of short-term strength.

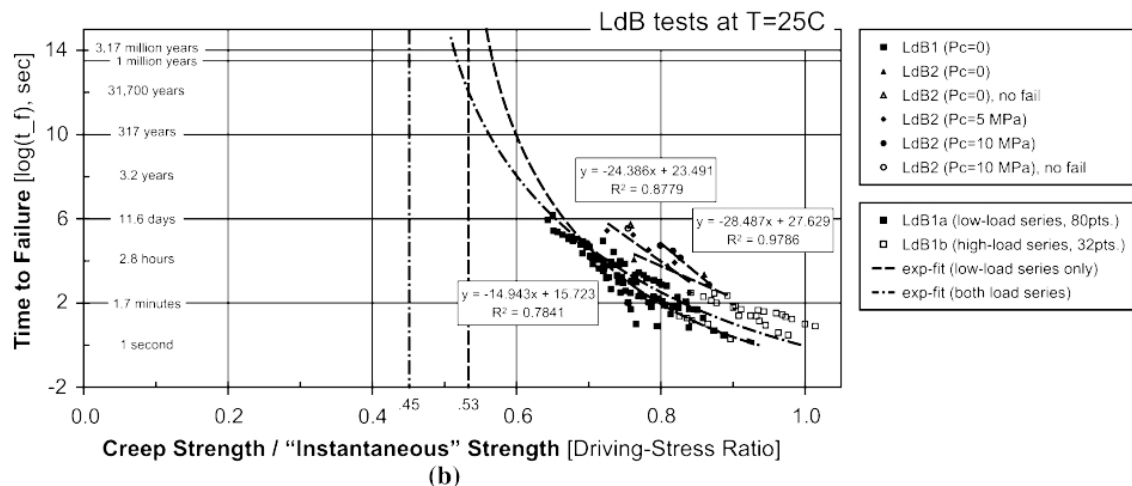


Figure 4-13. Creep test data for the Lac du Bonnet granite showing exponential extrapolation of test result data (Damjanac and Fairhurst 2010).

The SKB method description for compressive test (SKB MD 190.001) prescribes the use of the radial strain signal as the feed-back signal to control the compression. The loading rate is set to a radial strain rate of -0.025 %/min. In this way one can cope with the brittle rock sample's post-peak behaviour. Experimental differences, such as the loading rate, are important to recognise when comparing sample behaviour, curve interpretation and parameter definition details, from different test series or laboratories. However, for the issue of long-term strength the uncertainty in modelling will probably arise mainly from scarcity of laboratory data and from the inherent uncertainty while extrapolating from shorter time span data (cf Figure 4-13).

To verify the assumed long-time strength of the rock samples some laboratory test with longer loading periods will be specifically performed on Forsmark rock samples. These results will serve as a support to the previous results found in the literature regarding the relation between short-time and long-time strength for the intact rock.

For time dependent properties where fractured rock (i.e. the rock mass) is involved in the studied process, it has been shown by Glamheden and Hökmark (2006) that the time-dependent properties of the fractures will dominate over the intact rock properties (see further Section 5.7.4).

5 Single open fracture properties

This chapter is structured such that the first two sections, Section 5.1 and 5.2, present properties and parameters which certainly will be included in the future site descriptions. The way to summarize and present these properties will, to a large extent, follow the methodology applied in SDM-Site (Glamheden et al. 2007). The next three sections (Section 5.3 through 5.6) deal with fracture characteristics parameters, which will be added or modified compared with SDM-Site and it thus includes new methodology.

The subsequent Section 5.7 is a discussion that brings up various potential sources of bias or shortcomings in the results and models. These factors are brought forward to reflect and explain the complexity of mechanical processes and the limitations of the proposed parameters, but the strategy is not to describe them quantitatively in the site description.

5.1 Fracture normal and shear stiffness

The fracture normal and shear stiffnesses are determined from laboratory tests on small samples collected from drill cores. The methodology for new tests will be slightly modified compared to what was previously used in SDM-Site (SKB 2008). The scale and the type of test is of importance for the test results and the work on modifying the laboratory test procedures is ongoing within SKB R&D program (e.g. Siren et al. 2017, Larsson and Flansbjerg 2020).

During the SDM-Site investigation phase the laboratory fracture test performance was improved in three steps, which was reported in Glamheden et al. (2008). In SDM-Site an attempt was made to calibrate results from the different procedures such that all laboratory results could be used. However, since there still seems to be a tendency to systematic differences in results, the confidence in the latest test procedure “Test III” is considered higher. The foreseen choice for future updated descriptions is to include only existing results from the “Tests III” test procedure, together with new laboratory results when available.

The previous laboratory tests and modelling showed a large spread in results for normal stiffness (see Table 5-1 and Figure 5-1). This result is to be expected since all different types of fractures are lumped together and stiffness is sensitive to many factors, for example the fracture infillings and the matedness of fracture surfaces.

Table 5-1. Results from direct shear tests on open fracture sampled in fracture domain FFM01 and deformation zones (DZ). The tests include 29 samples from FFM01 and 10 samples from three DZs. (SKB 2008).

Parameter	FFM01		DZ	
	Mean/stdev Uncertainty	Min–Max	Mean/stdev Uncertainty	Min–Max
Normal stiffness (MPa/mm)	656/396 ± 22 %	159–1 833	662/729 ± 68 %	167–2 445
Shear stiffness, K_{s20} (MPa/mm)	34/10 ± 11 %	18–52	31/8 ± 16 %	19–44
Peak friction angle (°)	37/3 ± 3 %	29–42	35/2 ± 4 %	32–38
Peak cohesion (MPa)	0.8/0.3 ± 14 %	0.2–1.3	0.8/0.5 ± 39 %	0.0–1.7
Residual friction angle (°)	34.9/3.4 ± 4 %	28–42	35/2 ± 4 %	30–37
Residual cohesion (MPa)	0.3/0.2 ± 24 %	0.1–0.8	0.3/0.2 ± 41 %	0.0–0.6

Note: Shear stiffness determined under 20 MPa normal stress. The uncertainty of the mean is quantified for a 95 % confidence interval. Minimum and maximum truncation values are based on the observed min' and max' for the tested population.

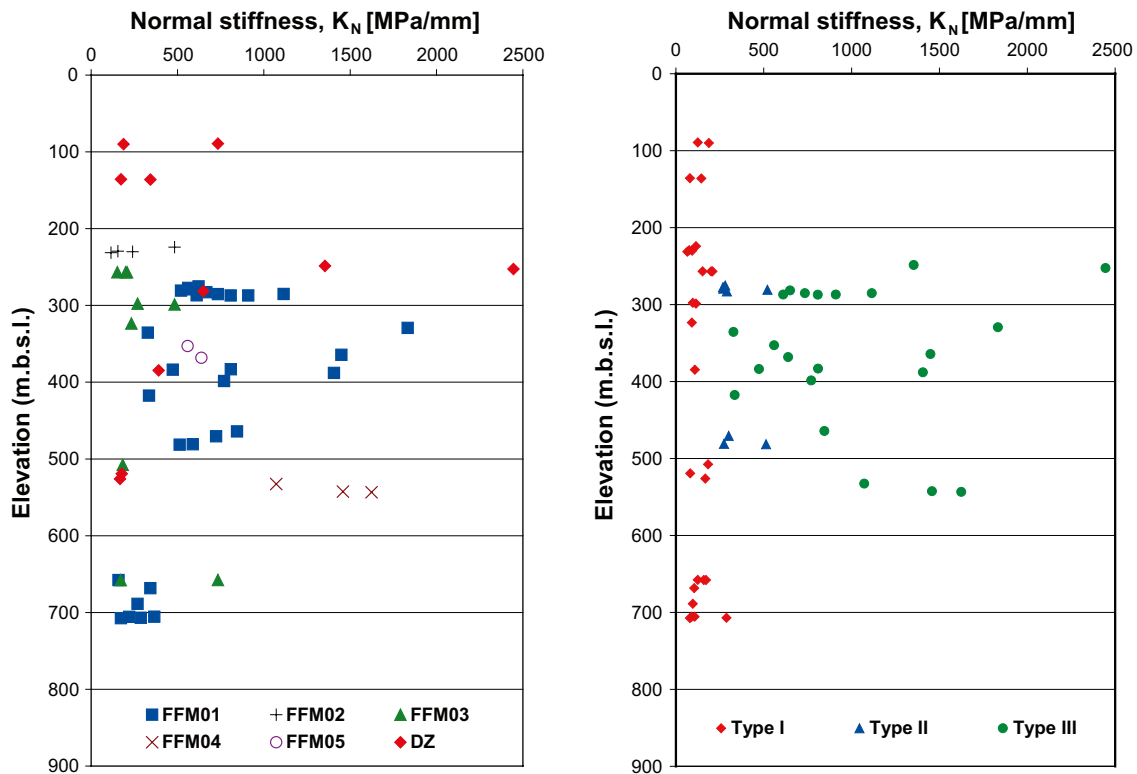


Figure 5-1. a) Normal stiffness k_n of all open fractures tested in laboratory from the SDM-Site stage (Glamheden et al. 2007). Type I and Type II results are “converted”, see text. b) The data available earlier at stage 2.2, with the result sorted based on the test type (without conversion) (Olofsson et al. 2007).

The laboratory tests on fractures up to date included two loading-unloading cycles with only normal loading, with a normal stress ranging from 0.5 MPa to 10–20 MPa, (see example in Figure 5-2), in which the normal stiffness parameter used is determined as a secant from the minimum and maximum stress points of the second loading curve (the maximum load has varied between tests, but it is most frequently 10 MPa).

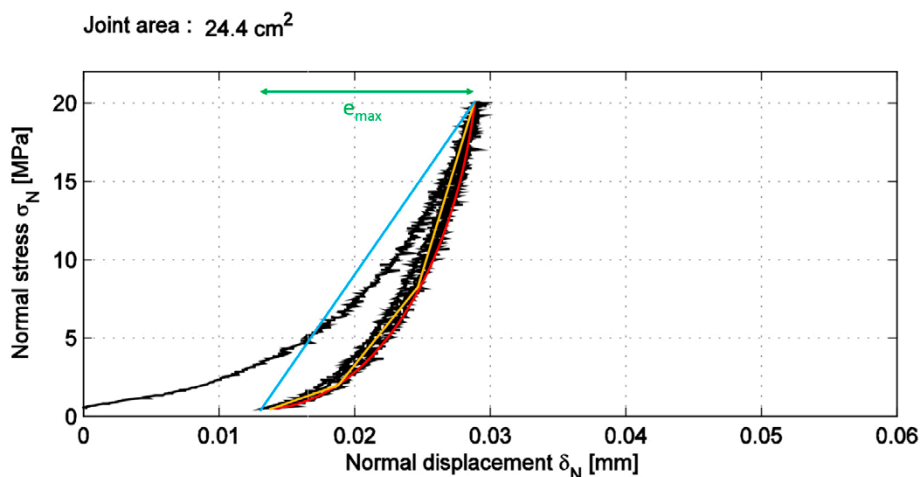


Figure 5-2. Example of the normal displacement directly measured using two crack opening displacement (COD) gauges (Jacobsson and Flansbjerg 2005). The strategy for next SDM is to fit an exponential function to the laboratory unloading curve using the approach by Zangerl et al. (2008) (red line added here). The orange dashed straight lines show how the laboratory result will also be described with three stiffness values for three stress intervals. The previous stiffness parameter was defined as a single secant (blue dotted line). The green arrow and parameter e_{max} indicate the maximum closure variation (e_{max} is used in the definition of a transmissivity-stress model, see Equation 5-2 and Figure 5-13 in Section 5.6).

For the future site description, the strategy is that stiffness is given as a normal stress dependent value, instead of the single value used previously. This will be made through a nonlinear elastic joint constitutive model using a new parameter, the “stiffness characteristic” following the proposal by Evans et al. (1992), further applied by Zangerl et al. (2008). It consists of a best fit semi-logarithmic function to the second unloading curve of a laboratory normal loading test (red line). The model is a function between the closure $-a_m$ to the effective stress σ'_n as in the following equation:

$$-\Delta a_m = \frac{1}{\frac{dk_n}{d\sigma'_n}} \ln (\sigma'_n / \sigma_n^{ref}) \quad \text{Equation 5-1}$$

Where $dk_n/d\sigma'_n$ is a constant denoted *stiffness characteristic* which together with the reference load σ_n^{ref} are the only parameters needed to describe the deformation curve. To obtain a certain total aperture the aperture at the starting reference load is also needed. For the Forsmark case the reference/start load will be 0.5 MPa, since this is the so-called seating load at which the normal stiffness measurements started. Apart from this functional description, three different normal stress level intervals are suggested to determine constant stiffness values, as previously using the secant of the second unloading curve, preliminary for the normal stress intervals (0.5–2 MPa, 2–8 MPa and 8– $\sigma_{n,max}$ MPa), see Figure 5-2.

This improvement, with several normal stiffness parameters, is planned because the rock mechanics analyses often include fracture processes at a wide range of normal stress levels and, as has been shown above, the stress level has a significant influence on the stiffness and therefore also on the results of the analyses.

A new methodology that in the future may be available for accurate measurements of small movements, such as in the fracture normal loading laboratory tests, is based on Digital Image Correlation (DIC). Because DIC is a non-contact technique it is flexible, and its applicability is promising. At present SKB is testing this technique within the R & D program (Jacobsson et al. 2021).

Another type of testing technique for fracture surface characterization, is the Leeb hardness test (LHT) (Corkum et al. 2018), and this technique will be evaluated within the work with the future rock mechanics descriptions. The LHT involves an instrument similar to the traditional Schmidt hammer but expected to be better suited to measure the thin joint surface materials because the size and energy impact of the hammer is less. The LHT will first be tried on intact rock surfaces (the wall rock to fractures) and the stiffness and strength compared with laboratory test results. If this “calibration” is successful, the LHT may be used on fracture samples in drill cores to support the description of fracture properties. The method further enables comparison of drill core fractures with fractures tested in the laboratory and may be utilized directly on fracture surfaces in the field during excavation. The LHT is fast and non-expensive and therefore attractive to use. Since many fractures can be tested at acceptable costs, this method may help in describing the variation within fractures planes and between different fracture sets of the network.

5.2 Fracture shear strength and dilation

The shear strength parameters are determined from laboratory tests on the same small samples from the drilled core first used for normal stiffness measurements. The methodology applied in previously performed laboratory tests is described in SKB method description (MD 190.005e) and in the P-reports of respective test series. A summary of results is presented in Table 5-1. These data will be retained, but the laboratory methodology may be slightly improved based on ongoing research, and some additional testing will probably be performed before the next SDM. Complementary fracture samples will be taken from existing and possibly from new core drill boreholes and these new tests are planned to use constant normal *stiffness* (CNS) procedures as opposed to the previously employed constant normal *load* (CNL) tests (see Section 5.7.1).

One aspect of fracture shear is that the shearing normally includes some degree of dilation, where dilation is the term for the fracture normal opening displacement that follows with shearing. The fracture surface roughness, the fracture surface minerals and the fracture wall strength will, together with the normal load applied, determine how large the dilation during shearing will be. The dilation is normally

expressed as an angle between the general fracture plane, being parallel with the shear load direction, and the actual movement direction, which with the dilation will be slightly upward. Dilation was part of the previous description with an estimated value for three different normal loads (0.5 MPa, 5 MPa, 20 MPa). As an example of previous results: the dilation was determined, on the average for fracture domain FFM01, to be 14.6° for a normal stress of 0.5 MPa and, clearly lower, 3.2° for a normal stress of 20 MPa (constant normal load tests) (Glamheden 2007).

In traditional laboratory fracture testing the normal load is often kept constant when shearing (CNL test), but in situ, and specially at depth during the actual process, the dilation due to shearing will cause the normal stress to increase significantly, since there is confinement which acts against the opening movement. This is why laboratory experiments are now frequently made instead as a constant normal stiffness test (CNS test), see example results in Figure 5-3. It is clear from this figure how the curve from CNL test (green) differs from CNS tests. At any moment of a CNS test, the dilation may be determined, and compared with results of CNL tests if desired. The dilation at peak load in the CNS experiment is normally one of the determined parameters, while after a long shearing the dilation normally decreases compared with the initial dilation, and this may be of importance for the modelling results.

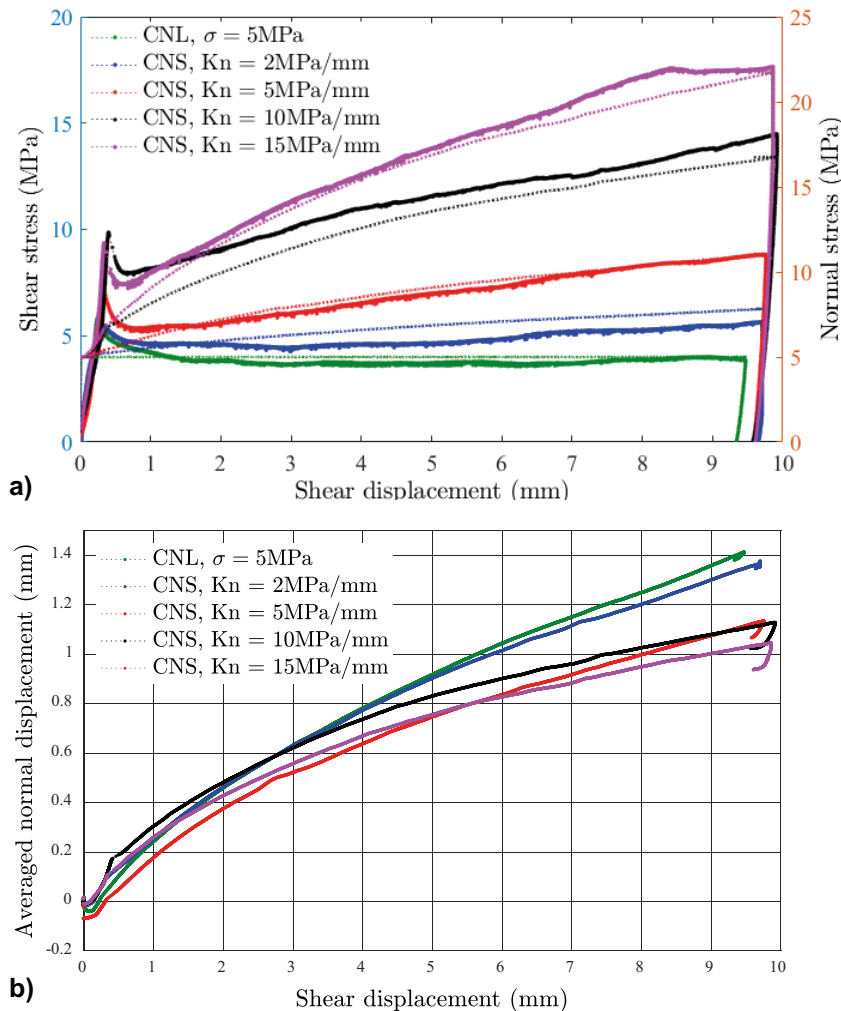


Figure 5-3. Example of results from constant normal stiffness shear test (CNS). (a) Shear stress and normal stress (dotted curves) versus shear displacement; (b) Averaged normal displacements versus shear displacement (Zou et al. 2020).

5.3 Fracture aperture

The description of the fracture surface geometry and aperture are key for deriving reasonable fracture physical properties (hydraulic, mechanic and coupled properties). The aperture is conceived as the spacing between fracture walls, i.e. a measure of the “thickness” of a fracture orthogonal to the general fracture surface orientation (Figure 5-4). Natural fractures are always more complex than the simplified parallel plate model where the fracture aperture and orientation are assumed constant. The walls of a fracture may be unambiguously defined only for fresh fractures with fracture walls as irregular and rough surfaces. In addition, any natural fracture contains some infilling materials like minerals, alteration, stagnant pores, micro cracks, sealed portions, gouge and small rock fragments (see Figure 5-4).

The geometric aperture is a pointwise entity over the fracture surface, the open distance perpendicular to the overall fracture plane. It is also known as the physical/mechanical/real aperture. The pointwise geometrical aperture can be determined in the laboratory using pointwise measurements, e.g. from photos of sections across the fracture or from fracture surface scanning. The average geometrical aperture, associated to portions of or entire fractures, can be deduced from the distribution of local values.

The hydraulic aperture, e_h , is another average quantity over a fracture, deduced from fracture transmissivity measurements (transmissivity T expressed in m^2/s) and from the so-called cubic law (see Equation 5-3). It reflects the capacity for a fracture to carry a certain amount of flow and is expressed as an equivalent aperture (see Equation 5-3).

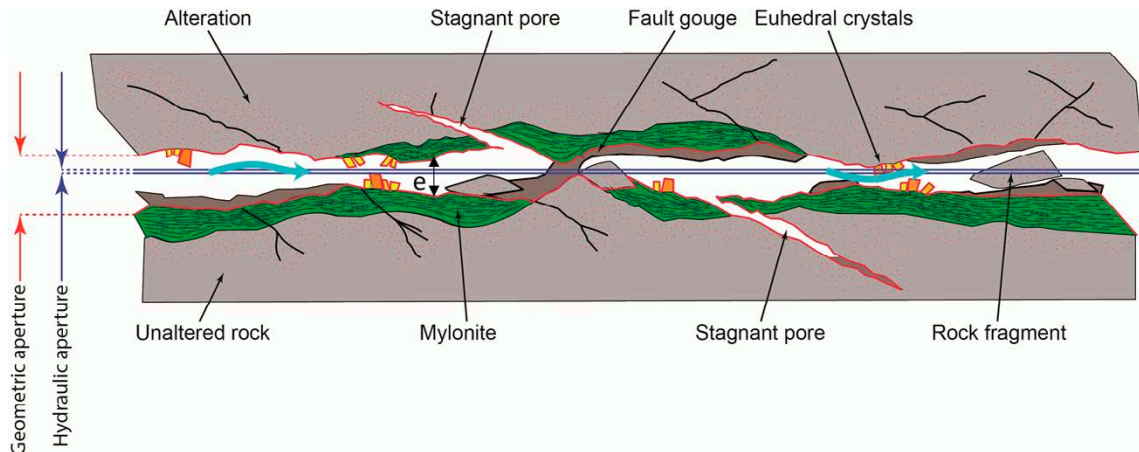


Figure 5-4. Schematic illustration of fracture surfaces, mineralogy, and different types of apertures on a cross section through a fracture: geometric aperture e (red colour) and hydraulic aperture e_h (blue colour). Modified from Winberg et al. (2000). See text for details.

5.4 Fracture surface geometry properties

5.4.1 Small scale surface geometry – Roughness

Small scale surface geometry typically refers to data samples from core diameter size (c 5 cm) up to a maximum of about a metre in size, hence dimensions which are manageable in laboratory conditions. Roughness is often understood as variations over fracture walls on a scale in the order of the aperture or smaller.

As part of the strategy for the future site modelling, results from fracture surface scanning will be added as a new component of the description of fractures. The strategy is to include a more quantitative and elaborate description of small-scale fracture surfaces, compared to previous models, while the details of this description have not yet been established.

Such measurements will be part of future laboratory fracture tests within the site investigations. Scanning techniques and surface characterization metrics are under development, but a standardized methodology is not yet finalized. Stigsson and Mas Ivars (2019) and Stigsson (2018) suggest the use of the fractal dimension parameter H (Hurst exponent) together with the standard deviation of height differences for points 1 mm apart (see also Section 6.7 in DFNMM1, (Selroos et al. 2022)). Finenko and Konietzky (2021) propose the use of the Hausdorff distance as a metric to quantify the 3D fracture aperture.

The metrics to be established from the lab scale and high resolution scanning techniques will be also compared with slightly larger scales and fracture surface roughness measured from tunnel fracture traces at depth as recently done at the ONKALO and Äspö HRL. Stigsson (2015) suggests, with some uncertainty, that the estimated parameters for the fractal surfaces do mimic the statistics of the traces and surfaces from ONKALO and Äspö HRL.

The objective of collecting such detailed surface geometry data is to enable future studies of the correlation between the surface geometry and the other laboratory test results, such as the shear strength, dilation and the normal and shear stiffnesses. Scanning results will provide accurate, objective data in 3D as a complement to the traditional index JRC (Barton and Choubey 1977) used to describe the fracture surface roughness. JRC will still be determined for new fracture samples to further enable demonstration of the coupling between JRC and surface scanning results. With improved understanding of the surface characteristics, it will also be easier to support the assessment of bias in laboratory results (see Section 5.7).

5.4.2 Large scale surface geometry – Undulation

Large scale surface geometry and possible undulation typically refer to fracture trace mapping with observations made over tunnel dimensions, from resolution in mapping usually down to 0.5 m and up to the standard length of tunnel sections (a few tens of meters), or fracture trace data from detailed outcrop mapping or outcrop drone surveys. Waviness generally refers to fracture surface irregularities much larger than the fracture aperture and undulation refers to large scale variation wavelength (metre scale).

Waviness and undulation measurements from fracture trace mapping also differ from roughness measurements in that they can often be simultaneously related to the fracture size scale itself. It is the case when fracture tips of a mapped fracture trace are observed, i.e. when the fracture trace is not fully crossing the observation. This is a major distinction relative to core and laboratory observation scales where sampled fractures generally are much larger than the scale over which they are analysed.

Trace map data collected at various sampling scales are already extensively used to construct DFN models (DFNMM1, (Selroos et al. 2022)). They can also be used in building improved models describing the surfaces at a scale closer to the actual scale of the main safety concern to be assessed, e.g. a critical shear of a very large fracture (See Section 2.5). By applying a stochastic approach these fracture surface models can be used to calculate the fracture shear strength as suggested by e.g. Casagrande et al. (2018).

Theoretical and numerical analyses by Lönnqvist and Hökmark (2015) have shown that if a large scale undulating fracture geometry is simplified into a regular “wavy” shape, the displacement due to a certain perturbation along this surface will decrease due to the change in angle of the sliding contact areas.

The strategy is therefore to try to collect supporting field data on fracture undulation from outcrops and future excavated walls of tunnels and caverns in the planned central area of the repository, and to express the surface description as a span for the angle deviation. This span can be used to better estimate the actual shear movement and shear resistance of undulating fractures (see also Section 5.5.3).

5.5 Influence of sample scale on fracture parameters

5.5.1 Fracture scale issue

Natural fractures of multiscale systems, as in Forsmark, are more complex than the idealized and simplified concept that a single fracture is a simple 2D planar surface of finite size. Real fractures are more complex than this with e.g. branching, infilling, alteration and fragments, and the larger the fractures the more complex they are.

This is acknowledged in the first steps (Chapter 1) of the DFN modelling methodology described in DFNMM1 (Selroos et al. 2022) where “the term DFN modelling defines how a fractured rock mass (the natural fracture system) can be equivalently and quantitatively represented as a population of individual, fracture-like, idealized tabular objects, including their geometrical and physical properties”.

Hence, defining relevant and appropriate geometrical and physical properties to large fractures, for instance to (major) faults, is at the core of the most important issues related to fractured rock modelling, including rock mechanics. Two scale issues can be distinguished (Figure 5-5):

- For a given fracture, the fracture sample available to measure the fracture mechanical properties, and laboratory testing conditions, is in most cases much smaller than the target fracture size scale of the problem at hand. This is called the sample scale issue.
- When the typical properties of a fracture belonging to a given size scale (e.g. a small, simple fracture) are known, how to extrapolate or demonstrate that the same properties are relevant also to fractures of different size scales (e.g. very large fractures are critical for earthquake modelling scenarios). This is called the size scale issue. This issue can be generalized to any type of fracture (possibly defined by reference to the geological history or the stress field and its orientation, etc).

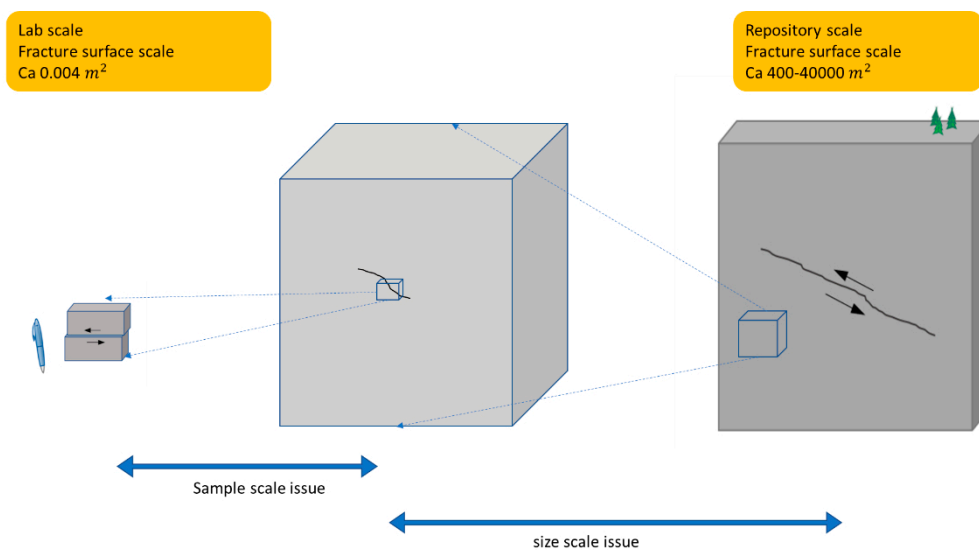


Figure 5-5. Schematic illustration of the size and sampling scale issues. The repository scale on the right symbolizes safety assessment relative to modelling the maximum shear that can be expected from earthquake triggered by the largest deformation zones at the repository scale.

Within the safety assessment, in particular, for the calculation of maximum possible shear that could occur on fractures intersecting the future repository (cf Section 2.5), the target fractures are in the order of 50–300 m in diameter (Lönnqvist and Hökmark 2010, Hökmark et al. 2019). The character and even the existence of such large fractures is hard to identify, study and verify in the field. Over this range of size scale, the fractures depart from single 2D shapes and likely gradually show increase in their structural complexity when increasing size scales (see Figure 5-6).

Figure 5-6a gives one example of the type of data available from outcrops in Forsmark. This type of mapped area provides fracture traces up to tens of meters in length. One can note the unclear transition between what could be considered an assembly of a large number of shorter fractures or one single weakness plane of a fractured zone. It is also notable that there are long fractures both along the bed-rock lithology pattern and in the direction across it. Some fractures terminate against each other, but some also intersect other fractures and create blocks of rock. The next scale that underpins the fracture size models of the Forsmark site is based on lineament studies (Figure 5-6b). In this type of maps the structures are documented as lines but the detailed internal structures could well be more complex, and the individual lineament often corresponds to a deformation zone rather than a single fracture.

The task to describe the site fracture network in 3D has been undertaken under the investigation phase in Forsmark (Fox et al. 2007, SKB 2008) and the work has continued thereafter (DFNMM1, (Selroos et al. 2022)). The very basic principles of DFN modelling are described in Section 2.6.1. The approach sets out to define the simplest possible description of the multiscale fracture population as a DFN model of *fracture-like* objects to which hydraulic and mechanical properties should be assigned. The approach has been to find a common stochastic description that connects the mapped patterns from the smaller scales, borehole and outcrops, as well as the larger scales. These discrete fracture networks (DFN) make it possible to make prognoses about the fracture intensity, fracture size and the orientation of fractures in the 3D space. The DFN model representation is the most relevant modelling workflow and data integrator to combine multiple size scales geometries and physical processes.

With regards to the earthquake safety assessment scenario, there is still a challenge in determining appropriate mechanical properties for the target size scale. To avoid the sample and size scale issues for determining the target fracture mechanical properties, the approach in the previous SDM stage was to assume conservative strength values, rather than using values based on actual measurements.

In the updated strategy it is recommended to introduce limits when using laboratory-derived data in assigning mechanical properties to specific fracture size ranges. While it is very difficult to measure fracture sizes in situ, it is suggested to use as much as possible indirect input information relative to fracture sizes to specify the abovementioned limits. One idea is to introduce a new fracture “class” based on water-bearing fractures (named PFL-fractures by reference to their identification using the Posiva Flow Logging tool, PFL (Rouhiainen and Sokolnicki 2005)). The specificity of the water bearing fractures is further discussed in Section 5.6.3.

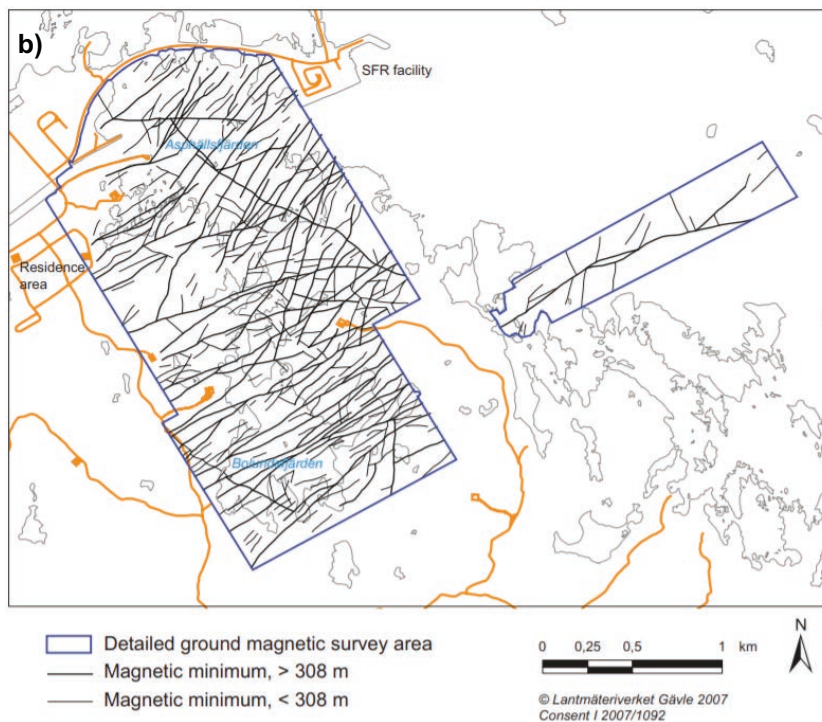
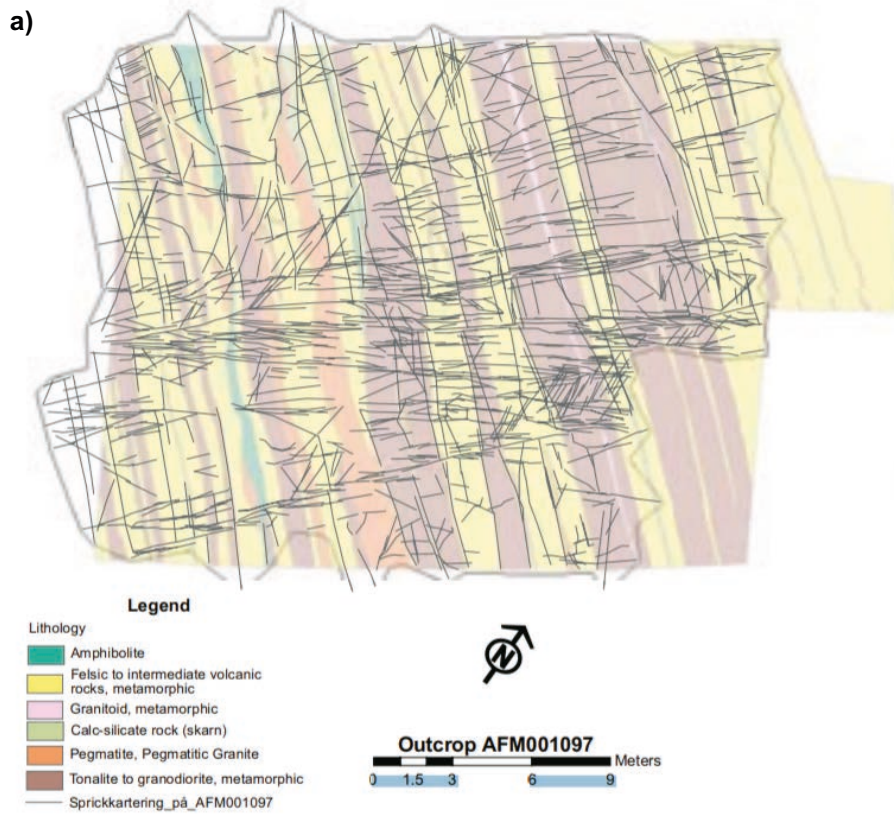


Figure 5-6. a) Example of mapped fracture traces and bedrock geology on outcrop AFM001097 in Forsmark. (Stephens et al. 2007). b) Lineament map based on magnetic minima based on the ground magnetic survey of the Forsmark site (Stephens et al. 2007).

5.5.2 Upscaling for smaller fractures

The sample scale issue, even if only considering single plane fractures of sizes less than a meter, is not an exhausted field of study. Researchers are still discussing the best approach based on current understanding. One recent work has been presented by Johansson (2016), who developed a theory to predict fracture peak shear strength based on adhesion theory, the fractal surface parameters and the knowledge of fracture surface matedness. Figure 5-7 shows an example of the results from this research, which indicates a lack of scale dependence between samples of 60 mm and 200 mm size, irrespective of the fracture being mated or unmated. The figure further shows that the fit between the conceptual model and the laboratory results is quite good for this test series.

Further experimental and analytical research has been carried out (e.g. Ríos Bayona 2019, 2022, Ríos-Bayona et al. 2021) to further develop the constitutive model of Johansson and Stille (2014) and Johansson (2016), in a project partly financed by SKB (Figure 5-9 and Figure 5-9). In this project the shear box at LTU has been used. Additionally, the newly built shear box at RISE in Borås as part of the POST2 and POST3 project (Jacobsson et al. 2021), which is co-financed by NWMO and SKB, is also being used for testing even larger fracture samples (e.g. 500 × 300 mm).

The strategy for updated description of fracture shear strength is currently to present the parameters for small scale samples, and to add a discussion on upscaling, including some upscaling alternatives based on the latest results available at the time. The intention is that the shear strength function chosen is corresponding to the fracture roughness description parameters chosen (Section 5.4.1).

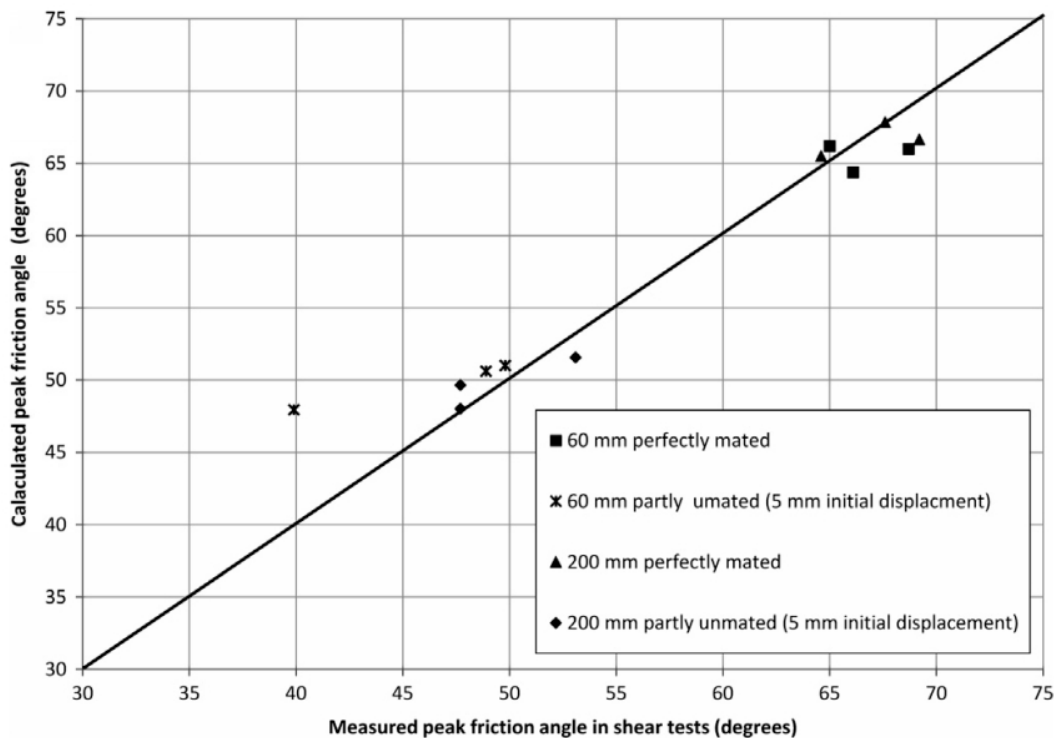


Figure 5-7. Comparison between calculated peak friction angle with a developed conceptual model and peak friction angles measured in shear tests using samples of two different sizes (Johansson 2016).

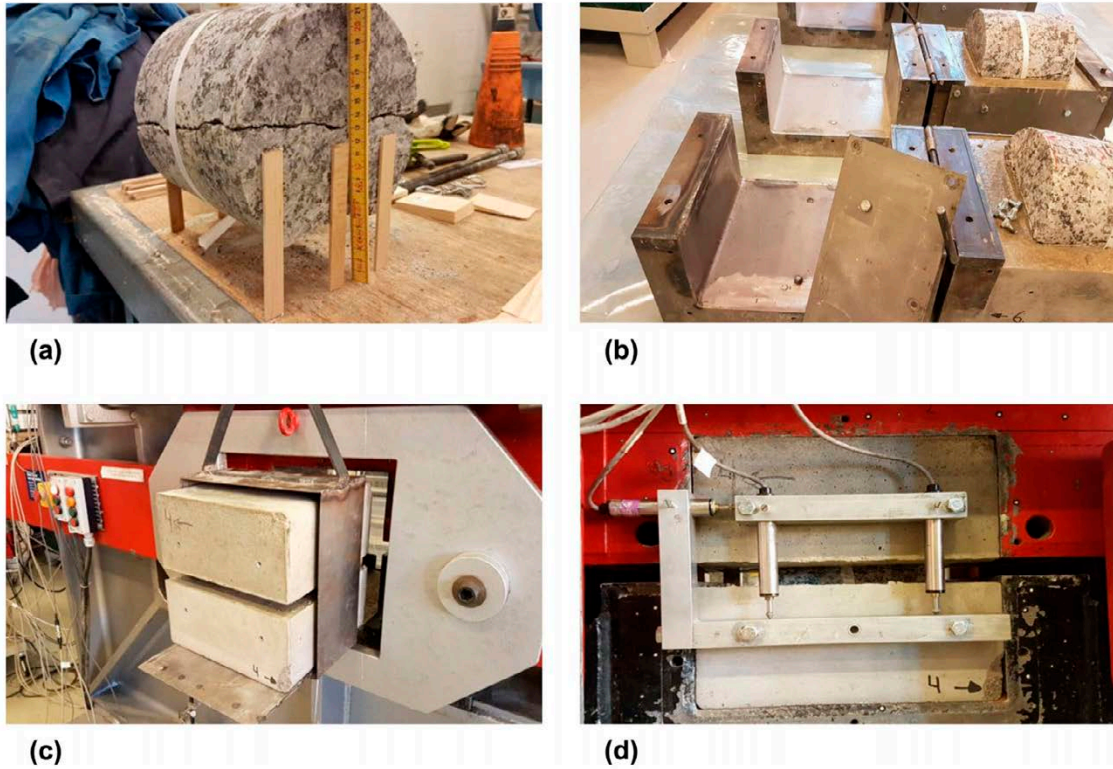


Figure 5-8. Example of laboratory constant normal load shear test set up on natural fractures where the size of the tested fracture is larger than what has been used previously. The size of the surfaces is about 200×200 mm. Images a) – d) show the steps of mounting the samples into the large shear loading frame (Rios Bayona et al. 2021).

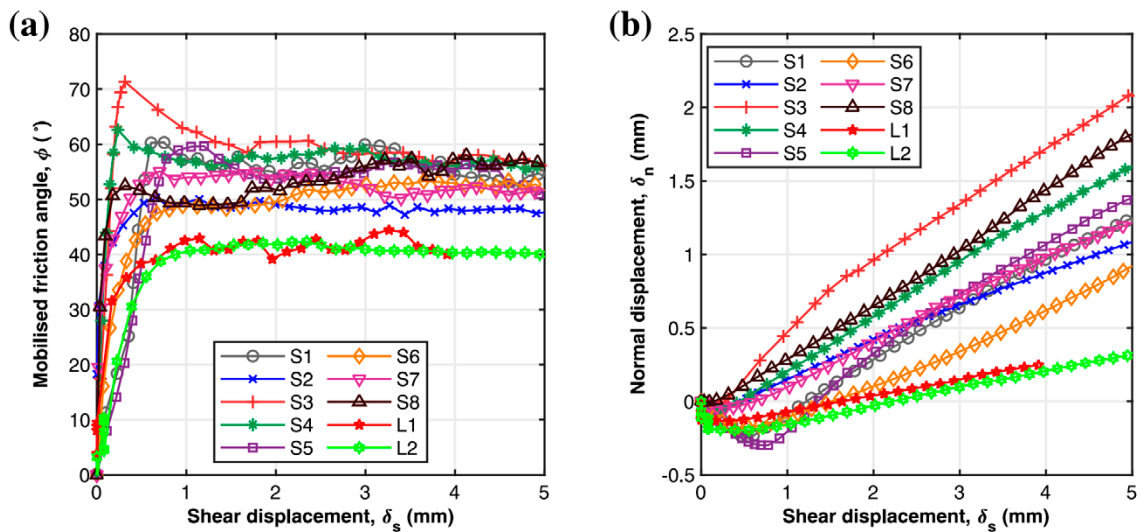


Figure 5-9. Example of results from large scale shear tests. The results from different fracture samples are shown as a) friction angle versus shear displacement and b) normal displacement versus shear displacement (Rios-Bayona et al. 2021).

The strategy for the next site description is to improve the support for different scale models and to provide some guidance for the fracture properties at the larger scales. The details of the methodology, and the specific parameters, for the scale dependence description are not fully determined, as they are part of ongoing research projects. If judged feasible specific tests will be performed on larger samples also from Forsmark, but the modelling may also be based on results from studies using samples from other sites with similar rock types, since the influence of scale can be assumed similar.

5.5.3 Strategy for mechanical property estimations for larger fractures

In previous safety analyses (Lönqvist and Hökmark 2015, Hökmark et al. 2019) the *friction angle* used for large fractures was chosen considerably lower than the friction angle measured on the small laboratory samples (30 degrees compared to the laboratory mean of 37 degrees for small-scale samples). No cohesion was assumed. For the *stiffness* parameters the values were chosen equal to the result from single fractures in laboratory. This illustrates the need for an expanded single fracture description, better representing the whole expected variety of fracture characteristics, in the future site descriptions. This will improve the traceability and consistency of values used in future analyses.

Some effort to estimate the strengthening influence of non-planarity analytically, which is one expected characteristic for larger fractures, has been made by Lönqvist and Hökmark (2015). They analysed the influence on shear displacement for generic shapes of ridges and wavy or saw-tooth large fracture surfaces and showed that the equivalent friction increased to some extent, depending on the orientation and location of the non-planar features.

To support the assumptions for large scale structures, some further theoretical analysis of different geometrical cases, such as rock bridges, may be performed. However, such methodology development is not yet decided or initiated. For further discussion on different fracture types, which may influence the expected mechanical properties of the fractures, see also Section 5.6 on the normal stiffness and hydro-mechanical properties.

When some additional geometry data are collected from relevant scales of fracture traces, these results could be used to support further analyses and possibly models with increased friction angles, corresponding to the estimated effect of the observed large-scale geometry (see Section 5.4.2). As long as new field information is lacking the approach for the site description will be to include what is judged as the lowest possible values for friction angle in the uncertainty span.

5.6 Coupled H-M properties of single fractures

5.6.1 The need for coupled models for fractures

The risk assessment for transport of radioactive nuclides from the canisters in the repository via the geosphere up to the biosphere can be performed with different approaches and levels of complexity, but consideration of hydro-mechanical (H-M) coupling is needed to predict the flow and the transport through the different future scenarios, including the heated period, glaciation cycles and effects of earthquakes.

The use of H-M models may be divided into two areas of application:

- 1) To help *explain* the existing distribution of transmissive fractures today, in the *initial* state. Why are they existing with a certain frequency and transmissivity distribution and why are some fractures more transmissive than others? Mechanical processes in the geological evolution of the site (and its boundaries) obviously play a major role in this.
- 2) To help *predict* the foreseen changes in the *future* fracture transmissivity and transport properties and their distribution. A main reason for conductivity changes will be the evolution of the stress field and associated mechanical processes in the bedrock.

The application area 1) is illustrated further in Section 5.6.3. The question raised is if the fractures tested in the laboratory are representative in the actual analyses where the mechanical property parameters are applied. The answer to this could vary depending on the application.

The application area 2) of the hydro-mechanical coupling applications is perhaps more important for the safety assessment in that it is needed for the prediction of future conditions, where our correct understanding of the site, acting processes and predictive capability is crucial for the result. Even if accepting and assuming correct the current model for the in situ situation as is, a model is needed to assess if the hydraulic conductivities should be expected to change during future loading scenarios and to what extent. In the assessment of SR-site, Hökmark et al. (2010), used a model directly coupling changes in rock stress with changes in fracture transmissivity, which will be explained further in Section 5.6.2.

5.6.2 Coupling fracture stress and transmissivity

In general, hydromechanical coupling in rock masses refers to three aspects:

- the effect of pore pressure on deformation and strength of the rock mass,
- the effect of mechanical deformation on pore pressures, and
- the effect of mechanical deformation on the bulk permeability.

The first two aspects are treated by the theory of poroelasticity for porous media (Biot 1955, Berryman 2016). For low intrinsic intact matrix rock permeability but fractured rock masses, both the mechanical and hydraulic behaviours are controlled to a great extent by the fractures. The coupling at the fracture scale, with the dependency of the fracture transmissivity to the in situ stress conditions (Brace et al. 1968b, Jaeger et al. 2007, Ranjram et al. 2015), is the major hydromechanical process for this type of medium. The mechanical processes involved are 1) the variation of fracture aperture in relation with normal stress and 2) the variation of fracture aperture resulting from the shearing or slipping of the fracture. They are discussed in this order in the remainder of this section.

The flow in fractures is often very complex in nature, due to the morphology, geometry and nature of fracture surfaces (Figure 5-4). Numerous laboratory studies have shown that the fracture transmissivity is affected by the stress conditions acting on the fracture. At scales from cm to tens of cm, laboratory and numerical experiments (e.g. Brace et al. 1968b, Kranzz et al. 1979, Walsh 1981b, Baghbanan and Jing 2008) show that flow decreases significantly when the confining stress increases, potentially following a power-law (Raven and Gale 1985) or an exponential (Liu et al. 2004, Hökmark et al. 2006) decay trend between transmissivity and normal stress. For scales relevant to in situ hydraulic tests, correlations between localized flow measurements and stress conditions display similar trends (Martin and Follin 2011, Follin and Stigsson 2013). The transmissivity dependency on stress can also be related to dilation and shear displacement, especially for critically stressed fractures (slipping regime, i.e. fractures whose shear stress is larger than their shear resistance (Min et al. 2004)). Barton et al. (1995) and Townend and Zoback (2000) suggest that most of the hydraulically conductive fractures (70 % – 80 %) appear to be critically stressed. Cotesta et al. (2004) show that stress may play an important role in controlling the anisotropy of the rock mass permeability of moderately fractured rocks. Recently Mattila and Follin (2019) analysed fracture and flow data from the Olkiluoto and Forsmark sites, a database with about 200 000 fractures, among which roughly 3 % display measurable flows. Only a weak correlation between critically stressed fractures and flowing fractures can be observed for the present-day stress conditions at the two sites.

All these observations underscore the need to quantify and model the hydro-mechanical coupling in order to evaluate its impact on the in situ flow and contaminant transport processes.

Understanding further the fracture H-M coupling can be approached from a single or two-step approach, with (Figure 5-10):

- a) First, a change in stress ($\Delta\sigma$ in Figure 5-10) over a fracture causes a change in the geometry of the surfaces in relation to each other (matedness), i.e. a change in the mechanical or geometric aperture Δe (Figure 5-4). The relation between stress and mechanical aperture is most commonly parameterized with a normal stiffness (k_n). Shear stiffness (k_s), strength and dilation are also of influence under certain circumstances. This avenue of research has been ongoing during the last 40 years (Bandis et al. 1983, Zimmerman 2008, Li et al. 2019, Zou et al. 2020).

- b) Second, a change in mechanical aperture distribution causes a change in the transmissivity distribution, which is also an active field of research (Brace et al. 1968a, Zimmerman and Main 2004, Zimmerman 2008, Li et al. 2019).
- c) Or a single step approach where the intermediate step between stress and mechanical aperture is bypassed and a direct link between stress and transmissivity is established (Walsh 1981, Liu et al. 2004, Baghbanan and Jing 2008).

The transmissivity (T) is often expressed as an equivalent hydraulic aperture (e_h), which has the same dimension as the mechanical aperture. The hydraulic aperture is the aperture of an equivalent parallel plate model that would lead to the same transmissivity and flow (defined by the cubic law in Equation 5-3 below).

Apart from laboratory-scale tests, there is also field evidence of fracture stress-flow and stress-transmissivity couplings. This is shown in Figure 5-11 through borehole hydraulic tests of different types from Rutqvist and Tsang (2008) with actual jacking tests in the fractures in situ. The tests reported by Rutqvist and Tsang (2008) were performed on individual fractures, located close to deformation zones along borehole KLX02 (Laxemar site) at depths from 267 to 338 m. The tested fractures with the highest initial transmissivities (e.g. “315 m” in Figure 5-11) are only weakly dependent on the injection pressure (and resulting effective normal stress). In some extreme cases the transmissivity variations vary over more than five orders of magnitude, mainly due to a transmissivity decrease effectively down to zero for high normal stresses. It appears from these few observations that the stress state is one of the controlling factors of a fracture transmissivity, but not the only one.

The stress-flow and stress-transmissivity coupling is also shown in Figure 5-12 with data from PFL testing (Rouhiainen and Sokolnicki 2005) of individual fractures in deformation zones at the Forsmark site (Follin and Stigsson 2013). The transmissivities are compiled by deformation zone, as the sum of the individual inflows (ΣT_{PFL}) observed in each of them (typically less than 5 distinct intercepts by zone). The stresses are deduced from the current Forsmark stress model (SKB 2008) and the DZ plane orientations. This analysis shows that, despite a significant heterogeneity of about 2.5 orders of magnitude (see the two parallel blue dashed lines in the figure), the global transmissivity decrease reaches four orders of magnitude and is compatible with an exponential decay. For the above mentioned in situ experiments, it is notable too that the different types of fractures/structures may have quite different transmissivity, even if subjected to the same normal stress. This could be explained by differences in the fractures filling and surface quality, typical sizes and geological histories, leading to the observed different characteristics.

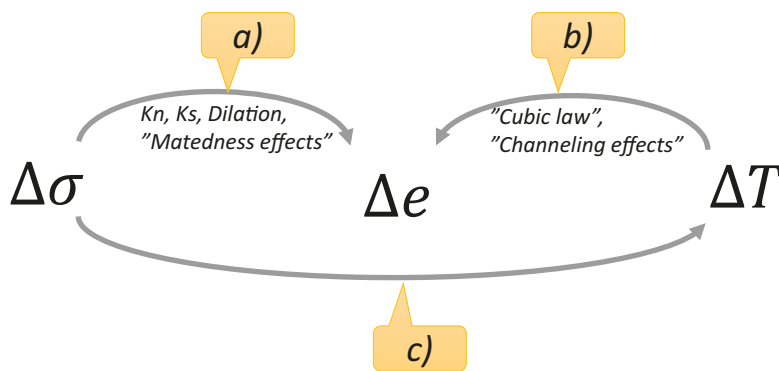


Figure 5-10. Summary scheme of research approaches, a), b) and c), to investigate the H-M-coupling for single fractures. The schemes a), b) and c) are explained in the text.

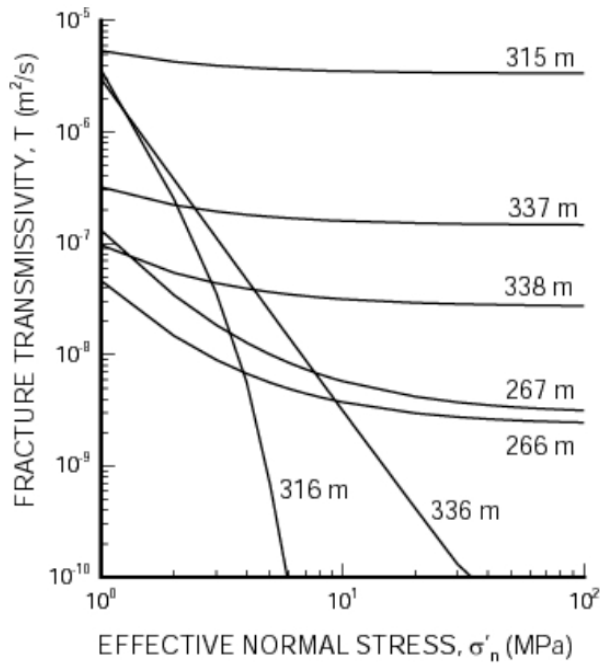


Figure 5-11. Transmissivity versus stress relationships estimated from in situ hydraulic jacking tests on single conductive fractures at the KLX02 borehole at Laxemar. Note that both the x- and y-axes are logarithmic. The curves start at 1 MPa effective normal stress. The figure is taken from Rutqvist and Tsang (2008).

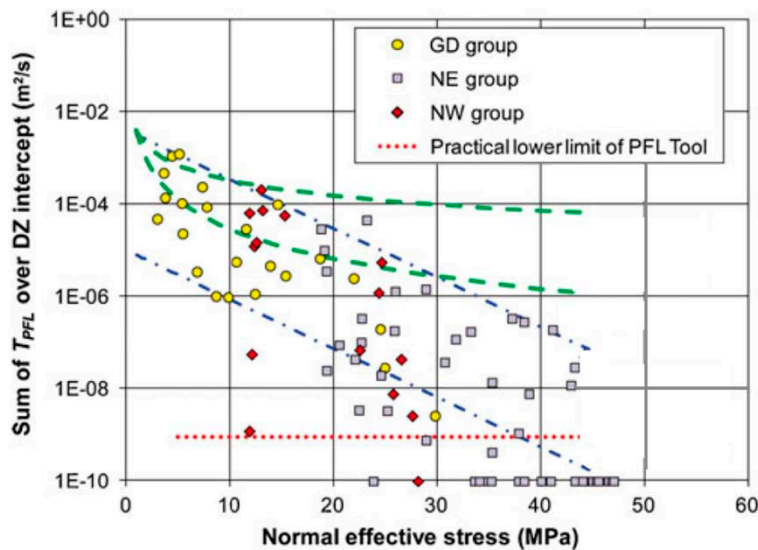


Figure 5-12. Calculated normal effective stress acting on the inferred transmissivity (ΣT_{PFL}) along the plane of the deformation zones. Each dot is coloured by reference to an orientation group – Gently Dipping (GD), North East (NE) and North West (NW). The dashed lines refer to i) the practical lower detection limit for T_{PFL} records (in red), ii) the lateral heterogeneity in T_{PFL} values based on the GD group and expressed as an exponential decay (in blue), and iii) the reference to existing lab-scale experiments and power-law model from Raven and Gale (1985) (in green). Figure adapted from figure 10 in Follin and Stigsson (2013).

A fracture transmissivity may also result from criticality and shear stress conditions. The current understanding of the THM (Thermo-Hydro-Mechanical) aspects in Forsmark and Laxemar (Hökmark et al. 2010) assumes that high normal stresses suppress the effect of fracture shear dilation on transmissivity. This effect, if existing at repository depth, is assumed to be very local, acting in the near field of the repository excavation boundaries. However, the effect at shallower depths and therefore, lower normal stress, is uncertain. At present there is still conflicting evidence about the effect of shear dilation on fracture transmissivity. An increase of the normal stress from 2 to 4 MPa appeared to suppress the increase of transmissivity very effectively in hydromechanical shear tests performed by Olsson (1998). On the other hand, increases in transmissivity of between one and two orders of magnitude were observed in tests performed by Esaki et al. (1999) under high normal stresses on artificially created granite fractures after about 5 mm of shear. It is not clear whether the behaviour of the artificial fractures is representative of natural fractures. An experiment performed with a normal stress of 20 MPa, and repeated shear in the opposite direction, gave insignificant transmissivity effects for shear displacements up to 10 mm.

Ultimately any T-H-M-analysis requires a model to couple the normal stress-induced aperture change with transmissivity change. The methodology previously used by SKB in SR-Can (Hökmark et al. 2010), which will be retained for the future assessment, is to use the model of Liu et al. (2004). This model fits an exponential function to laboratory normal loading results (see Figure 5-2) and assumes that the mechanical deformation over the fracture due to change in normal stress is equal to the change in the hydraulic aperture, which is given by Equation 5-2.

$$e_h(\sigma_N) = e_r + e_{max} \exp(-\alpha \cdot \sigma_N) \quad \text{Equation 5-2}$$

Where σ_N is the effective normal stress, e_r is the residual hydraulic aperture, e_{max} is the maximum deviation between the residual and the maximum hydraulic apertures and α reflects the intensity of the exponential decrease with the normal stress.

Equation 5-2 can either be expressed in terms of hydraulic aperture (e_h) or in terms of transmissivity (T), using the cubic law (Snow 1965, Witherspoon et al. 1980), to switch from one to the other. The cubic law is recalled below:

$$T = \frac{\rho g}{12\mu} e_h^3 \quad \text{Equation 5-3}$$

where μ is the fluid viscosity ($Pa \cdot s$), ρ is fluid density ($kg \cdot m^{-3}$), g is gravitational acceleration ($m \cdot s^{-2}$).

Two parametrizations of a stress-transmissivity model were selected in the previous SR-Can program, as recalled in Table 5-2 below:

- Model A in the Figure 5-13, was calibrated using in situ flow logging data.
- Model B in the Figure 5-13, was based on the mechanical aperture and stiffness laboratory testing mentioned above (Figure 5-2).

Table 5-2. Parameters of the models A and B (Equation 5-2) used by SKB in SR-Can (Hökmark et al. 2010).

Model	e_r (μm)	e_{max} (μm)	α
A	20	42	0.15
B	20	13	0.13

Both models can be equally expressed as hydraulic aperture (right axis in Figure 5-13) or as normalized transmissivity (left axis in Figure 5-13). The normalized transmissivity, $\frac{T}{T_0}$, is defined from T_0 , the transmissivity for an arbitrary selected normal stress σ_{N0} (with $\sigma_{N0} = 20 \text{ MPa}$ in Figure 5-13, left axis). The normalized expression can be expressed either as $\frac{T}{T_0}$ or $\frac{e_h}{e_0}$, with $\frac{T}{T_0} = \left(\frac{e_h}{e_0}\right)^3$ as derived from the cubic law and with e_0 as the hydraulic aperture at the reference effective normal stress σ_{N0} .

There are pro and con arguments regarding the parametrization of a relevant stress-transmissivity model. The strength of the laboratory-based model (model B) is that it is based on direct measurements of fracture closure under increasing normal stresses. The weakness is the laboratory scale of the

measurement itself, as it is very likely only partially representative of in situ conditions and typical size scales of the fractures relevant to the flow. Moreover, the inherent constraints of laboratory experiments, e.g. the minimum stress (0.5 MPa) under which no closure measurement can be done, lead to advising caution when extrapolating the stress transmissivity relation over untested ranges of stress.

Model A is based on in situ hydraulic (PFL) tests and therefore represents size scales more adapted to typical sizes for which the HM coupled model will be used. However, the deduction of both normal stress and equivalent transmissivities relies on additional modelling assumptions, going from a larger size scale in situ stress model to local normal stresses and from drawn-down in groundwater head and flowrates to individual fracture transmissivities.

The approach in safety assessment needs to be conservative and conclusions drawn from sensitivity analyses with respect to the fracture properties and parameters covering the most extreme fracture stress-transmissivity couplings. It is presently recommended to continue using the stress-transmissivity model proposed initially by Liu et al. (2004) and used by SKB in SR-CAN (Hökmark et al. 2010). It is also recommended to determine, when relevant, several parametrizations of the law (e_r , e_{max} and α) and clearly identify the type and size scale used to derive the parameters and the type and size scale at which the parametrized law shall be used. This is particularly relevant when considering the in situ water-bearing structures (see Section 5.6.3).

Although no major changes of the methodology used in SR-Site for the coupling models are planned, significant changes are suggested. This involves the introduction of variability in the parameters and the introduction of different categories of fractures for which all the parameters relevant to mechanical and hydromechanical modelling should, to the extent possible, be identified and differentiated from one category to the other. It is recommended to consider these categories based on:

- Typical size scale of fractures (when possible).
- Belonging to the identified set of fractures which are bearing some flow in situ (the so-called PFL-fractures).
- Fracture typical infilling minerals, internal geometrical characteristics, etc.

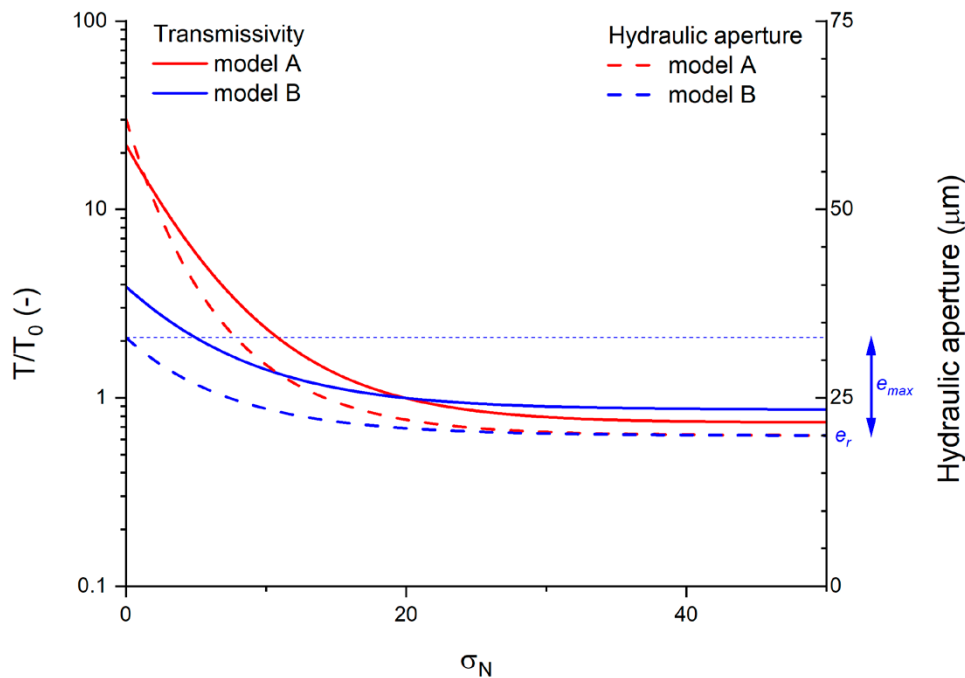


Figure 5-13. Illustration plot of the stress-transmissivity models (A and B) selected in the previous SR-Can program (Hökmark et al. 2010), with the model defined in Equation 5-2 and the model parameters recalled in Table 5-2 and a normalized transmissivity $\sigma_{N0} = 20$ MPa. Normalized transmissivities (left axis, log scale) are plotted in continuous lines. Equivalent hydraulic apertures (right axis, linear scale) are plotted as dashed lines. The model parameter e_{max} for model B is plotted as a blue arrow on the hydraulic aperture axis.

The complementary data and parameters to be compiled should not be limited to the hydromechanical properties but also encompass the basic mechanical ones. As an example, a change in mechanical normal stiffness will induce a change in the coupling parameters. Lower stiffnesses will result in higher values of e_{max} in the stress – transmissivity model. There is yet no clear consensus on which are the most important parameters, among the aforementioned ones, to define the fracture stress dependent transmissivity relation. Literature studies as well as theoretical, numerical and laboratory research is ongoing in order to increase the understanding in this regard. As a complement to this fundamental research, systematic sensitivity analyses will help to tighten the range of possibilities for safety assessment applications.

The characteristics of PFL-fractures, including their correlation with typical fracture sizes, are further discussed in the next section.

5.6.3 Water-bearing fractures – PFL fractures

The PFL-fractures introduced in Section 5.5.1 are all the individual fractures over which inflows are detected during in situ Posiva Flow Logging tests. Several conditions must be met for a fracture to be PFL-fracture (also denoted PFL-f): the fracture has to intersect the borehole over which the hydraulic test is performed, its transmissivity is not null, and it has to belong to a connected network of conductive fractures connecting to the hydraulically active boundaries of the flow test. In these conditions, the population of PFL-fractures should be different from the complete fracture population, in terms of fracture type, size scale, orientation and hydromechanical properties.

This is conceptually illustrated in Figure 5-14a (with indicative fracture frequencies noted P_{10}). Among the intercepts of all fractures (fracture frequency $P_{10,a}$) recorded over a borehole, one defines several categories. First the fracture frequency of apparently open fractures ($P_{10,o}$) is defined by removing the apparently sealed intersecting fractures. On average in the Forsmark site roughly 80 % of the total fracture surface area at depth is sealed and therefore not transmissive (Follin et al. 2014, Doolaeghe 2021). While there exists no consensus yet on how the sealing is distributed throughout the fractures, existing modelling and sensitivity analyses tend to show a positive correlation between fracture size and (degree of) openness. The open fractures category further divides into isolated open ($P_{10,o}$) and connected open ($P_{10,cof}$) fractures, considering the connectivity between hydraulically active boundaries with the intersecting borehole. The last category ($P_{10,PFL}$) groups the open and connected fractures for which a positive inflow can be measured during the PFL test, i.e. when the inflow is above the detection limit. The fracture frequency tends to decrease from all the intersecting fractures ($P_{10,a}$) to the PFL intersecting fractures ($P_{10,PFL}$). Over the whole fracture population, this decrease is likely coupled with a change in size distribution of the different fracture categories (Figure 5-14b), with a tendency to increase the proportion of larger fractures compared to smaller ones (in a scaling relationship). This tendency naturally arises from the DFN connectivity structure and may be increased if the transmissivity is positively correlated with fracture size.

Apart from in situ hydraulic tests and DFN modelling, recent laboratory data analyses show that stiffnesses for PFL-fracture tends to be lower than the average fracture population stiffness. If confirmed this would result in higher values of e_{max} (Figure 5-2) for the PFL-fractures. There are also theoretical arguments for defending a correlation between fracture size and fracture aperture, as discussed in depth by for example Olson (2003).

It is therefore recommended to evaluate if fracture categories and/or fracture size dependency should be introduced in the parametrization of the stress-transmissivity relationship (Equation 5-2). To sum up, the current strategy assumes that the type of fracture samples used in laboratory tests are likely *not* representative of the transmissive fractures, and that the stiffness parameters are preferably described as a separate group (see also Section 5.5.3). Combined this supports the strategy to have a separate description of the different mechanical parameters for fracture sub-groups (e.g. the PFL-fractures). The work will consist of additional analysis of already available investigation data and probably some additional sampling and testing, specifically for the PFL-fractures.

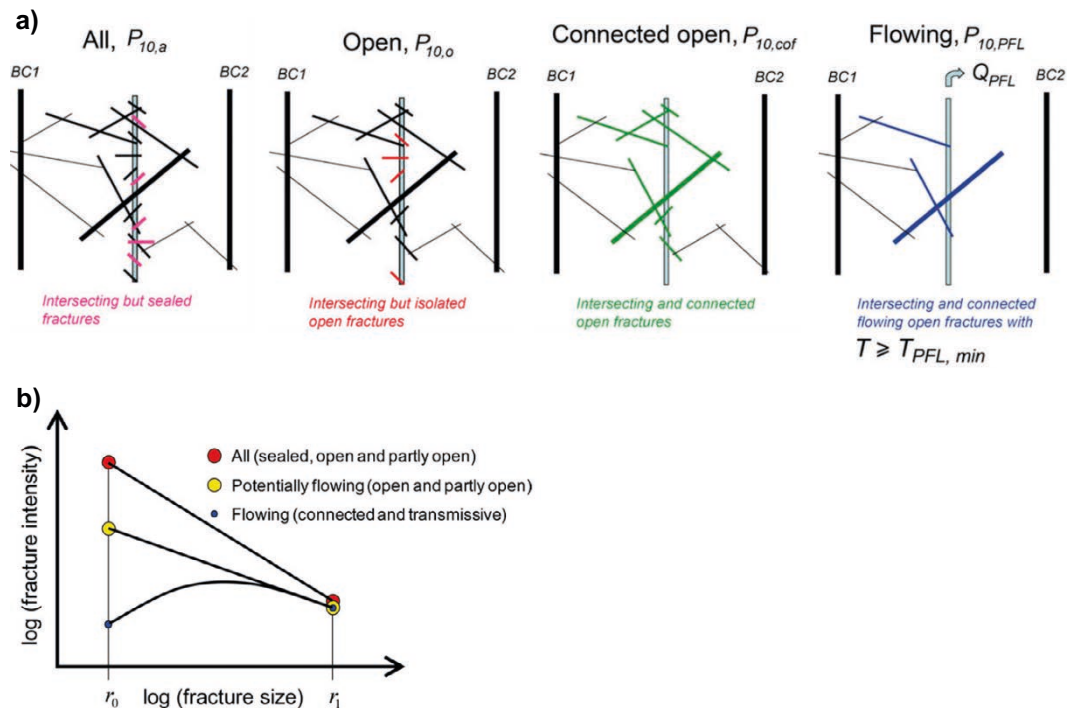


Figure 5-14. a) Definition of different types of fractures with regard to flow. $P_{10,PFL}$ is the frequency of “flowing connected open fractures” identified with the PFL-f method. BC1 and BC2 represent hydraulic boundary conditions, e.g. the surface and/or nearby deformation zone which is connected to the surface. (SKB 2008). b) Envisaged relationship between the probability density functions of all, open, and flowing fractures for a power law fracture-size probability-density distribution. Figure modified from Follin et al. (2014) and SKB (2008).

5.7 Additional influencing factors on laboratory fracture test results and property models

In this section different factors influencing the modelling results are discussed. However, the strategy is not to put much further effort into quantifying these factors. The user of the description will have to judge if these factors need to be addressed or further adjusted for in the specific application. A motivation for having factors in this less prioritized category is given.

5.7.1 Boundary conditions during laboratory testing

One of the reasons that mechanical properties for the large single fractures are needed is that the large fractures are important elements in safety analyses for the future repository. For example, Lönnqvist and Hökmark (2015) and Hökmark et al. (2019) describe analyses to estimate the maximum possible shear movement due to earthquakes on large fractures potentially intersecting the repository, and identify the critical fracture size prone to generate the maximum accepted shear movements in conjunction with earthquake events. Hökmark et al. (2010) also analyse the fracture movements due to a glaciation cycle induced loads and the thermal loads that the heat generating waste will cause.

In these analyses the property parameters as well as the type of loading are important factors. The laboratory data that are used to find fracture property parameters should, as far as possible, resemble and reflect the actual situation. The way to represent the actual in situ situation in a laboratory test is by using representative boundary conditions. Shear tests on fracture samples may be performed either under constant normal load (CNL), i.e., the same load acting on the fracture surface throughout the whole shearing, or under constant normal stiffness (CNS) boundary conditions.

As was explained in Section 5.1 the normal stress dependency of the mechanical dilation has been characterized in small scale laboratory tests on core fracture samples at different constant normal stress levels (0.5 MPa, 5 MPa and 20 MPa). Obviously, mechanical dilation decreases with increasing normal stress, and this is one of the main reasons why CNL conditions are not as suitable for analysing fracture behaviour in a stiff rock at depth. The rock mass surrounding each fracture at depth in Forsmark is very stiff, and this stiffness causes the normal stress on the fracture plane to increase as the fracture tries to dilate due to shear. This interlocking effect is not captured well under CNL conditions. Additionally, CNS conditions inhibit mechanical dilation. During the shear test the normal stress will continuously increase and, as a consequence, the shear strength of the fracture will also increase. Therefore, CNS conditions produce a more realistic representation of the actual conditions at depth.

The strategy for future site modelling is to combine the results from previous CNL tests with some additional new CNS tests. Normal stress dependent shear stiffness, strength and dilation can be determined from both types of tests. The preliminary assumption is that the results will not deviate dramatically between old and future new types of tests, and that it will be possible to make the description based on both. The potential bias and errors that are a result of the difference in boundary conditions between field and laboratory will not be investigated in depth because, apart from being extremely difficult to study practically, it is judged that other influencing factors, such as the scale and sample representativity issues constitute a more significant part of the uncertainty.

5.7.2 Variation in fracture infilling materials and side wall alteration

Most fracture surfaces have some amount of infilling material and mineral coatings. The character of this infilling can, in particular if the thickness of the infilling is larger than the asperity height, fully determine the mechanical behaviour of the fracture. Therefore, it is useful that the tested fractures are described also with respect to fracture infilling. A small number of tests have already been performed by SKB on samples with fractures which were clearly not mated or with fracture surfaces with a significant infilling layer (Jacobsson 2016). However, most of the fractures in the drill cores mapped within SDM-Site contained a limited amount of infilling material (Drake et al. 2006).

Therefore, for the future descriptive models in Forsmark, the strategy is to, as previously, pool the laboratory test results together and to treat the *open* fracture property variation statistically rather than to try and subdivide the different fractures with respect to different amount of fracture infilling minerals, surface anisotropy or fracture orientation. At the selected deposition hole positions the fractures intersecting are expected to be single open fractures or sealed fractures, where the sealed fractures will be described separately (Chapter 6). Any larger complex structures (faults), which often exhibit larger amounts of infilling material, will be avoided at the deposition holes, i.e., the deposition holes will be located at a certain distance from these structures, and no attempt will be made to describe their individual mechanical properties. The infilling material will, however, be part of the judgement of large fracture (fault) parameters (Section 5.5.3) and PFL-fracture properties (Section 5.6.3).

5.7.3 Coupling between temperature and fracture properties

Temperature increase will change the fracture mechanical property parameters, but the influence is small due to limited estimated temperature increase (< 100 °C) of crystalline rocks (e.g. Chen et al. (2017)) and the strategy is to not make any specific studies for the Forsmark rock types.

Lima et al. (2019) studied the temperature effect on fracture transmissivity and found that the apertures decreased with increasing temperature, even if the normal stress over the fracture was kept constant. This result can be interpreted as an effect of expanding minerals inside open voids of the fracture aperture. However, the strategy is to not include any specific parameter description for the potential temperature effect on the fractures as these effects are typically expected to produce a reduction in transmissivity (fracture closure).

Additionally, the temperature will make the rock mass expand and the expansion will lead to increased stress in the studied rock volume. A temporary increase in temperature closest to the deposition areas will therefore, in general, induce fracture closure due to increase in fracture normal stress. However,

some fractures may experience shear and shear dilation. This mechanism does not require any additional mechanical parameter than what is already included in the description (thermal expansion and fractures stiffnesses, strength and dilation angle) for its analysis.

5.7.4 Creep – Time dependent behaviour for single fractures

Glamheden and Hökmark (2006) discuss the issue of long-term strength and creep shear movement on fractures, in the context of analysing the maximum expected shear on fractures intersecting the repository. It is not possible to know how the fractures will behave in the long term, after several ice-loading cycles, etc and Glamheden and Hökmark (2006) suggest treating this issue in safety assessment by simply assuming extremely low friction. For studies of shear due to earthquake events, Fälth et al. (2019) used a friction of 30 degrees in all cases, for the analysed fractures at the repository. The stiffness and cohesion applied for studied fractures may also have influence on the results. This demonstrates the need for a more comprehensive description of the parameters, including discussion on time-dependent behaviour, such that the assumptions made in the safety assessment are traceable and that adopted uncertainty spans are explained. The strategy for the future site modelling is to not perform any specific laboratory tests or site investigations (apart from what is mentioned regarding fracture surface geometry in Section 5.3) but to make an updated literature review on the subject, including potential recent research results.

6 Sealed fracture properties

6.1 Frequency of sealed fractures

In the Forsmark area the investigations have so far shown that sealed fractures and so-called sealed fracture networks are common (SKB 2008). Figure 6-1 shows an example of how a sealed fracture may look like in a core sample. The frequency of sealed fractures is generally higher than the frequency of open fractures, which is illustrated by the diagram in Figure 6-2. In this diagram the data from boreholes at the planned area of the repository are plotted, with the access area separated. A certain decrease in frequency with depth may be noted for the open fractures but the sealed fractures have a fairly constant frequency in the volume. At 470 m depth the frequency of sealed fractures is around five fractures per meter, which means that with this level of frequency, the eight-meter-long deposition holes should be expected to be intersected by many sealed fractures, and the potential influence in safety assessment is discussed in the next section. This is followed by a section outlining the strategy for new parameters to add for sealed fractures in the future site-descriptive models.

Before mechanical test



After mechanical test



Figure 6-1. Example of sealed fracture tested in the laboratory. The lower images are the fracture surfaces after the shear test has broken the sealed fracture (Jacobsson and Flansbjer 2006).

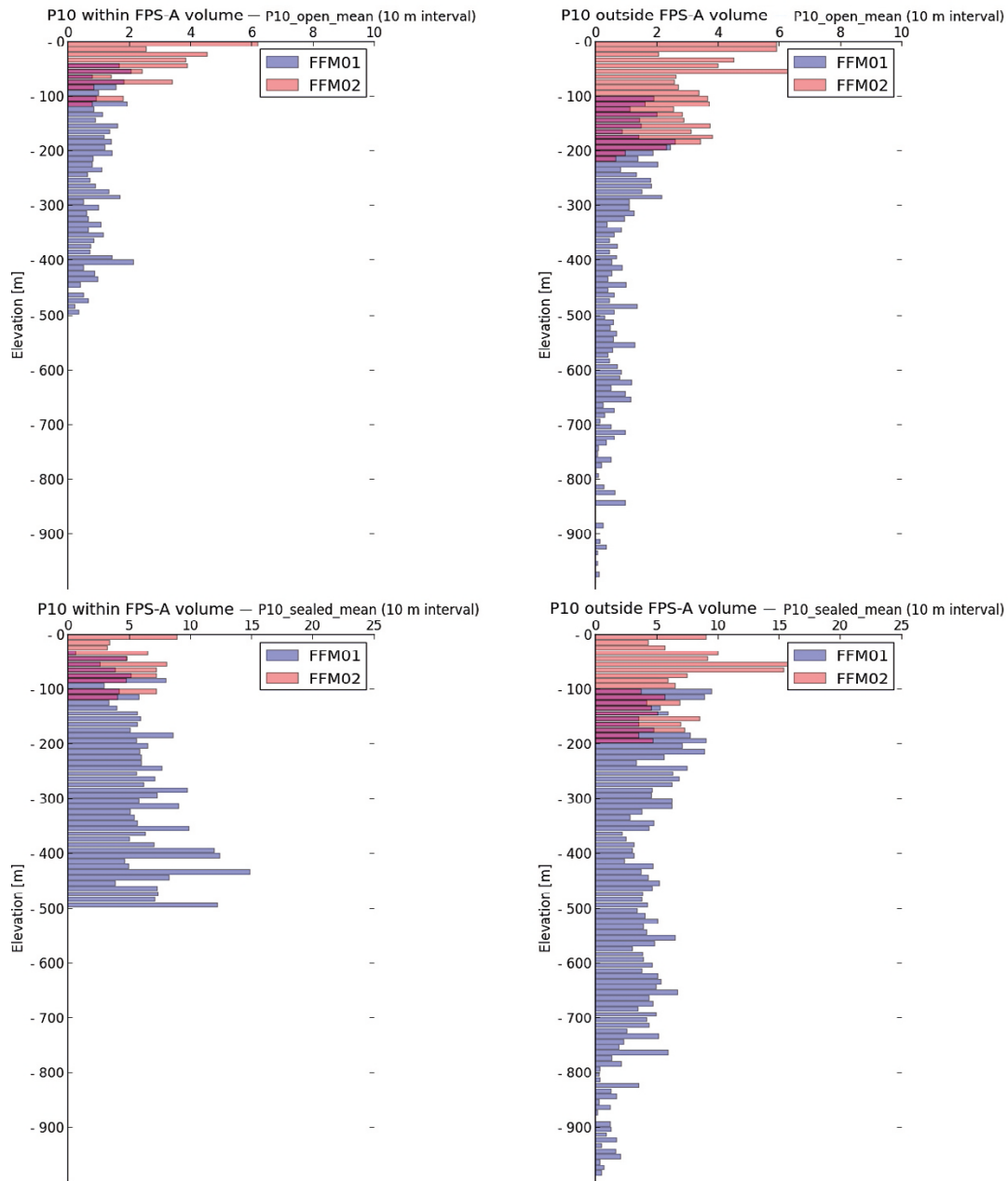


Figure 6-2. Terzaghi corrected fracture frequency inside and outside the access volume. Upper diagrams are for the open fractures and lower diagrams for the sealed fractures. Note that x-scales are different (Follin 2019).

6.2 Potential influence on safety assessment from sealed fractures

In the absence of open fractures, if *sealed* fractures exist in the rock surrounding the excavated deposition hole, it is likely that any failure around the hole will take place at the sealed fractures primarily, and *before* spalling in the intact matrix rock takes place, this since the sealed fractures are expected to be weaker than the intact matrix rock. A few laboratory tests on sealed fractures have been performed in the site investigation (Figure 6-3). These results showed that the cohesion for the sealed fractures was in the order of 3 MPa while the cohesion for intact rock type 101057 is about 28 MPa.

If we, as an example, assume a frequency of sealed fractures similar to what was reported in the previous SDM-Site, a situation in a cross section through a deposition hole could look like in Figure 6-4. Two vertical fracture sets intersect the rock volume in this case and there is a possibility to have small fallouts of wedges created by the sealed fractures, depending on where they are located. There is a criterion limiting the open void between the bentonite and the rock wall, due to the requirements on the bentonite properties after swelling out in the void volume. As long as the drilled diameter of the deposition hole is not larger than the design target value (1 750 mm), there is still room within the span of the acceptance volume criteria for some fallouts of some kind. However, if the drilled diameter is close to the maximum allowed diameter there will be a very limited acceptance for failures and loosened fragments in the deposition hole's wall. For this reason, there is a need for an improved description of the sealed fractures and their mechanical properties, such that the potential for this problem can be assessed.

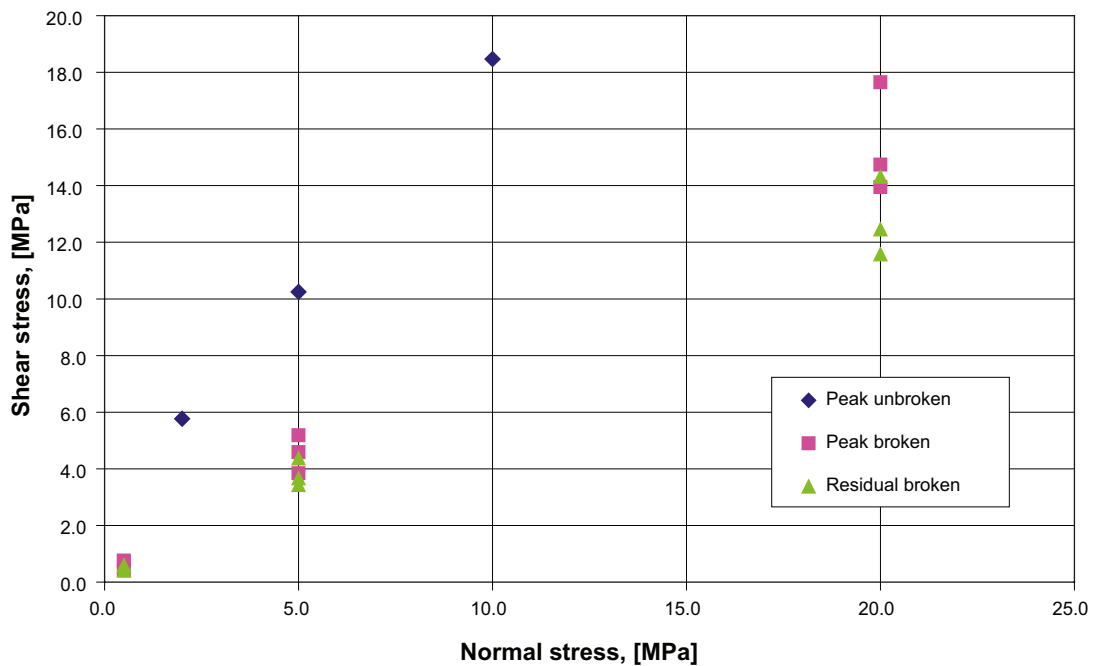


Figure 6-3. Example of shear test results on three samples of a sealed fracture from borehole KFM01D, elevation 459 m. The peak unbroken values are the values that represents the sealed fracture before they are broken and the three values (diamonds) are used to evaluate a cohesion and a friction angle for the sealed fracture (Glamheden et al. 2007).

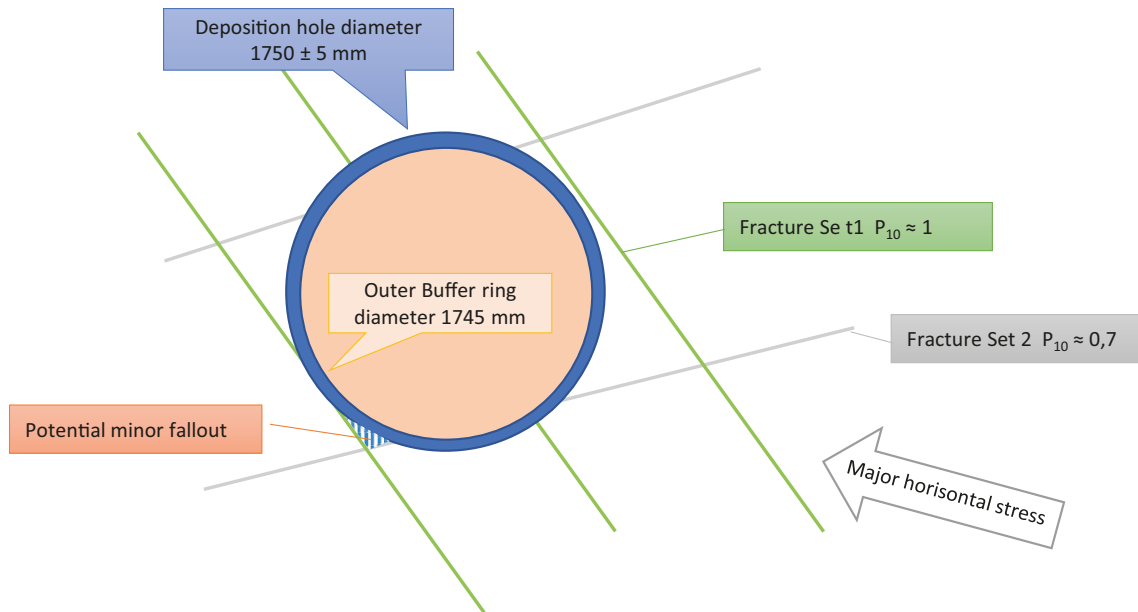


Figure 6-4. Sketch of possible cross-section through a deposition hole with two vertical sealed fracture sets. There is a limitation for the acceptable total gap volume between the buffer ring and the rock wall. The failure in the wall must therefore be limited and only show small fallout volumes. The amount will depend both on the frequency of sealed fractures and on their strength and stress conditions.

6.3 Selection of parameters for sealed fracture description

The parameters for the description of sealed fractures will be the same or similar to the parameters for the open fractures. A difference is that the properties depend on the sealing material, at least if it has proven to make a significant difference for the strength. Since there are very few results from the previous site description the details of the parameters will be decided based on new acquired data.

Ongoing work focuses on doing some core sampling and laboratory testing of sealed fractures of different types, and on collecting the data already available concerning the sealed fractures. The methods to be used in the additional laboratory analyses will mainly be the same as used for open fractures, i.e., shear tests, but also the indirect tensile strength test may be used on samples with sealed fractures. Indirect tensile strength tests may not give a well-defined outcome, because of difficulties with sample preparation and complex testing procedures, but they would unquestionably be able to demonstrate any significant strength difference compared with intact matrix rock without the sealed fractures.

The plan is to determine *shear* stiffness and strength parameters for sealed fractures, based on laboratory tests on drill core samples. Furthermore, the *tensile* strength will be estimated for the direction perpendicular to the sealed fracture plane. These parameters are added compared to previous SDM.

7 Rock mass properties of fracture domains and deformation zones

The term “rock mass” is defined as the equivalent material consisting of intact matrix rock and fractures together, looking at a larger scale. This term may be used for the rock inside the “ordinary” rock volumes in a Fracture Domain. It can also be used for the rock inside a deformation zone. Properties of the rock mass inside Fracture Domains and Deformation Zones can be determined using the same methodology.

7.1 DFN-based analytical approach

The modelling concepts of a DFN-based rock mass description are described in Section 2.6.1. The rock mass is viewed as an ensemble of discrete fractures (the DFN) embedded in an intact rock. The previously applied approach, denoted “theoretical approach” during SDM-Site (Staub et al. 2002) has evolved and is now called DFN-based approach.

7.1.1 Rock mass effective elastic and strength properties

The DFN-based approach predicts, at present, the effective elastic properties of a rock mass (Modulus and Poisson’s ratio for simple cases and more generally all the terms of the compliance tensor), relative to the intact rock and embedded DFN properties (geometry and mechanical properties), the scale of interest and the remote stress conditions (Figure 7-1). It is analytical and as such eliminates the computational burden of numerical limitations inherent to numerical rock mass modelling. It provides a relevant means to understand further which characteristics of the fractured system (i.e., DFN model) are critical for the mechanical behaviour, and therefore to relate DFN model metrics to rock mass properties using simplified relationships. Details about this new approach can be found in the report (Darcel et al. 2021). Additionally, the fundamental developments are found in Davy et al. (2018) and one application to the Forsmark site FFM01 Fracture Domain in Darcel et al. (2018).

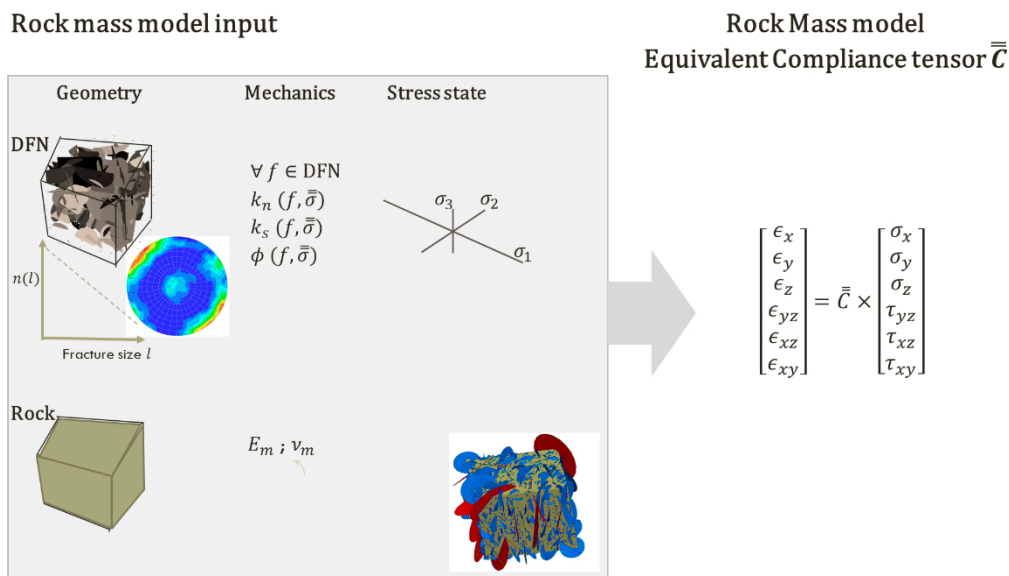


Figure 7-1. Sketch of the input parameters and output of the DFN based approach to derive rock mass effective elastic properties. The numerical set up, as referred in Darcel et al. (2021), is called PyRockMassTool and was written as a Python set of functions. PyRockMassTool computes the equivalent compliance tensor of a rock mass specimen defined from a DFN description of the fracture system embedded in a rock mass sample, as well as rock and fracture mechanical properties and remote stress conditions.

The method may be summarized as follows. It first calculates the contribution, to the rock mass deformation, of each individual disk-shaped fracture embedded in it. The individual contributions of each fracture are added and combined according to effective medium theory, to finally define the rock mass deformation resulting from a stress input. These are finally combined to derive the equivalent compliance tensor components.

The suitability of the DFN-based approach to define the rock mass elastic properties was tested against a wide range of DFN geometrical and rock mechanical conditions. In practice, rock mass specimens (DFN embedded in a rock) were built and tested numerically with the geomechanical code 3DEC. Results of the comparison between the DFN based approach and the direct numerical modelling (Figure 7-2) are satisfactory over the complete range tested and down to ratios of effective rock mass to intact rock equal to 0.3.

The DFN-based method is directly applicable to evaluate the effective elastic properties of a Fracture Domain (Darcel et al. 2021) or a Deformation Zone (Åkerlind 2019), as illustrated in Figure 7-3. In the selected example the rock mass effective modulus estimated for rock mass block dimensions of 20 meters or more, is decreased by maximum 25 % when compared to the intact rock modulus. The prediction also emphasizes two critical aspects which are anisotropy and scale effect: i) the observed anisotropy (expressed as the ratio of the apparent moduli in the vertical direction, E_{zz} , and horizontal direction, E_{xx} or E_{yy}) is of about 15 %, ii) whatever the tested direction, the effective elastic properties show a scale effect (smooth decrease from the intact rock to the stabilized values) which vanishes beyond about 10 meters.

Moreover, the approach is a key component to further fundamental understanding of the rock mass mechanical behaviour, as it is based on its constituent characteristics (DFN statistics, fracture and intact rock mechanical properties). Davy et al. (2018) demonstrate that the contribution of each fracture to rock mass deformation is largely controlled by the relative size of the fracture with respect to the ratio of the intact rock modulus to the fracture shear stiffness (noted $l_s = E_m/k_s$). Moreover, over the full range of fracture sizes smaller than l_s , the controlling factor is the DFN metric called percolation parameter (see Section 2.6.1), while for the full range of fracture sizes larger than l_s , the DFN controlling metric is the so-called P_{32} (see Section 2.6.1). For power-law distributed fracture size distributions, such as those found in Forsmark, the multiscale nature of the fractured system therefore induces, by itself, a scale effect on the effective mechanical properties, as it is observed in Figure 7-3. The extent of the scale effect is controlled by l_s . It is noted that, for an extreme case where k_s is close to zero, whatever the fracture size (i.e., conditions equivalent to frictionless fractures), the scale effect would be endless (plotted as dashed lines in Figure 7-3). Such analyses, including alternative realistic and extreme cases, are useful: they provide lower bound estimates; they emphasize which scales are “mechanically” critical; they overall improve the quantitative understanding of the rock mass characteristics.

As it was already stated in the previous strategy report, discontinuum models (e.g. 3DEC) can be used for determining the strength. The approach may still be used but, since performing a large number of numerical tests is tedious, further developing the DFN-based approach is suggested for coming descriptions. This new strategy for rock mass strength follows the abovementioned DFN-based approach. The same philosophy – i.e., fundamental developments, use of numerical modelling, testing and methodology development – will be pursued to determine the link between the strength of the rock mass and again its constituents (DFN statistics, rock and fracture strength models).

By first making actual discontinuum models and thereafter correlating with analytical relationships, the methodology for strength prediction will arise. This work is now in an ongoing stage.

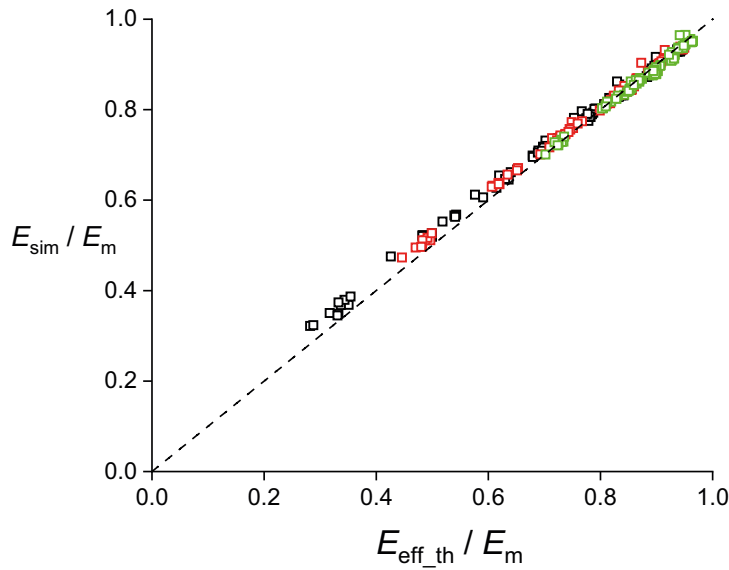


Figure 7-2. Comparison between rock mass moduli predicted with the effective theory estimate (E_{eff_th}) and derived from a complete numerical set up in 3DEC (E_{sim}). Both values are plotted normalized by the intact rock modulus (E_m). Various DFN geometrical and mechanical properties are defined (the black, red and green symbols respectively represent increasing values for fracture shear stiffness). The condition $E_{eff_th} = E_{sim}$ is depicted by the black dashed line. The figure is slightly modified from Davy et al. (2018).

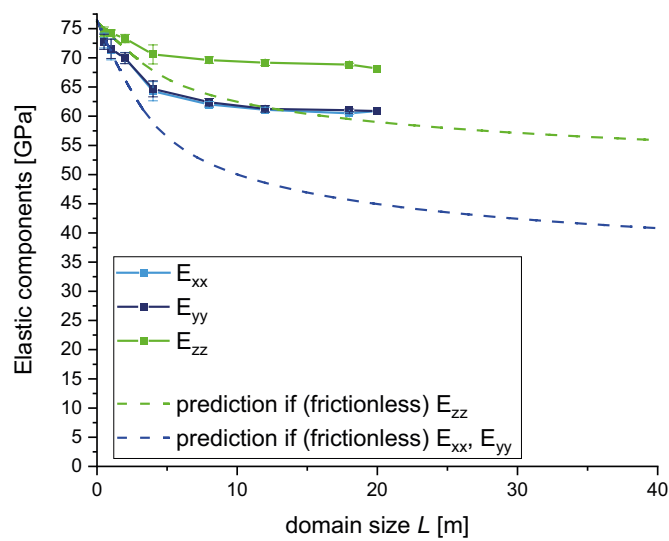


Figure 7-3. Evolution, with rock mass domain size, of the apparent effective elastic Modulus in the EW (E_{xx}), NS (E_{yy}) and vertical directions (E_{zz}). Two cases of fracture mechanical properties are shown: k_s and k_n values relevant to the FFM01 unit of Forsmark (lines with symbols) and generic values used for the frictionless case, with very high normal stiffness and null shear stiffness (dashed lines). The figure is adapted from Darcel et al. (2021) and the parameters were adjusted to FFM01 unit at Forsmark.

7.1.2 Stress dependent rock mass equivalent permeability

In situ stress variations do impact fracture transmissivities and therefore likely change the rock mass equivalent permeabilities, both their intensity and anisotropy (Brace et al. 1968b, Jaeger et al. 2007, Ranjram et al. 2015). Although there is no possibility to directly measure in situ both the stress and the equivalent permeability over well-defined rock mass dimensions, some studies emphasize the stress dependence through plots of equivalent permeability decrease when increasing depth (Rutqvist and Stephansson 2003, Achtziger-Zupančič et al. 2017). However, no established framework exists to relate the rock mass permeability and stress tensors.

The equivalent permeability of a rock mass arises from a combination of multiple factors: the DFN geometric and connectivity structure, the individual fracture transmissivities, the relation between stress and transmissivity (see Section 5.6), and the stress field itself.

Ongoing research supported by SKB aims at deriving an effective theory approach to define the rock mass stress permeability relationship. The work initially relies on a DFN-based approach. First the stress state on each fracture of a DFN is derived from remote stress boundary conditions coupling to DFN-based stress fluctuations. Second, transmissivities are calculated and complete equivalent permeability tensors are obtained from DFN-based flow simulations. This numerical approach is the foundation for developing the effective theory and builds an equivalent continuum stress permeability relation, with a parametrization based on DFN connectivity and fracture transmissivity stress relation.

7.2 DFN-based numerical approach

Another way to use the DFN to analyse mechanical properties of rock mass is to use discrete element codes where the fractured rock volume is numerically simulated, with separate material models for the intact rock parts and the embedded fractures. In Figure 7-2 results were presented from the 3DEC code which uses continuum models for the blocks between the fractures. Another numerical approach is applied when using PFC (Particle Flow Code) to simulate the rock. In this code the material consists of many particles with bond elements between them, and the bond properties are then clearly different between particles in the intact part and between particles on each side of discontinuity planes. The fracture network (faults, joints, veins, defects, grain boundaries, etc) of a rock mass can be explicitly represented together with the intact matrix rock part in between the fractures. In this way, both the fractures and the intact components can deform and fail in the numerical simulation.

This numerical technique is also denoted synthetic rock mass (SRM) and was introduced first by Potyondy and Cundall (2004) and refined by Potyondy (2012, 2014) with regard to intact rock modelling and further applied and developed by several researchers with regard to rock mass modelling (e.g. Mas Ivars et al. 2011, Potyondy 2012, Poulsen et al. 2015, Zhang et al. 2018, Castro-Filgueira et al. 2020).

To exemplify the capability of this approach, the diagrams in Figure 7-4 show the results from a series of simulations by Zhang et al. (2018) where triaxial loading of a “rock mass sample” (ca $3 \times 3 \times 3$ m size) is numerically simulated and the left and right column of the figure refers to different stress cases. With “regular” triaxial testing the stresses in all horizontal (confining) directions (x and y) are the same, and in the “true” triaxial testing the x and y confinement stresses are different. When principal stresses in the rock are different in different directions the deviatoric stress increases and this explains why the strength of the fractured rock block decreases, as is seen from the differences between the left and right column diagrams. This work by Zhang et al. (2018) illustrates how the numerical approach can be used to improve the understanding of different behaviour, like the pre- and post-peak behaviour and influence of different fracture network properties, even if empirical methods sometimes are used to calibrate the model input parameters. Fracture parameters (friction and cohesion) were in this case chosen to give results that are equal to the corresponding Mohr-Coulomb model for the uniaxial loading condition, and the SRM analyses could then be used to predict strength and behaviour under the true triaxial conditions.

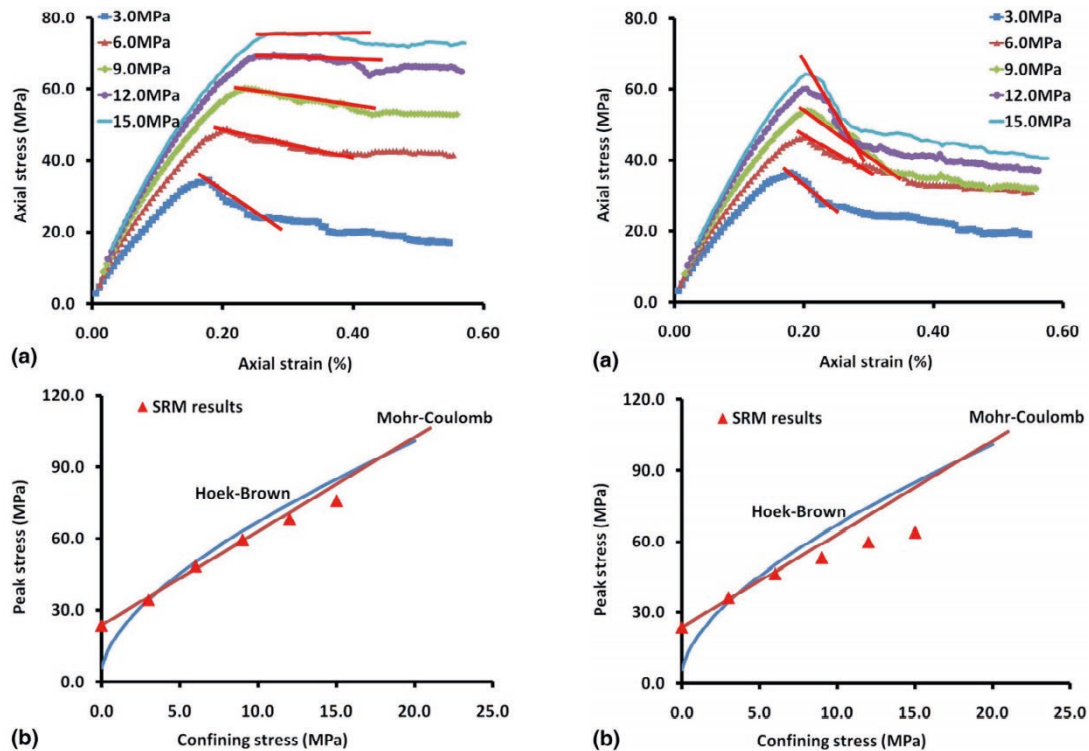


Figure 7-4. Results from DFN-based numerical rock mass simulation using PFC (Synthetic Rock Mass, SRM). Left column: Regular triaxial testing. a) Axial stress versus axial strain with varied confining stress and b) comparison between the SRM strength and the Hoek-Brown and Mohr-Coulomb criteria. Right column: True triaxial testing. a) Axial stress versus axial strain with constant stress of 5 MPa in the X direction and varied stress in the Y direction and b) comparison between the SRM and the Hoek-Brown and Mohr-Coulomb criteria. (Zhang et al. 2018).

7.3 Empirical approach

The empirical indices Q or Q_{bas} (Barton 2002, NGI 2015) and RMR or RMR_{bas} (Bieniawski 1989) have been determined for every metre of mapped drill core in Forsmark. These results will be retained and if new boreholes are drilled their Q_{bas} and RMR_{bas} data for the associated drill cores will be added to the database.

The difference in methodology is that only the statistics for empirical indices will be presented and the mechanical property parameters will *not* be derived from the empirical indices. It is believed that the indices are more useful and understood as is, and that the improved theoretical and DFN-based approach is better for determining rock mass parameters. One reason for not relying too much on empirical relations is the uncertainty regarding applicability in the very competent and sparsely fractured rock at depth in Forsmark.

As a first trade-off between purely empirical and purely quantitative approaches, the Hoek-Brown (HB) constitutive model of failure (Hoek and Brown 2018) relates a semi-empirical description of the rock mass to rock mass strength properties. The HB model takes as input the so-called Geological Strength Index (GSI) with the intact rock UCS and modulus parameters (plus an engineering index D for the geotechnical construction, known as the disturbance factor) (Hoek et al. 1995). The GSI refers to the fractured system, or the DFN structure, with two components, one relative to fracture surface quality and one to the level of blockiness or interlocking. For the latter, especially for scarcely fractured rock, the apparent spacing between fractures observed along core logs is taken as the proxy for rock mass block size and as such used in the GSI index. Improvements to the GSI approach were suggested by Cai et al. (2004) where the GSI is coupled to a quantitative estimate of the average rock block

volume, making the GSI index more objectively defined. Since the work of Cai et al. (2004), several attempts have been made to reinforce the quantitative character of the GSI index. In this way, although the HB model remains an empirical constitutive model of failure criteria, the definition of its input parameters, especially the geometrical information (level of interlocking or rock block size), is possibly quantitative.

The recent work of Kim et al. (2015) introduces two quantitative aspects. First, the use of a 3D DFN model to assess rock block volumes in 3D, and second, the use of statistical models and Monte-Carlo based approach to evaluate the distribution of likely values of GSI indexes rather than to reduce the prediction to a single and unique value (Figure 7-5). These two aspects contribute to improve the prediction by resorting to a more complete (3D) and quantitative representation of the fractured system with a DFN model. Hence, Kim et al. (2015) arrive at the index GSI distribution and from this calculate the distribution for the uniaxial strength of the rock mass.

These latest improvements to decrease the subjectivity in the empirical methods and to estimate their parameters in a more quantifiable manner go on the right direction. However, the DFN-based approach is founded on a common discrete theoretical framework that brings together the fields of geology, rock mechanics and hydrogeology and it is better suited for the analysis of complex coupled processes in fractured hard rock masses. Therefore, the DFN-based approach, rather than the empirical, is chosen as the primary methodology to support rock mass parameters of the future rock mechanics models.

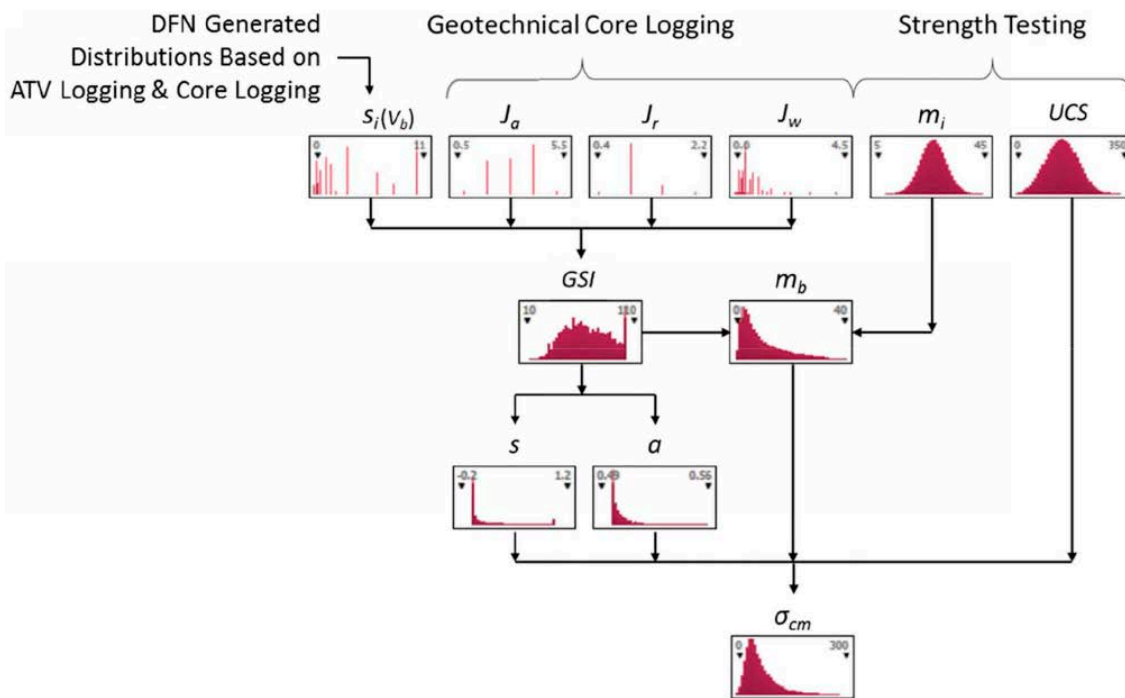


Figure 7-5. Monte Carlo procedure for estimating rock mass strength based on core logging and intact rock strength from Kim et al. (2015). The figure summarizes the path used to evaluate the distribution of Hoek–Brown parameters using the DFN derived block volumes, geotechnical core logging and strength testing data. The geometrical input for the GSI chart $S_i(V_b)$ is derived from a set of DFN realizations (Monte Carlo procedure) and combined to the core logging observations (classical J_a , J_r and J_w coefficients from the Q index (Barton et al. 1974)) in a statistical approach.

8 Rock mechanics modelling improvement strategy

In this report the different areas where rock mechanics modelling methodology is developed, compared to the rock mechanics model of SDM-Site, have been presented. Certain developments are already performed and other are merely planned and recommended. These different subjects have been dealt with in the preceding chapters of this report and in Figure 8-1 the different new items of the methodology are summarized, sorted for the different property areas (in the same way as in Figure 2-26 where the link to specific rock mechanics safety concerns was presented). Some of the methodology improvements deal with the interpretation of laboratory data and how to model or analyse further the measured results to make the most relevant site description (left column), while other suggested improvements include collection of a new type of data using new measurement methods (right column). Apart from these added components most of the previously applied methodology described in Glamheden et al. (2007) and SKB (2008) will also be retained and all available data will together constitute the basis for future site description.

Rock mechanics parameters required	New approaches to modelling methodology	New instruments and data collection
In situ stress <i>Chapter 3</i> 	<ul style="list-style-type: none"> • Updated numerical modelling procedures • Tensorial presentation of stress data • System for QA of overcoring data • Analyses of diskings occurrence 	<ul style="list-style-type: none"> • Overcoring in tunnel wall • Ring diskings analyses • Overcoring with improved tools in boreholes
Intact rock properties <i>Chapter 4</i> 	<ul style="list-style-type: none"> • Fracture toughness • Sample size effects • Long-term loading effects • Analyses for rock type variations 	<ul style="list-style-type: none"> • Fracture toughness test, pCT • Point Load Tester • Leeb hardness test • CAI
Single fracture properties <i>Chapter 5 and 6</i> 	<ul style="list-style-type: none"> • Water-bearing fracture description • Sealed fracture description • Improved normal stiffness parameters • Fracture transmissivity and stress coupling • Fracture undulation analyses • Surface roughness analyses 	<ul style="list-style-type: none"> • Surface laser scanning • CNS laboratory shear test • Leeb's hammer • Ground surface laser data
Rock mass properties <i>Chapter 7</i> 	DFN-based approach to <ul style="list-style-type: none"> • Rock mass elastic properties • Rock mass strength properties • Rock mass equivalent permeability stress dependency 	Refer to DFN Modelling Methodology Report, DFNMM1

Figure 8-1. Summary of recommended new or modified components in the future rock mechanics modelling methodology, compared to SDM-Site, which have been addressed in this report.

References

SKB's (Svensk Kärnbränslehantering AB) publications can be found at www.skb.com/publications. SKBdoc documents will be submitted upon request to document@skb.se.

Achtziger-Zupančič P, Loew S, Mariethoz G, 2017. A new global database to improve predictions of permeability distribution in crystalline rocks at site scale. *Journal of Geophysical Research: Solid Earth* 122, 3513–3539.

Alber M, Yaralı O, Dahl F, Bruland A, Käsling H, Michalakopoulos T N, Cardu M, Hagan P, Aydın H, Özarslan A, 2013. ISRM suggested method for determining the abrasivity of rock by the CERCHAR abrasivity test. *Rock Mechanics and Rock Engineering* 47, 261–266.

Andersson C, Söderhäll J, 2001. Rock mechanical conditions at the Äspö HRL. A study of the correlation between geology, tunnel maintenance and tunnel shape. SKB R-01-53, Svensk Kärnbränslehantering AB.

Andersson J C, 2007. Äspö Hard Rock Laboratory. Äspö Pillar Stability Experiment. Final report. Rock mass response to coupled mechanical thermal loading. SKB TR-07-01, Svensk Kärnbränslehantering AB.

Andersson J, Christiansson R, Hudson J, 2002. Site investigations. Strategy for rock mechanics site descriptive model. SKB TR-02-01, Svensk Kärnbränslehantering AB.

Ask D, 2011. Semi-integration of overcoring stress data and review of rock stress data at the Olkiluoto site. Posiva Working Report 2011-16, Posiva Oy, Finland.

Ask D, Cornet F, Brunet C, Fontbonne F, 2007. Forsmark site investigation. Stress measurements with hydraulic methods in boreholes KFM07A, KFM07C, KFM08A, KFM09A and KFM09B. SKB P-07-206, Svensk Kärnbränslehantering AB.

Back P-E, Sundberg J, 2022. Methodology for modelling of thermal properties of the Forsmark site. Part 1 – Recommended data and interpretation methods. SKB R-20-18, Svensk Kärnbränslehantering AB.

Backers T, Meier T, Gipper P, Stephansson O, 2014. Rock Mechanics – Confidence of SKB's model for predicting the occurrence of spalling. Main review phase. SSM Technical Note 2014:10, Swedish Radiation Safety Authority.

Baghbanan A, Jing L, 2008. Stress effects on permeability in a fractured rock mass with correlated fracture length and aperture. *International Journal of Rock Mechanics and Mining Sciences* 45, 1320–1334.

Bandis S C, Lumsden A C, Barton N R, 1983. Fundamentals of rock joint deformation. *International Journal of Rock Mechanics and Mining Sciences & Geomechanics Abstracts* 20, 249–268.

Barton C A, Zoback M D, Moos D, 1995. Fluid flow along potentially active faults in crystalline rock. *Geology* 23, 683–686.

Barton N, 2002. Some new Q-value correlations to assist in site characterisation and tunnel design. *International Journal of Rock Mechanics & Mining Sciences* 39, 185–216.

Barton N, Choubey V, 1977. The shear strength of rock joints in theory and practice. *Rock Mechanics* 10, 1–54.

Barton N, Lien R, Lunde J, 1974. Engineering classification of rock masses for the design of tunnel support. *Rock Mechanics* 6, 189–236.

Berryman J G, 2016. Role of fluid injection in the evolution of fractured reservoirs. *International Journal of Engineering Science* 103, 45–58.

Bieniawski Z T, 1989. Engineering rock mass classifications: a complete manual for engineers and geologists in mining, civil, and petroleum engineering. New York: Wiley.

Biot M A, 1955. Theory of elasticity and consolidation for a porous anisotropic solid. *Journal of Applied Physics* 26, 182–185.

- Bonnet E, Bour O, Odling N E, Davy P, Main I, Cowie P, Berkowitz B, 2001.** Scaling of fracture systems in geological media. *Reviews of Geophysics* 39, 347–384.
- Brace W F, Walsh J, Frangos W, 1968a.** Permeability of granite under high pressure. *Journal of Geophysical Research* 73, 2225–2236.
- Brace W F, Walsh J B, Frangos W T, 1968b.** Permeability of granite under high pressure. *Journal of Geophysical Research* 73, 2225–2236.
- Cai M, Kaiser P K, 2014.** In situ rock spalling strength near excavation boundaries. *Rock Mechanics and Rock Engineering* 47, 659–675.
- Cai M, Kaiser P K, Uno H, Tasaka Y, Minami M, 2004.** Estimation of rock mass deformation modulus and strength of jointed hard rock masses using the GSI system. *International Journal of Rock Mechanics & Mining Sciences* 41, 3–19.
- Casagrande D, Buzzi O, Giacomini A, Lambert C, Fenton G, 2018.** A new stochastic approach to predict peak and residual shear strength of natural rock discontinuities. *Rock Mechanics and Rock Engineering* 51, 69–99.
- Castro-Filgueira U, Alejano L R, Mas Ivars D, 2020.** Particle flow code simulation of intact and fissured granitic rock samples. *Journal of Rock Mechanics and Geotechnical Engineering* 12, 960–974.
- Chen Y-L, Wang S-R, Ni J, Azzam R, Fernández-Steegeer T M, 2017.** An experimental study of the mechanical properties of granite after high temperature exposure based on mineral characteristics. *Engineering Geology* 220, 234–242.
- Corkum A G, Lorig L J, DeGagne D O, 2012.** Continuum representation of brittle rock failure bulking-induced displacements around tunnels. In *Proceedings of 46th US Rock Mechanics/ Geomechanics Symposium, Chicago, 24–27 June 2012*. American Rock Mechanics Association.
- Corkum A G, Asiri Y, El Nagggar H, Kinakin D, 2018.** The Leeb hardness test for rock: an updated methodology and UCS correlation. *Rock Mechanics and Rock Engineering* 51, 665–675.
- Cotesta L, Kaiser P K, Cai M, 2004.** The effects of the full stress tensor on permeability anisotropy in moderately fractured rock – an application of 3D stress modelling and advanced visualization tools. *MIRARCO Mining Innovation Laurentian University*. Report No: 06819-REP-01300-10080-R00.
- Damjanac B, Fairhurst C, 2010.** Evidence for a long-term strength threshold in crystalline rock. *Rock Mechanics and Rock Engineering* 43, 513–531.
- Darcel C, Davy P, Le Goc R, Mas Ivars D, 2018.** Rock mass effective properties from a DFN approach. In *Proceedings of 2nd International Discrete Fracture Network Engineering Conference, Seattle, 20–22 June 2018*. American Rock Mechanics Association.
- Darcel C, Le Goc R, Doolaege D, Ghazal R, Davy P, 2021.** Rock mass effective properties from a DFN approach. Phase 1 – Elastic properties. SKB R-20-05, Svensk Kärnbränslehantering AB.
- Davy P, Darcel C, Le Goc R, Mas Ivars D, 2018.** Elastic properties of fractured rock masses with frictional properties and power-law fracture size distributions. *Journal of Geophysical Research: Solid Earth* 123, 6521–6539.
- Delgado-Martin J, Muñoz-Ibáñez A, Herbón-Penabad M, Alejano L R, 2021.** Fracture toughness using pseudo-compact tension (*p*CT) test and semi-circular bending specimen (SCB) test. SKB P-21-02, Svensk Kärnbränslehantering AB.
- Dershowitz W S, Herda H H, 1992.** Interpretation of fracture spacing and intensity. In *Proceedings of the 33th U.S. Symposium on Rock Mechanics (USRMS), Santa Fe, New Mexico, June 1992*. American Rock Mechanics Association.
- Doolaege D, 2021.** Colmatage des réseaux de fractures, modèles et conséquences hydrologiques. PhD thesis. Géosciences, Université de Rennes, France. (In French.)
- Drake H, Sandström B, Tullborg E-L, 2006.** Mineralogy and geochemistry of rocks and fracture fillings from Forsmark and Oskarshamn: Compilation of data for SR-Can. SKB R-06-109, Svensk Kärnbränslehantering AB.

- Ericsson L, Thörn J, Christiansson R, Lehtimäki T, Ittner H, Hansson K, Butron C, Sigurdsson O, Kinnbom P, 2015.** A demonstration project on controlling and verifying the excavation-damaged zone. Experience from the Äspö Hard Rock Laboratory. SKB R-14-30, Svensk Kärnbränslehantering AB.
- Ericsson L O, Vidstrand P, Christiansson R, Morosini M, 2018.** Comparison between blasting and wire sawing regarding hydraulic properties of the excavated damaged zone in a tunnel – Experiences from crystalline rock at the Äspö Hard Rock Laboratory, Sweden. In Proceedings of 52th US Rock Mechanics Symposium, Seattle, Washington, 17–20 June 2018. American Rock Mechanics Association.
- Esaki T, Du S, Mitani Y, Ikusada K, Jing L, 1999.** Development of a shear-flow test apparatus and determination of coupled properties for a single rock joint. *International Journal of Rock Mechanics and Mining Sciences* 36, 641–650.
- Evans K F, Kohl T, Rybach L, Hopkirk R J, 1992.** The effects of fracture normal compliance on the long term circulation behavior of a hot dry rock reservoir: a parameter study using the new fully-coupled code ‘fracture’. *Geothermal Resources Council Transactions* 16, 449–456.
- Figueiredo B, 2019.** Study of stress heterogeneity at Forsmark. Itasca Consultants AB. SKBDoc 1992068 ver 1.0, Svensk Kärnbränslehantering AB.
- Finenko M, Konietzky H, 2021.** Hausdorff distance as a 3D fracture aperture metric. *Rock Mechanics and Rock Engineering* 54, 2355–2367.
- Follin S, 2019.** Multidisciplinary description of the access area of the planned spent nuclear fuel repository in Forsmark prior to construction. SKB R-17-13, Svensk Kärnbränslehantering AB.
- Follin S, Stigsson M, 2014.** A transmissivity model for deformation zones in fractured crystalline rock and its possible correlation to in situ stress at the proposed high-level nuclear waste repository site at Forsmark, Sweden. *Hydrogeology Journal* 22, 299–311.
- Follin S, Hartley L, Rhén I, Jackson P, Joyce S, Roberts D, Swift B, 2014.** A methodology to constrain the parameters of a hydrogeological discrete fracture network model for sparsely fractured crystalline rock, exemplified by data from the proposed high-level nuclear waste repository site at Forsmark, Sweden. *Hydrogeology Journal* 22, 313–331.
- Follin S, Kokinen L, Suikkanen J, Riihiliuoma N, Kantia P, Kiuru R, Mustonen S, 2021.** Characterization of EDZ for final disposal facility of spent nuclear fuel in Olkiluoto. Posiva 2021-16, Posiva Oy, Finland.
- Fox A, Hermanson J, Öhman J, 2007.** Statistical geological discrete fracture network model Forsmark modelling stage 2.2. SKB R-07-46, Svensk Kärnbränslehantering AB.
- Fransson Å, 2009.** Literature survey: Relations between stress change, deformation and transmissivity for fractures and deformation zones based on in situ investigations. SKB R-09-13, Svensk Kärnbränslehantering AB.
- Fälth B, Lönnqvist M, Hökmark H, 2019.** Co-seismic secondary fracture displacements under different stress conditions. Posiva Working Report 2019-10, Posiva Oy, Finland.
- Gerolymatou E, 2019.** A novel tool for simulating brittle borehole breakouts. *Computers and Geotechnics* 107, 80–88.
- Glamheden R, Hökmark H, 2006.** Creep in jointed rock masses. State of knowledge. SKB R-06-94, Svensk Kärnbränslehantering AB.
- Glamheden R, Fredriksson A, Röshoff K, Kalsson J, Hakami H, Christiansson R, 2007.** Rock mechanics Forsmark. Site descriptive modelling Forsmark stage 2.2. SKB R-07-31, Svensk Kärnbränslehantering AB.
- Glamheden R, Lanaro F, Karlsson J, Lindberg U, Wrafter J, Hakami H, Johansson M, 2008.** Rock mechanics Forsmark. Modelling stage 2.3. Complementary analysis and verification of the rock mechanics model. SKB R-08-66, Svensk Kärnbränslehantering AB.
- Glamheden R, Fälth B, Jacobsson L, Harrström J, Berglund J, Bergkvist L, 2010.** Counterforce applied to prevent spalling. SKB TR-10-37, Svensk Kärnbränslehantering AB.

- Gorski B, Conlon B, Ljunggren B, 2007.** Forsmark site investigation. Determination of the direct and indirect tensile strength on cores from borehole KFM01D. SKB P-07-76, Svensk Kärnbränslehantering AB.
- Hagros A, Johansson E, Hudson J, 2008.** Time dependency in the mechanical properties of crystalline rocks. A literature study. Posiva Working Report 2008-68, Posiva Oy, Finland.
- Hakala M, 1999.** Numerical study on core damage and interpretation of *in situ* state of stress. Posiva 99-25, Posiva Oy, Finland.
- Hakala M, 2000.** Interpretation of the Hästholmen *in situ* state of stress based on core damage observations. Posiva 2000-01, Posiva Oy, Finland.
- Hakala M, 2022.** SKB MD 181.002e Method description for LVDT-cell rock stress measurement method. SKBdoc 1981591 ver 1.0, Svensk Kärnbränslehantering AB.
- Hakala M, Hudson J A, Christiansson R, 2003.** Quality control of overcoring stress measurement data. International Journal of Rock Mechanics and Mining Sciences 40, 1141–1159.
- Hakala M, Siren T, Kempainen K, Christiansson R, Martin D, 2013.** In situ stress measurement with the new LVDT-Cell-method description and verification. Posiva Working Report 2012-43, Posiva Oy, Finland.
- Hakala M, Ström J, Valli J, Juvani J, 2019.** Structural control on stress variability at Forsmark. SKB R-19-23, Svensk Kärnbränslehantering AB.
- Hakami E, 2011.** Rock stress orientation measurements using induced thermal spalling in slim boreholes. SKB R-11-12, Svensk Kärnbränslehantering AB.
- Hakami E, Olofsson S-O, 2000.** Thermo-mechanical effects from a KBS-3 type repository. Performance of pillars between repository tunnels. SKB TR-00-05, Svensk Kärnbränslehantering AB.
- Hakami E, Hakami H, Cosgrove J, 2002.** Strategy for a Rock Mechanics Site Descriptive Model. Development and testing of an approach to modelling the state of stress. SKB R-02-03, Svensk Kärnbränslehantering AB.
- Hermanson J, Petersson J, 2022.** Methodology for deterministic geologic modelling of the Forsmark site. Application to the development of the final repository for spent nuclear fuel. SKB R-20-10, Svensk Kärnbränslehantering AB.
- Hoek E, Brown E T, 1997.** Practical estimates of rock mass strength. International Journal of Rock Mechanics and Mining Sciences 34, 1165–1186.
- Hoek E, Brown E T, 2018.** The Hoek-Brown failure criterion and GSI–2018 edition. Journal of Rock Mechanics Geotechnical Engineering 11, 445–463.
- Hoek E, Kaiser P K, Bawden W F, 1995.** Support of underground excavations in hard rock. Rotterdam: Balkema.
- Hudson J A, Bäckström A, Rutqvist J, Jing L, Backers T, Chijimatsu, Christiansson R, Feng X-T, Kobayashi A, Koyama T, Lee H-S, Neretnieks I, Pan P-Z, Rinne M, Shen B-T, 2008.** Characterising and modelling the excavation damaged zone (EDZ) in crystalline rock in the context of radioactive waste disposal. Environmental Geology 57, 1275–1297.
- Hökmark H, Fälth B, Wallroth T, 2006.** T-H-M couplings in rock. Overview of results of importance to the SR-Can safety assessment. SKB R-06-88, Svensk Kärnbränslehantering AB.
- Hökmark H, Lönnqvist M, Fälth B, 2010.** THM-issues in repository rock. Thermal, mechanical, thermo-mechanical and hydro-mechanical evolution of the rock at the Forsmark and Laxemar sites. SKB TR-10-23, Svensk Kärnbränslehantering AB.
- Hökmark H, Fälth B, Lönnqvist M, Munier R, 2019.** Earthquake simulations performed to assess the long-term safety of a KBS-3 repository. Overview and evaluation of results produced after SR-Site. SKB TR-19-19, Svensk Kärnbränslehantering AB.
- ISRM, 2014.** The ISRM suggested methods for rock characterization, testing and monitoring: 2007–2014. Oxford: Pergamon.
- Itasca, 2016.** UDEC – User’s manual, version 6.0. Minneapolis, MN: Itasca Consulting Group.

- Itasca, 2017.** PFC suite – Particle Flow Code in 3 dimensions, version 6.0. Minneapolis, MN: Itasca Consulting Group.
- Itasca, 2020.** 3DEC – Three Dimensional Discrete Element Code, version 7.0. Minneapolis, MN: Itasca Consulting Group.
- Jacobsson L, 2016.** Parametrisation of fractures – Direct shear tests on calcite and breccia infilled rock joints from Äspö HRL under constant normal stiffness condition. Posiva Working Report 2016-19, Posiva Oy, Finland.
- Jacobsson L, Bäckström A, 2005.** DECOVALEX. Uniaxial compression tests of intact rock specimens at dry condition and at saturation by three different liquids: distilled, saline and formation water. SKB IPR-05-33, Svensk Kärnbränslehantering AB.
- Jacobsson L, Flansbjer, 2005.** Forsmark site investigation. Borehole KFM05A. Normal stress test with direct and indirect deformation measurement together with shear tests on joints. SKB P-05-141, Svensk Kärnbränslehantering AB.
- Jacobsson L, Flansbjer M, 2006.** Borehole KFM01D Shear tests on sealed joints. Forsmark site investigation. SKB P-06-215, Svensk Kärnbränslehantering AB.
- Jacobsson L, Sjöström J, 2019.** Forsmark – Laboratory tests for investigation of the influence of rock type, oxidation and other factors in borehole breakouts. Borehole KFM01A, KFM04A, KFM05A KFM24. Thermal properties by TPS method and uniaxial compression and indirect strength tests of intact rock. SKB P-18-08, Svensk Kärnbränslehantering AB.
- Jacobsson L, Appelquist K, Lindqvist J-E, Åkesson U, 2018.** Spalling initiation experiments on large hard rock cores. SKB R-14-12, Svensk Kärnbränslehantering AB.
- Jacobsson L, Mas Ivars D, Kasani H, Johansson F, Lam T, 2021.** Experimental program on mechanical properties of large rock fractures. In Proceedings of Eurock, Torino, Italy, 20–25 September 2021.
- Jaeger J C, Cook N G W, Zimmerman R, 2007.** Fundamentals of rock mechanics. 4th ed. Malden MA: Blackwell.
- Johansson F, 2016.** Influence of scale and matedness on the peak shear strength of fresh, unweathered rock joints. *International Journal of Rock Mechanics and Mining Sciences* 82, 36–47.
- Johansson F, Stille H, 2014.** A conceptual model for the peak shear strength of fresh and unweathered rock joints. *International Journal of Rock Mechanics and Mining Sciences* 69, 31–38.
- Jonsson M, Bäckström A, Feng Q, Berglund J, Johansson M, Mas Ivars D, Olsson M, 2009.** Äspö Hard Rock Laboratory. Studies of factors that affect and controls the Excavation Damaged/ Disturbed Zone. SKB R-09-17, Svensk Kärnbränslehantering AB.
- Kaiser P K, Diederichs M S, Martin C D, Sharp J, Steiner W, 2000.** Underground works in hard rock tunnelling and mining. International Conference on Geotechnical & Geological Engineering, Melbourne, November 2000. Lancaster, PA: Technomic Publishing, 841–926.
- Kim B-H, Peterson R, Katsaga T, Pierce M, 2015.** Estimation of rock block size distribution for determination of Geological Strength Index (GSI) using discrete fracture networks (DFNs). *Mining Technology* 124, 203–211.
- Kranzz R L, Frankel A D, Engelder T, Scholz C H, 1979.** The permeability of whole and jointed Barre Granite. *International Journal of Rock Mechanics and Mining Sciences & Geomechanics Abstracts* 16, 225–234.
- Kröhn K-P, Lanyon B, 2016.** Observation of hydraulic and transport “Skin effects”. SKB Task Force Workshop, Prague, 9–12 May 2016.
- Lan H, Martin C D, Hu B, 2010.** Effect of heterogeneity of brittle rock on micromechanical extensile behavior during compression loading. *Journal of Geophysical Research: Solid Earth*. Volume 115. doi:10.1029/2009JB006496
- Larsson J, Flansbjer M, 2020.** An approach to compensate for the influence of the system normal stiffness in CNS direct shear tests. *Rock Mechanics and Rock Engineering* 53, 2185–2199.

- Li B, Li Y, Zhao Z, Liu R, 2019.** A mechanical-hydraulic-solute transport model for rough-walled rock fractures subjected to shear under constant normal stiffness conditions. *Journal of Hydrology* 579, 124153. doi:10.1016/j.jhydrol.2019.124153
- Lim S S, 2013.** In situ stress magnitude and core diskings. PhD thesis. Department of Civil and Environmental Engineering, University of Alberta, Canada.
- Lim S S, Martin C D, 2010.** Core diskings and its relationship with stress magnitude for Lac du Bonnet granite. *International Journal of Rock Mechanics and Mining Sciences* 47, 254–264.
- Lima M G, Vogler D, Querci L, Madonna C, Hattendorf B, Saar M O, Kong X-Z, 2019.** Thermally driven fracture aperture variation in naturally fractured granites. *Geothermal Energy* 7, 23. doi:10.1186/s40517-019-0140-9
- Liu H-H, Rutqvist J, Zhou Q, Bodvarsson G S, 2004.** Upscaling of normal stress-permeability relationships for fracture networks obeying fractional Levy motion. *Elsevier Geo-Engineering Book Series Elsevier* 2, 263–268.
- Lönnqvist M, Hökmark H, 2010.** Assessment of potential for glacially induced hydraulic jacking at different depths. SKB R-09-35, Svensk Kärnbränslehantering AB.
- Lönnqvist M, Hökmark H, 2015.** Assessment of method to model slip of isolated, non-planar fractures using 3DEC. In *Proceedings of the 13th ISRM International Congress of Rock Mechanics*, Montreal, Canada, May 2015.
- Martin C D, 2005.** Preliminary assessment of potential underground stability (wedge and spalling) at Forsmark, Simpevarp and Laxemar sites. SKB R-05-71, Svensk Kärnbränslehantering AB.
- Martin C D, 2007.** Quantifying in situ stress magnitudes and orientations for Forsmark. Forsmark stage 2.2. SKB R-07-26, Svensk Kärnbränslehantering AB.
- Martin C D, Follin S, 2011.** Review of possible correlations between in situ stress and PFL fracture transmissivity data at Forsmark. SKB R-08-69, Svensk Kärnbränslehantering AB.
- Martin C D, Kaiser P K, Christiansson R, 2003.** Stress, instability and design of underground excavations. *International Journal of Rock Mechanics and Mining Sciences* 40, 1027–1047.
- Martino J B, Chandler N A, 2004.** Excavation-induced damage studies at the underground research laboratory. *International Journal of Rock Mechanics and Mining Sciences* 41, 1413–1426.
- Mas Ivars D, 2005.** Äspö Pillar Stability Experiment. Hydromechanical data acquisition experiment at the APSE site. SKB IPR-05-21, Svensk Kärnbränslehantering AB.
- Mas Ivars D, 2020.** Äspö Hard Rock Laboratory. Äspö Pillar Stability Experiment. Three-dimensional mechanical discontinuum modelling of the de-stressing slot drilling at the APSE site. SKB P-17-22, Svensk Kärnbränslehantering AB.
- Mas Ivars D, Pierce M E, Darcel C, Reyes-Montes J, Potyondy D O, Young R P, Cundall P A, 2011.** The synthetic rock mass approach for jointed rock mass modelling. *International Journal of Rock Mechanics and Mining Sciences* 48, 219–244.
- Mas Ivars D, Veiga Ríos M, Shiu W, Johansson F, Fredriksson A, 2014.** Long term stability of rock caverns BMA and BLA of SFR, Forsmark. SKB R-13-53, Svensk Kärnbränslehantering AB.
- Mas Ivars D, Lope Álvarez D, Sánchez Juncal A, Ghazal R, Damjanac B, 2015.** Parametrisation of fractures – Estimation of fracture shear displacement due to excavation of new slots at the TASQ tunnel via numerical modeling. *Posiva Working Report 2015-28*, Posiva Oy, Finland.
- Masoumi H, Saydam S, Hagan P C, 2016.** Unified size-effect law for intact rock. *International Journal of Geomechanics* 16. doi:10.1061/(ASCE)GM.1943-5622.0000543
- Mattila J, Follin S, 2019.** Does in situ state of stress affect fracture flow in crystalline settings? *Journal of Geophysical Research: Solid Earth* 124, 5241–5253.
- Milnes A G, 2006.** Understanding brittle deformation at the Olkiluoto site. Literature compilation for site characterization and geological modelling. *Posiva Working Report 2006-25*, Posiva Oy, Finland.

- Min K-B, Rutqvist J, Tsang C-F, Jing L, 2004.** Stress-dependent permeability of fractured rock masses: a numerical study. *International Journal of Rock Mechanics and Mining Sciences* 41, 1191–1210.
- Munier R, 2004.** Statistical analysis of fracture data, adapted for modelling Discrete Fracture Networks-Version 2. SKB R-04-66, Svensk Kärnbränslehantering AB.
- Muñoz Ibáñez A, 2020.** Experimental investigation of mode I rock fracture toughness. PhD thesis. University of A Coruña, Spain.
- NGI, 2015.** Using the Q-system: Rock mass classification and support design. Oslo: NGI.
- Nicksiar M, Martin C D, 2012.** Evaluation of methods for determining crack initiation in compression tests on low-porosity rocks. *Rock Mechanics and Rock Engineering* 45, 607–617.
- Nordlund E, Zhang P, Dineva S, Saiang C, Mainali G, 2014.** Impact of fire on the stability of hard rock tunnels in Sweden. BeFo Report 136, Rock Engineering Research Foundation, Sweden.
- Olofsson I, Simeonov A, Stephens M, Follin S, Nilsson A-C, Röshoff K, Lindberg U, Lanaro F, Fredriksson A, Persson L, 2007.** Site descriptive modelling Forsmark, stage 2.2. A fracture domain concept as a basis for the statistical modelling of fractures and minor deformation zones, and interdisciplinary coordination. SKB R-07-15, Svensk Kärnbränslehantering AB.
- Olson J E, 2003.** Sublinear scaling of fracture aperture versus length: An exception or the rule? *Journal of Geophysical Research: Solid Earth* 108. doi:10.1029/2001jb000419
- Olsson R, 1998.** Mechanical and hydromechanical behaviour of hard rock joints: a laboratory study. PhD thesis. Chalmers University of Technology, Sweden.
- Perras M A, Diederichs M S, 2014.** A review of the tensile strength of rock: concepts and testing. *Geotechnical and Geological Engineering* 32, 525–546.
- Perras M A, Diederichs M S, 2016.** Predicting excavation damage zone depths in brittle rocks. *Journal of Rock Mechanics and Geotechnical Engineering* 8, 60–74.
- Posiva, 2012.** Olkiluoto site description. Posiva 2011-02, Posiva Oy, Finland.
- Potyondy D O, 2012.** A flat-jointed bonded-particle material for hard rock. In *Proceedings of 46th U.S. Rock Mechanics/Geomechanics Symposium*, Chicago, 24–27 June 2012.
- Potyondy D O, 2014.** The bonded-particle model as a tool for rock mechanics research and application: current trends and future directions. *Geosystem Engineering* 18, 1–28.
- Potyondy D O, Cundall P A, 2004.** A bonded-particle model for rock. *International Journal of Rock Mechanics and Mining Sciences* 41, 1329–1364.
- Poulsen B A, Adhikary D P, Elmoultie M K, Wilkins A, 2015.** Convergence of synthetic rock mass modelling and the Hoek-Brown strength criterion. *International Journal of Rock Mechanics and Mining Sciences* 80, 171–180.
- Quiñones J, Arzúa J, Alejano L R, García-Bastante F, Mas Ivars D, Walton G, 2017.** Analysis of size effects on the geomechanical parameters of intact granite samples under unconfined conditions. *Acta Geotechnica* 12, 1229–1242.
- Ranjram M, Gleeson T, Luijendijk E, 2015.** Is the permeability of crystalline rock in the shallow crust related to depth, lithology or tectonic setting? *Geofluids* 15, 106–119.
- Raven K, Gale J, 1985.** Water flow in a natural rock fracture as a function of stress and sample size. *Proceedings of International Journal of Rock Mechanics and Mining Sciences & Geomechanics Abstracts* 22, 251–261.
- Read R S, 2004.** 20 years of excavation response studies at AECL's Underground Research Laboratory. *International Journal of Rock Mechanics and Mining Sciences* 41, 1251–1275.
- Read R, Martin C, 1996.** Technical summary of AECL's Mine-by Experiment phase I: Excavation response. AECL-11311, COG-95-171, Whiteshell Laboratories, Manitoba, Winnipeg.
- Ríos Bayona F, 2019.** Analytical and numerical approaches to estimate peak shear strength of rock joints. Licentiate thesis. KTH Royal Institute of Technology, Sweden.

- Ríos Bayona F, 2022.** Towards a methodology for field assessment of the peak shear strength of rock joints. PhD thesis. KTH Royal Institute of Technology, Sweden.
- Ríos-Bayona F, Johansson F, Mas-Ivars D, 2021.** Prediction of peak shear strength of natural, unfilled rock joints accounting for matedness based on measured aperture. *Rock Mechanics and Rock Engineering* 54, 1533–1550.
- Rouhiainen P, Sokolnicki M, 2005.** Forsmark site investigation. Difference flow logging in borehole KFM06A. SKB P-05-15, Svensk Kärnbränslehantering AB.
- Rutqvist J, Stephansson O, 2003.** The role of hydromechanical coupling in fractured rock engineering. *Hydrogeology Journal* 11, 7–40.
- Rutqvist J, Tsang C-F, 2008.** Review of SKB:s work on coupled THM processes within SR-Can. External review contribution in support of SKI:s and SSI:s review of SR-Can. SKI Report 2008:08, Swedish Nuclear Power Inspectorate.
- Röshoff K, Lanaro F, Jing L, 2002.** Strategy for a rock mechanics site descriptive model. Development and testing of the empirical approach. SKB R-02-01, Svensk Kärnbränslehantering AB.
- Saceanu M C, Paluszny A, Zimmerman R W, Ivars D M, 2022.** Fracture growth leading to mechanical spalling around deposition boreholes of an underground nuclear waste repository. *International Journal of Rock Mechanics and Mining Sciences* 152, 105038. doi:10.1016/j.ijrmms.2022.105038
- Selroos J-O, Mas Ivars D, Munier R, Hartley L, Libby S, Davy P, Darcel C, Trincherro P, 2022.** Methodology for discrete fracture network modelling of the Forsmark site. Part 1 – concepts, data and interpretation methods. SKB R-20-11, Svensk Kärnbränslehantering AB.
- Siren T, Hakala M, Valli J, Christiansson R, Mas Ivars D, Lam T, Mattila J, Suikkanen J, 2017.** Parametrisation of fractures – Final report. Posiva 2017-01, Posiva Oy, Finland.
- Sjöberg J, Lindfors U, Perman F, Ask D, 2005.** Evaluation of the state of stress at the Forsmark site. Preliminary site investigation Forsmark area – version 1.2. SKB R-05-35, Svensk Kärnbränslehantering AB.
- Sjöberg J, Berglund J, Mas Ivars D, 2007.** Äspö Hard Rock Laboratory. Core disk study in the TASQ (APSE) tunnel, Äspö HRL. SKB IPR-07-18, Svensk Kärnbränslehantering AB.
- SKB, 1992.** SKB 91 – Final disposal of spent nuclear fuel. Importance of the bedrock for safety. SKB TR 92-20, Svensk Kärnbränslehantering AB.
- SKB, 2008.** Site description of Forsmark at completion of the site investigation phase SDM-Site Forsmark. SKB TR-08-05, Svensk Kärnbränslehantering AB.
- SKB, 2010.** Data report for the safety assessment SR-site. SKB TR-10-52, Svensk Kärnbränslehantering AB.
- SKB, 2011.** Long-term safety for the final repository for spent nuclear fuel at Forsmark. Main report of the SR-Site project. SKB TR-11-01, Svensk Kärnbränslehantering AB.
- SKB, 2013.** Site description of the SFR area at Forsmark at completion of the site investigation phase. SDM-PSU Forsmark. SKB TR-11-04, Svensk Kärnbränslehantering AB.
- Snow D T, 1965.** A parallel plate model of fractured permeable media. PhD thesis. University of California.
- SSM, 2018.** Strålsäkerhet efter slutförvarets förslutning, Beredning inför regeringens prövning. Slutförvaring av använt kärnbränsle. Report 2018:07, Swedish Radiation Safety Authority. (In Swedish.)
- Staub I, Fredriksson A, Outters N, 2002.** Strategy for a Rock Mechanics Site Descriptive Model. Development and testing of the theoretical approach. SKB R-02-02, Svensk Kärnbränslehantering AB.
- Stephens M B, Simeonov A, 2015.** Description of deformation zone model version 2.3, Forsmark. SKB R-14-28, Svensk Kärnbränslehantering AB.
- Stephens M, Fox A, Simeonov A, Isaksson H, Hermanson J, 2007.** Geology Forsmark. Site descriptive modelling Forsmark stage 2.2. SKB R-07-45, Svensk Kärnbränslehantering AB.

- Stigsson M, 2015.** Parameterization of fractures – methods and evaluation of fractal fracture surfaces. Posiva Working Report 15-27, Posiva Oy, Finland.
- Stigsson M, 2018.** Finally, an objective way to infer JRC from digitized fracture traces. In Proceedings of 52nd US Rock Mechanics/Geomechanics Symposium, 2018. American Rock Mechanics Association.
- Stigsson M, Mas Ivars D, 2019.** A novel conceptual approach to objectively determine JRC using fractal dimension and asperity distribution of mapped fracture traces. *Rock Mechanics and Rock Engineering* 52, 1041–1054.
- Thörn J, 2015.** The impact of fracture geometry on the hydromechanical behaviour of crystalline rock. PhD thesis. Chalmers University of Technology, Sweden.
- Townend J, Zoback M D, 2000.** How faulting keeps the crust strong. *Geology* 28, 399–402.
- Valli J, Hakala M, Suikkanen J, Heine J, Simelius C, 2016.** Parametrisation of fractures – PUSH test execution and back-analysis. Posiva Working Report 2016-52, Posiva Oy, Finland.
- Walsh J B, 1981.** Effect of pore pressure and confining pressure on fracture permeability. *Proceedings of International Journal of Rock Mechanics and Mining Sciences & Geomechanics Abstracts* 18, 429–435.
- Walton G, Lato M, Anshütz H, Perras M A, Diederichs M S, 2015.** Non-invasive detection of fractures, fracture zones, and rock damage in a hard rock excavation – Experience from the Äspö Hard Rock Laboratory in Sweden. *Engineering Geology* 196, 210–221.
- Winberg A, 2017.** Modelling scales applicable to detailed site investigations in the Forsmark area. SKBdoc 1409070 ver 1.0, Svensk Kärnbränslehantering AB.
- Winberg A, Andersson P, Hermanson J, Byegård J, Cvetkovic V, Birgersson L, 2000.** Äspö Hard Rock Laboratory. Final report of the first stage of the tracer retention understanding experiments. SKB TR-00-07, Svensk Kärnbränslehantering AB.
- Witherspoon P A, Wang J S Y, Iwai K, Gale J E, 1980.** Validity of cubic law for fluid flow in a deformable rock fracture. *Water Resources Research* 16, 1016–1024.
- Wu S, Wu H, Kemeny J, 2018.** Three-dimensional discrete element method simulation of core diskings. *Acta Geophysica* 66, 267–282.
- Zangerl C, Evans K F, Eberhardt E, Loew S, 2008.** Normal stiffness of fractures in granitic rock: a compilation of laboratory and in situ experiments. *International Journal of Rock Mechanics and Mining Sciences* 45, 1500–1507.
- Zhang Y, Ren F Y, Yang T H, Wang S Y, Zhang W F, Yu M X, 2018.** An improved rock mass characterization method using a quantified geological strength index and synthetic rock mass model. *Rock Mechanics and Rock Engineering* 51, 3521–3536.
- Zhang Z X, 2002.** An empirical relation between mode I fracture toughness and the tensile strength of rock. *International Journal of Rock Mechanics and Mining Sciences* 39, 401–406.
- Zimmerman R, 2008.** A simple model for coupling between the normal stiffness and the hydraulic transmissivity of a fracture. In Proceedings of the 42nd U.S. Rock Mechanics Symposium (USRMS), San Francisco, June 2008. American Rock Mechanics Association.
- Zimmerman R, Main I, 2004.** Hydromechanical behavior of fractured rocks. *International Geophysics* 89, 363–422.
- Zou L, Li B, Mo Y, Cvetkovic V, 2020.** A high-resolution contact analysis of rough-walled crystalline rock fractures subject to normal stress. *Rock Mechanics and Rock Engineering* 53, 2141–2155.
- Åkerlind A, 2019.** Elastic properties of the Singö zone from a discrete approach. Master thesis. KTH Royal Institute of Technology, Sweden.

SKB is responsible for managing spent nuclear fuel and radioactive waste produced by the Swedish nuclear power plants such that man and the environment are protected in the near and distant future.

skb.se